

GENERAL NOTES

REFERENCE DRAWINGS

PROJ. NO.	REV. NO.	LOC.	REVISIONS	REVISED BY DATE	CHECKED BY DATE	APPROVED BY DATE



THIS DRAWING IS PREPARED FOR:



**NYSEG SENECA CASE PROJECT
STORAGE WELL SITE PLAN**

DESIGN BY: KS	DATE: 11/11	DRAWN BY: HH	DATE: 11/11	SCALE: 1 INCH=200 FEET
CHECKED BY: KS	DATE: 11/11	APPROVED BY: KS	DATE: 11/11	PROJECT NO:
FILE NAME: 50756B-GP-001	DRAWING NO: 50756B-GP-001	LATEST REVISION:	▲	

External Memorandum

To: Mr. Jim M. McHenry
Project Manager
PB Energy Storage Services, Inc.
16285 Park Ten Place, Suite 400
Houston, TX 77084

cc: Dr. Joe L. Ratigan, PB Energy Storage Services, Inc.
Dr. John D. Osnes, RESPEC
Project Central File 2040 — Category A

From: Mr. Joel D. Nieland
Staff Consultant
RESPEC
P.O. Box 725
Rapid City, SD 57709

Date: October 4, 2011

Subject: Thermodynamic Evaluation of Proposed New York State Electric & Gas Corporation
Compressed Air Energy Storage Cavern Design

The purpose of this memorandum is to present the results of a study to investigate the thermodynamic performance of the proposed cavern design for the compressed air energy storage (CAES) facility that New York State Electric & Gas Corporation (NYSEG) is planning to develop about 4 miles north of Watkins Glen, New York. The air storage caverns will be developed in the bedded salt deposits of the Syracuse Formation at a depth of about 2,400 feet below the ground surface. The performance issues examined here include: (1) cavern air storage capacity, (2) surface and underground pressures and temperatures, and (3) casing string (liner) sizes for the anticipated operations.

1.0 BACKGROUND

The proposed NYSEG CAES facility has a rated capacity between approximately 135 and 210 MW and will provide energy during peak periods in support of market needs. WorleyParsons Group, Inc. [2011] provided a typical daily air flow cycle that meets the power generation needs of the facility. The hourly flow rates for the typical cycle are listed in Table 1 and are shown graphically in Figure 1. The cycle has air injected into the cavern during off-peak hours and air is withdrawn from the cavern to generate power during peak periods. An air injection temperature at the wellhead of 95°F is specified. The daily cycle requires a total working gas of 17.7 million pounds of air. It was assumed in this analyses that there will not be any flow during weekend hours.

Table 1. Flow Rates for Typical Daily Cycle

Time of Day	Hours of Operation	Flow Rate ^(a) (lb/s) ^(b)
12 am – 5 am	5	639
5 am – 6 am	1	441
6 am – 8 am	2	-351
8 am – 9 am	1	0
9 am – 1 pm	4	-617
1 pm – 2 pm	1	0
2 pm – 4 pm	2	-617
4 pm – 5 pm	1	-510
5 pm – 10 pm	5	0
10 pm – 12 am	2	639

- (a) Positive values indicate injection into cavern and negative values indicate withdrawal for power generation.
- (b) lb/s = pounds per second.

RSI-2040-11-001

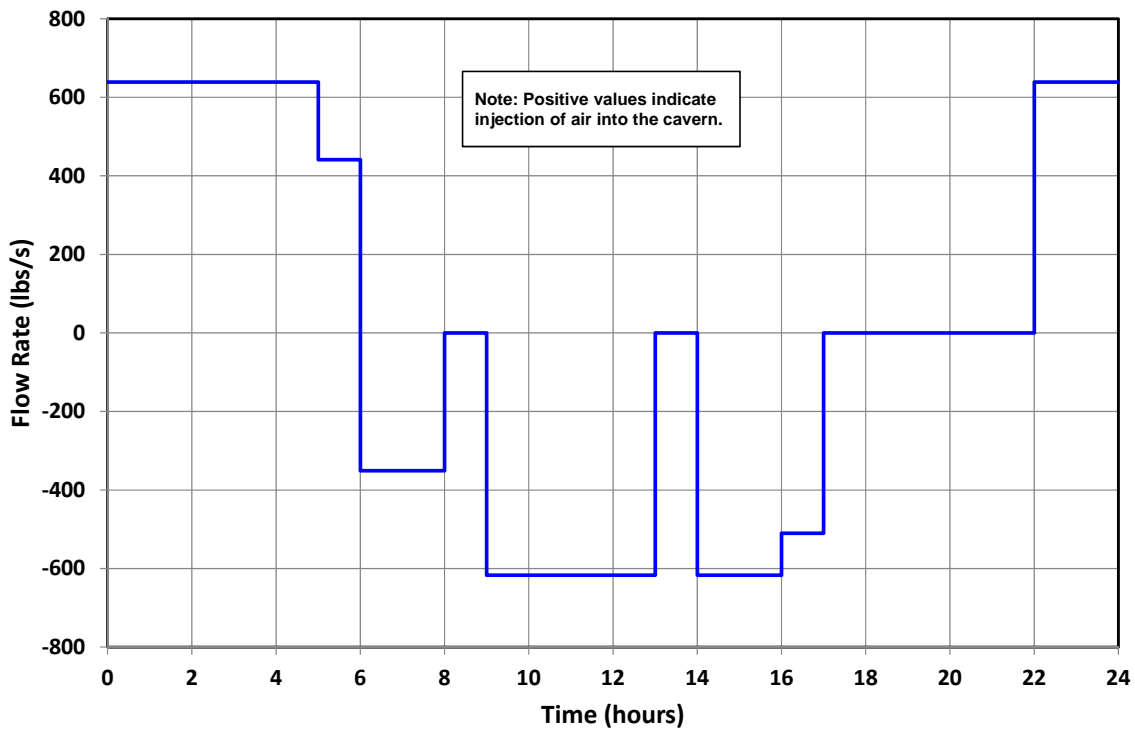


Figure 1. Typical Daily Air Flow Cycle.

Preliminary geomechanical analyses determined that an operating wellhead pressure range of 1,150 psi to 1,500 psi (about 1,260 psi to 1,630 psi within the cavern) will result in a structurally stable cavern. Based on preliminary thermodynamic analyses, a cavern volume of roughly 3 million barrels (MMbbls) is required to provide the required working gas for this pressure range. The rate of cavern volume development is governed by a brine disposal rate of about 350 gallons per minute (gpm) and it is estimated that approximately 6 years will be required to develop a cavern volume of 3 MMbbls. Because of solution-mining limitations and also to provide partial interim operation, three caverns each having a volume of approximately 1 MMbbls will be developed.

2.0 TECHNICAL APPROACH

The investigative analyses presented here were conducted with the Salt Cavern Thermal Simulator (SCTS) [Nieland, 2004], a program developed by PB Energy Storage Services, Inc. and RESPEC for simulating the thermodynamics and heat transfer related to the storage of natural gas in underground salt caverns. It accounts for the thermal effects associated with gas compression and expansion; the mass transfer during injection and withdrawal; and the heat transfer between the gas and its surroundings, both in the wellbore and in the cavern. Because the release version of SCTS only simulates natural gas storage, a modified version which allows the simulation of compressed air and hydrogen storage was used for this study.

The proposed cavern design analyzed in this study [Eyermann, 2011a] is based on solution-mining calculations performed following the preliminary analyses described above. The radius of the cavern design as a function of depth is shown in Figure 2. This cavern design has a mined volume of about 970,000 barrels (bbls) of which about 940,000 bbls can be dewatered and used for air storage. The roof of the cavern is at a depth of 2,402 feet (50 feet below the top of salt) and has a dewatered depth of about 2,525 feet. The casing seat is assumed to be at a depth of 2,360 feet, about 8 feet below the top of the salt¹.

In SCTS, the heat transfer between the air in the cavern and the surrounding rock is estimated using a one-dimensional spherical heat transfer model containing a single material (salt properties were used in this case). SCTS uses a parameter (the volume-to-area ratio) to modify the spherical model to approximate the actual shape of the cavern. The ratio of the volume to surface area of the proposed cavern design is 30.0 ft³/ft². The heat transfer between the air in the wellbore and surrounding rock is estimated using a stacked series of one-dimensional radial heat transfer models with properties assigned based on the surrounding rock. The stratigraphy used in the simulations of the wellbore heat transfer is based on local geology described by Eyermann [2011b]. Densities for the rock units are based on a density log conducted in Well No. 59 [Osnes and Eyermann, 1996]. Typical thermal properties [Croff et al., 1985; Callahan, 1981] for shale, sandstone, carbonates (limestone and dolomite), and salt were assigned to the units. The stratigraphic units and the properties assumed for them are listed in Table 2. The undisturbed in situ temperature profile assumed in this study is based on temperature logs conducted in Well No. 59 and is described in Table 3.

¹ This selection for the casing seat depth is based on the following: (1) the casing seat needs to be set in the salt, (2) placing the casing seat too close to the cavern roof will make mechanical integrity testing difficult or impossible, and (3) increasing the distance between the cavern roof and casing seat results in a lower amount of casing strain.

RSI-2040-11-002

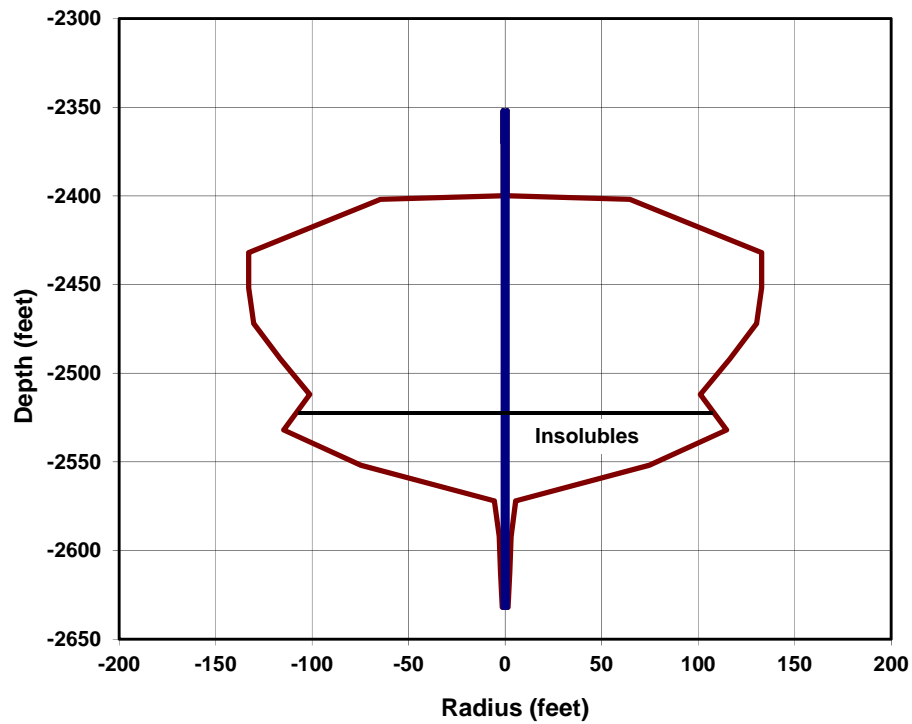


Figure 2. Simulated Shape of the Proposed Compressed Air Energy Storage Cavern Design [Eyermann, 2011a].

Table 2. Thermal Properties and Rock Densities

Unit - Lithology	Depth Range (ft)	Density (lb/ft ³)	Thermal Conductivity (Btu/hr-ft-°F)	Specific Heat (Btu/lb-°F)
Genesee - Shale	0-830	164	0.804	0.190
Tully - Limestone	830-847	167	1.775	0.123
Hamilton - Shale	847-1,768	165	0.804	0.190
Marcellus - Shale	1,768-1,866	165	0.804	0.190
Onondaga - Limestone	1,866-1,911	164	1.775	0.123
Tristates Group - Sandstone	1,911-1,948	167	1.966	0.170
Oriskany - Sandstone	1,948-1,956	167	1.966	0.170
Helderberg Group - Limestone	1,956-2,106	168	1.775	0.123
Cobleskill/Akron - Dolostone	2,106-2,166	169	1.775	0.123
Bertie - Dolostone	2,166-2,255	175	1.775	0.123
Camillus - Shale	2,255-2,352	170	0.804	0.190
Syracuse - Salt	2,352-2,360	130	3.000	0.200

Table 3. In Situ Temperature Profile

Surface Temperature = 45.6°F	
Depth Range (ft)	Temperature Gradient (°F/ft)
0 – 1,110	0.0085
1,110 – 1,866	0.0225
Below 1,866	0.0088

In the thermodynamic simulations, properties of the brine and air are calculated in SCTS based on the fluid composition (or salinity) and are functions of the temperature and pressure. These properties include density, compressibility, thermal conductivity, specific heat, and viscosity. The assumed air composition is shown in Table 4.

Table 4. Air Composition

Component	Mole Percent
Nitrogen	78.0
Oxygen	21.0
Argon	1.0

The air storage simulations were preceded by leaching and dewatering of the cavern. The leaching was simulated over 730 days with a flow rate of 350 gpm. A freshwater injection temperature of 52°F at the wellhead was assumed during leaching. After leaching the cavern, the cavern was dewatered and filled with air at a wellhead pressure of 1,350 psi. The cavern was then depressurized to about 1,160 psi at the wellhead, which is representative of the wellhead pressure at the end of a weekend in the simulations. The conditions at this point were used as the starting point for all of the following compressed air storage simulations.

3.0 RESULTS

The results of the analyses are given in terms of well casing liner size selection and cavern performance, including storage capacity and estimated surface and down-hole pressures and temperatures.

3.1 Casing Liner Size Selection

The wellbores of the CAES caverns will be completed with stainless-steel liners to help prevent corrosion. Liner sizes were determined to ensure the operational air velocities will not result in excessive erosion of the liner surface and also to keep pressure losses in the wellbore to a reasonable level. Air velocities will depend on the air flow rate, the air density, and the cross-sectional area of the wellbore. Pressure losses in the wellbore will depend on the air flow rate,

the cross-sectional area of the wellbore, and the smoothness of the wellbore. New stainless-steel casing has an absolute roughness of about 0.0018 inch and this value was used in all of the calculations.

After all three caverns are developed and are operating in parallel, the maximum flow rate for each of the caverns will be one-third of the maximum total flow rate. However, after the first cavern is developed, it is desired to begin CAES operations while the other caverns are being developed, and likewise, to use the second cavern as the third cavern is being developed. Also, after all three caverns are developed, it is desirable to be able to operate with any two of the caverns so that a cavern may be taken off-line for any required maintenance. It is anticipated that while operating with less than all three caverns, that operations will be conducted at full power (i.e., at the flow rates specified in Table 1); albeit, for shorter periods than specified by the full operational cycle. Maximum flow rates under this assumption for the various cavern configurations are listed in Table 5.

Table 5. Maximum Cavern Air Flow Rates

Operating Configuration	Maximum Cavern Injection Flow Rate (lb/s)	Maximum Cavern Withdrawal Flow Rate (lb/s)
One Cavern	639	617
Two Caverns	319.5	308.5
Three Caverns	213	205.7

To evaluate casing size, the maximum injection flow rate for each of the operating configurations was evaluated for liners with outer diameters (OD) ranging from 6.625 inches to 24 inches. A wall thickness of ¼ inch was assumed for all liners. The liners were evaluated at the minimum wellhead pressure of 1,150 psi when the air density is at its lowest value and thus velocities are at their highest.

The maximum allowable air velocities to prevent casing erosion were calculated using the following equation provided by the American Petroleum Institute (API) [1991]:

$$V_e = \frac{C}{\sqrt{\rho}} \quad (3-1)$$

where:

V_e = velocity above which erosion may occur (ft/s)

C = empirical constant

ρ = density of the fluid (lb/ft³).

For continuous service flow with solids-free fluids where a corrosion-resistant alloy is used (in this case, stainless steel) the API recommends C values in the range of 150 to 200. As a conservative measure, the lower-end value of 150 was used in this study.

The velocities were evaluated at the casing seat (2,360-foot depth) and at the wellhead, as shown in Figures 3 and 4, respectively. The air velocities at the wellhead are slightly higher because the air is at a lower density. The maximum allowable velocities that mitigate erosion are about 57 to 60 feet per second (ft/s). Thus to prevent erosion, the recommended liner sizes are a 20-inch OD liner for a flow rate of 639 lb/s, a 14-inch OD liner for a flow rate of 320 lb/s, and a 10³/₄-inch OD liner for flows of 213 lb/s.

The pressure losses in the wellbore liner are a result of the friction between the flowing air and the wellbore liner surface. Friction losses will result in increased power consumption while air is injected into the cavern and a decrease in power recovery as the air is withdrawn from the cavern. Figure 5 shows the estimated wellbore liner pressure losses for the same flow rates as a function of liner diameter. The results indicate that the pressure losses for the maximum flow rate of 639 lb/s will increase significantly for wellbore liner diameters of less than about 20 inches. Thus the 20-inch liner is recommended for the first cavern developed and is expected to have a pressure loss of about 35 psi at the maximum flow rate of 639 lb/s. The pressure loss in the 20-inch liner will decrease to about 15 psi when two caverns are operating and to about 10 psi when all three caverns are operating.

To have comparable pressure losses in the case when any two caverns are being operated (a maximum flow rate of 320 lb/s), it is recommended to install 16-inch liners in the second and third caverns developed. The caverns with the 16-inch liners are expected to have pressure losses of about 30 psi when two caverns are operating and about 17 psi when all three caverns are operating.

3.2 Cavern Performance

The air storage capacity of a solution-mined cavern is governed by the gas equation-of-state, which, for a real gas, is defined as:

$$m = \frac{VPM}{zRT} \quad (3-2)$$

where:

m = mass of stored gas

V = cavern volume

P = absolute gas pressure in the cavern

M = molecular weight of the gas

z = compressibility factor of the gas

R = universal gas constant

T = absolute temperature of gas.

RSI-2040-11-003

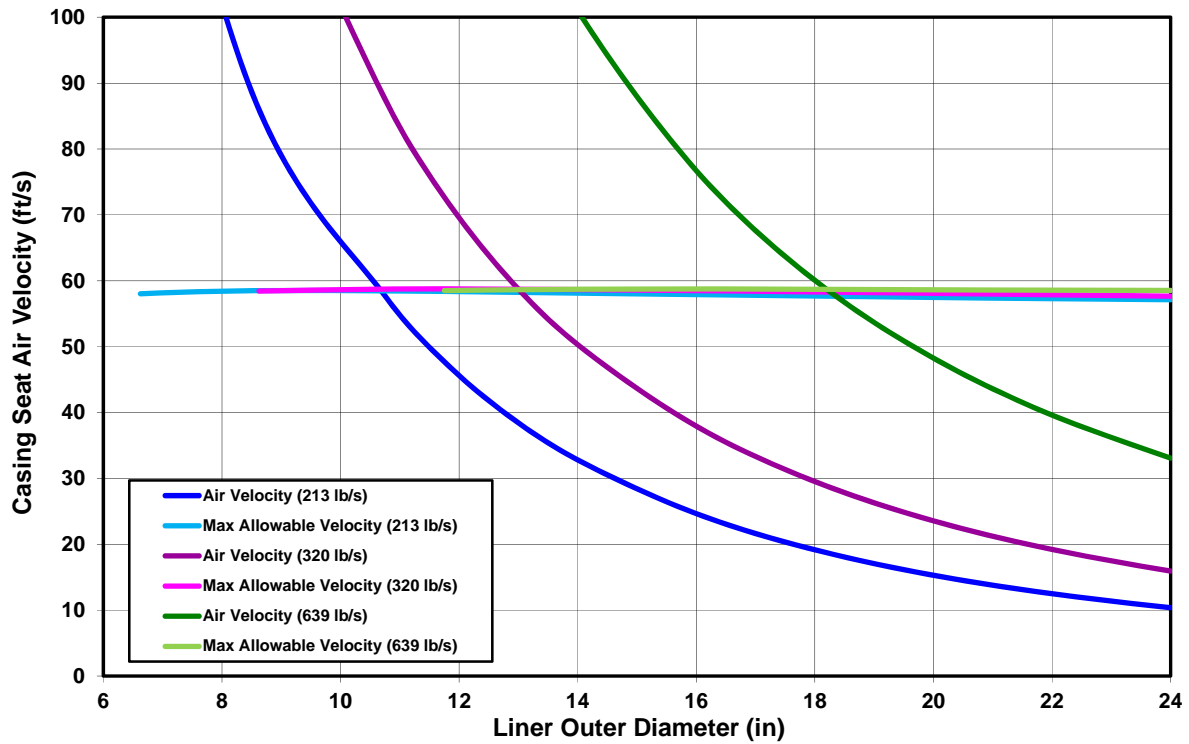


Figure 3. Air Velocities and Maximum Allowable Velocities at the Casing Seat.

RSI-2040-11-004

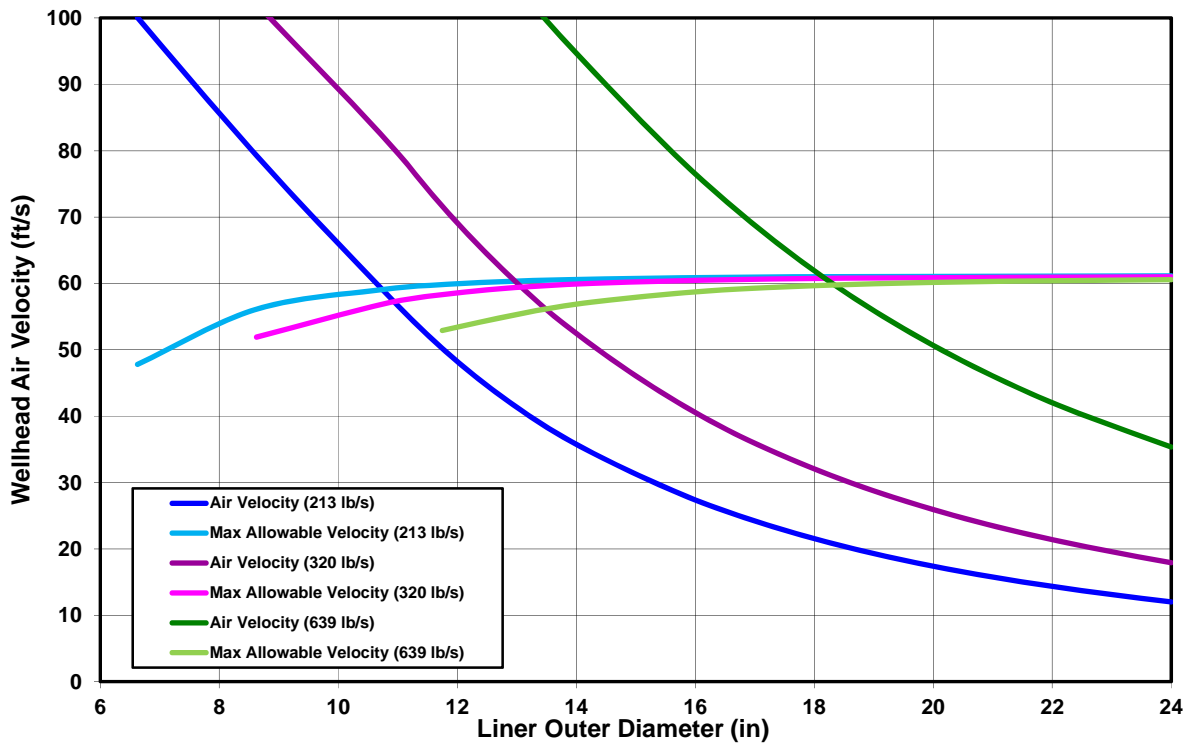


Figure 4. Air Velocities and Maximum Allowable Velocities at the Wellhead.

RSI-2040-11-005

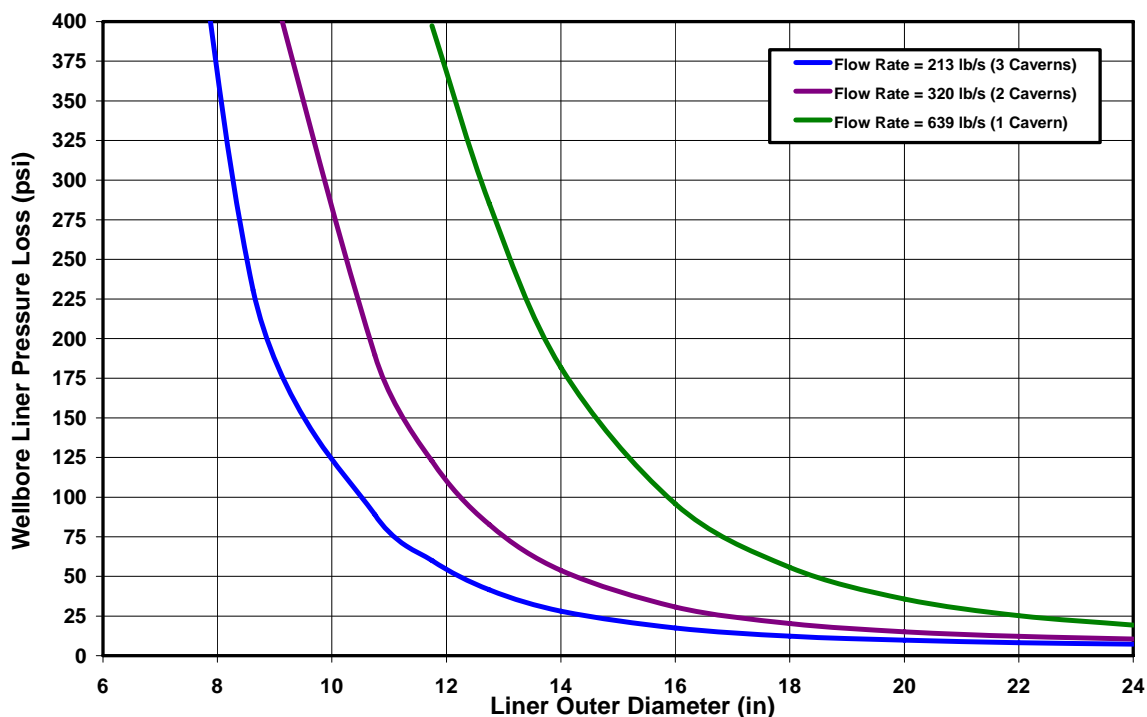


Figure 5. Calculated Wellbore Liner Pressure Losses for Various Air Flow Rates.

The storage pressure range is usually governed by cavern stability, regulation, or compressor capacity. In the case of the planned NYSEG CAES caverns, the maximum wellhead pressure of 1,500 psi is governed by the compressor capacity. The minimum pressure of 1,150 psi at the wellhead is based on preliminary cavern stability studies. The usable cavern volume of the solution-mining design is 940,000 bbls (5.3 million ft³). Assuming the air composition will be relatively constant, the main variable that will affect air storage capacity is air temperature in the cavern, which will be a function of the air injection temperature (95°F), the in situ rock temperature (estimated to be about 77°F), and the storage pressure cycle.

3.2.1 Typical Storage Cycle

To determine the storage capacity of the cavern design, a 5-year simulation was conducted in a single cavern (assuming three caverns are operating in parallel) where the flows of the typical daily cycle (Figure 1) were scaled to maintain the wellhead pressure between 1,150 psi and 1,500 psi. Because the salt around the cavern is cooled during leaching, the cavern gas temperature gradually warms with time during the 5-year simulation, as shown in Figure 6. Because of this gradual warming of the cavern, the amount of air that the cavern can hold gradually decreases with time, as shown in Figure 7. The scale factor of the flow rates of the typical daily cycle decreased from about 0.38 immediately after dewatering to 0.34 at the end of 5 years but is not expected to decrease significantly after that because thermal equilibrium is nearly reached. Thus developing three caverns similar to the cavern design should provide full capacity to operate with the typical daily cycle.

RSI-2040-11-006

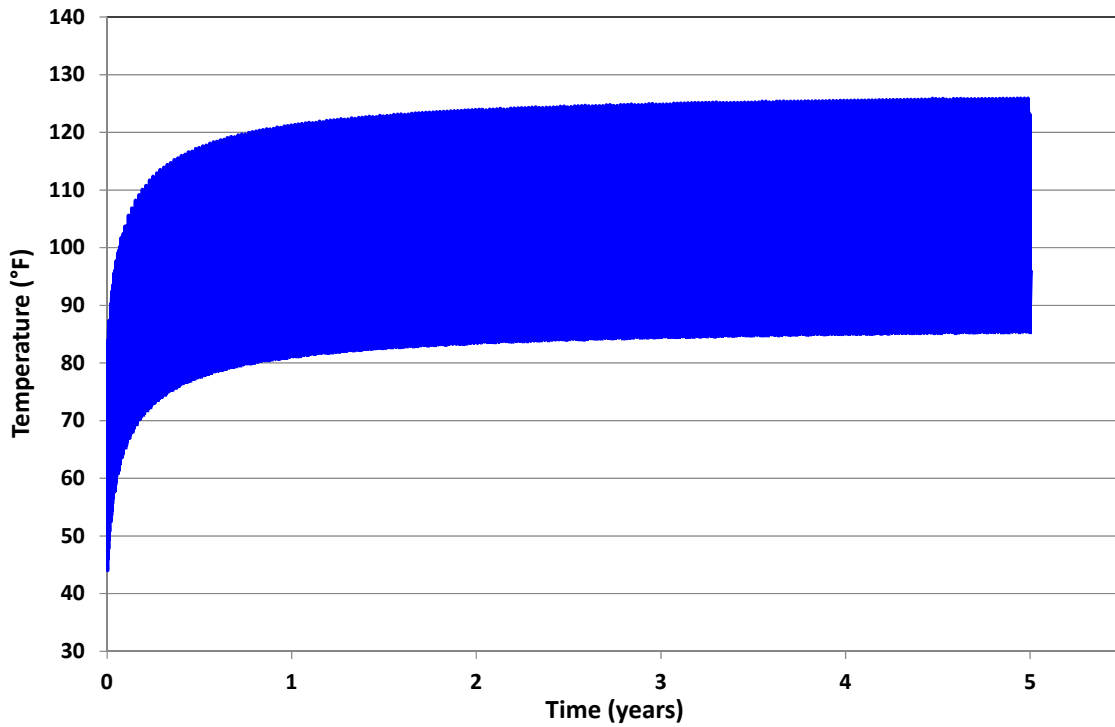


Figure 6. Cavern Air Temperature During 5-Year Simulation of Scaled Typical Daily Cycle in a Single Cavern (Assuming Three Caverns Operating in Parallel).

RSI-2040-11-007

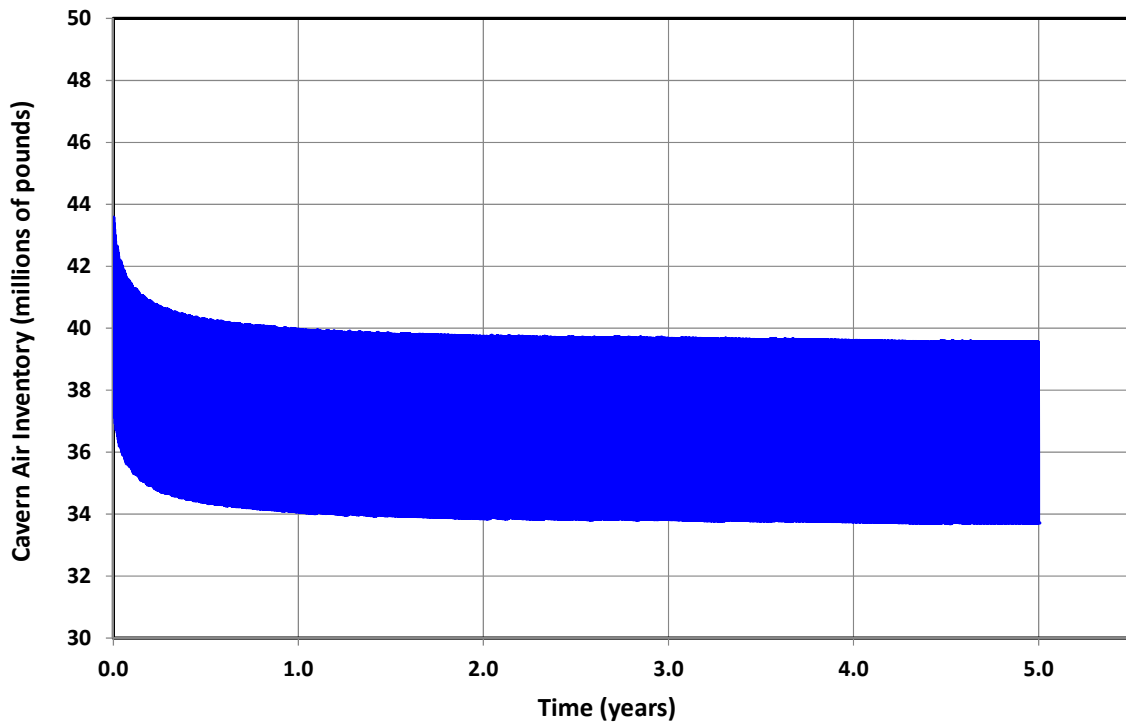


Figure 7. Cavern Air Inventory During 5-Year Simulation of Scaled Typical Daily Cycle in a Single Cavern (Assuming Three Caverns Operating in Parallel).

Figure 8 shows the wellhead and cavern pressures during a 1-week period at the end of the 5-year simulation. As shown in the figure, the cavern pressure is about 120 psi higher than the wellhead pressure. Figure 9 shows the estimated average cavern air temperature and the cavern wall temperature during this 1-week period. The average cavern air temperature is expected to vary between a minimum of 85°F and a maximum of about 126°F. Because the cavern temperature gradually warms over the weekend when there is no air flow, the highest temperature is expected after the first fill of the week. The cavern wall temperature is expected to range from about 91°F to 119°F. Figure 10 shows the estimated wellhead temperature. The wellhead temperature (shown in Figure 10) is expected to range from about 71°F at the end of the weekend to a maximum of about 101°F at the start of daily withdrawals.

Figure 11 shows the air flow rate and cavern air inventory during a 1-week period at the end of the 5-year simulation. The injection air flow rate at the beginning of the week required to pressurize to a wellhead pressure of 1,500 psi (about 211 lb/s) is slightly less than that during the rest of the week (about 217 lb/s) because of the gradual pressurization that occurs over the weekend. The withdrawal flow rates required to depressurize the wellhead pressure to 1,150 psi (about 207 lb/s) is nearly constant during the week and is about one-third of the total required withdrawal rate.

3.2.2 Operation With Partial Storage Capacity

To evaluate operations at partial storage capacity (i.e., when two caverns are in operation or when just a single cavern is in operation), the daily cycle was simplified to a single daily injection at the maximum injection rate of 639 lb/s and a single daily withdrawal at the maximum withdrawal rate of 617 lb/s. When operating with two caverns, half of these maximum flow rates were applied to each of the two caverns, and when operating with a single cavern, the full flow rates were applied to the single cavern. The durations of the flow periods were adjusted to keep the wellhead pressures below the maximum specified 1,500 psi and the cavern pressure above the minimum cavern pressure² of 1,260 psi predicted for the full power case.

The two-cavern operation simulation was conducted using a 16-inch OD liner. Figure 12 shows the air flow rate and cavern inventory for each cavern during a 1-week period of two-cavern operation. Air was injected into each cavern at a rate of 317.5 lb/s for about 4.78 hours to fill the caverns and was withdrawn at a rate of 308.5 lb/s for about 4.92 hours to bring the caverns down to minimum pressure. This results in a daily withdrawal of about 5.45 million pounds from each cavern or a total of 10.9 million pounds of air from both caverns—about 62 percent of full capacity. The pressure and temperature swings in the cavern, as shown in Figures 13 and 14, are comparable to those for the three-cavern operation. With the higher flow rates as compared to the three-cavern operation, the pressure losses in the wellbore are greater (note the peaks on the wellhead pressures in Figure 13 at the beginning and end of flow periods)

² Minimum cavern pressure is used here because it will dictate cavern stability. The higher flow rates required per cavern for the partial storage capacity cases will result in higher pressure losses in the wellbore (i.e., larger pressure differentials between the wellhead and the cavern). The maximum pressure is still limited at the wellhead as dictated by the compressor.

and filling of the cavern must be stopped prematurely to avoid exceeding 1,500 psi at the wellhead. By reducing the injection rate from 639 lb/s to 213 lb/s (while still withdrawing at RSI-2040-11-008

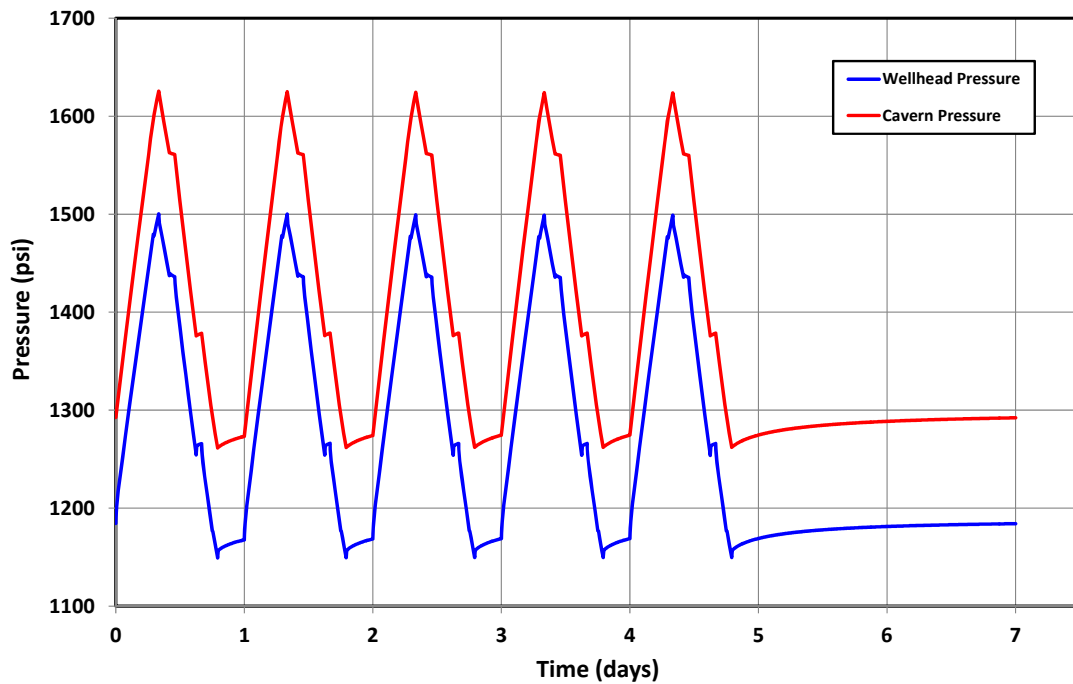


Figure 8. Wellhead and Cavern Pressure During a 1-Week Period After 5 Years of Operation of Scaled Typical Daily Cycle in a Single Cavern (Assuming Three Caverns Operating in Parallel).

RSI-2040-11-009

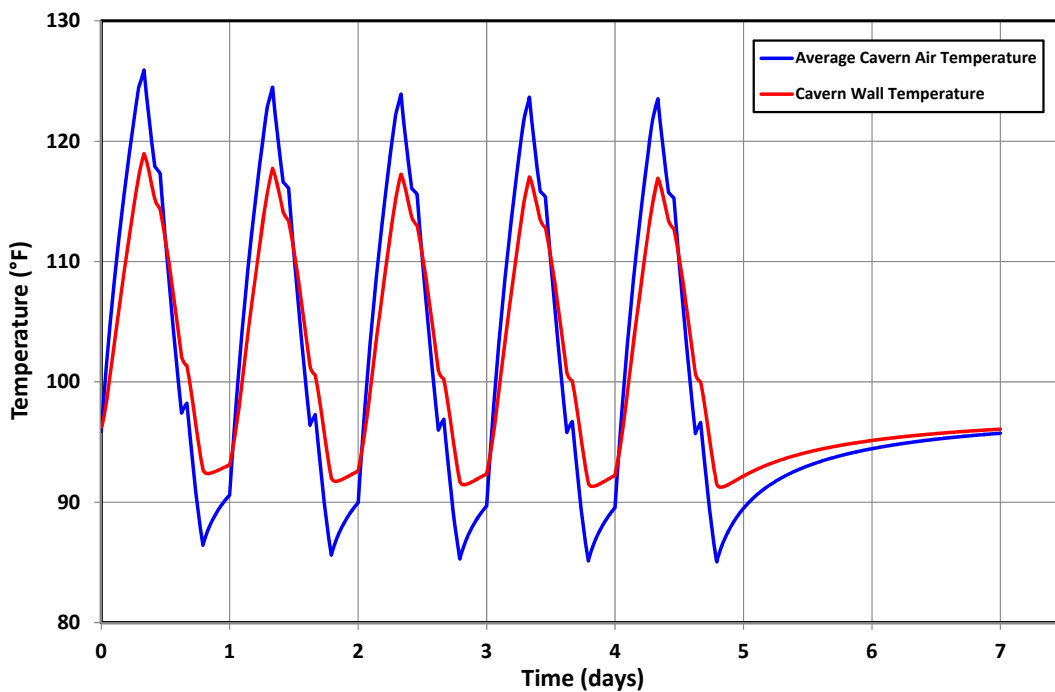


Figure 9. Average Cavern Air Temperature and Cavern Wall Temperature During 1-Week Period After 5 Years of Operations of Scaled Typical Daily Cycle in a Single Cavern (Assuming Three Caverns Operating in Parallel).

RSI-2040-11-010

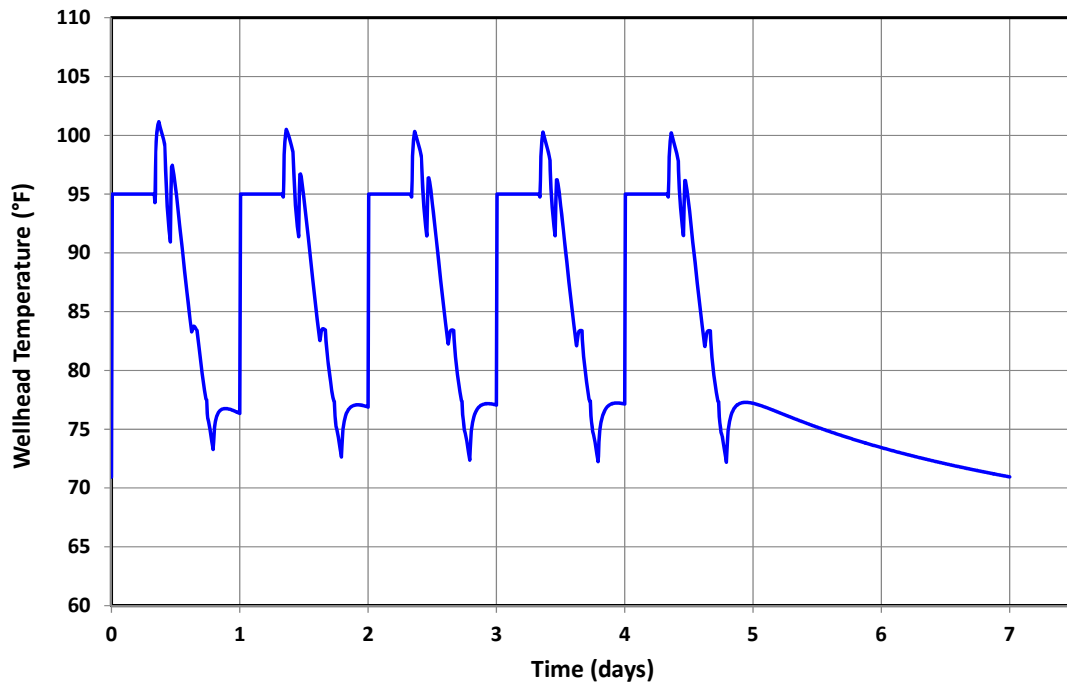


Figure 10. Air Temperature at the Wellhead During a 1-Week Period After 5 Years of Operations of Scaled Typical Daily Cycle in a Single Cavern (Assuming Three Caverns Operating in Parallel).

RSI-2040-11-011

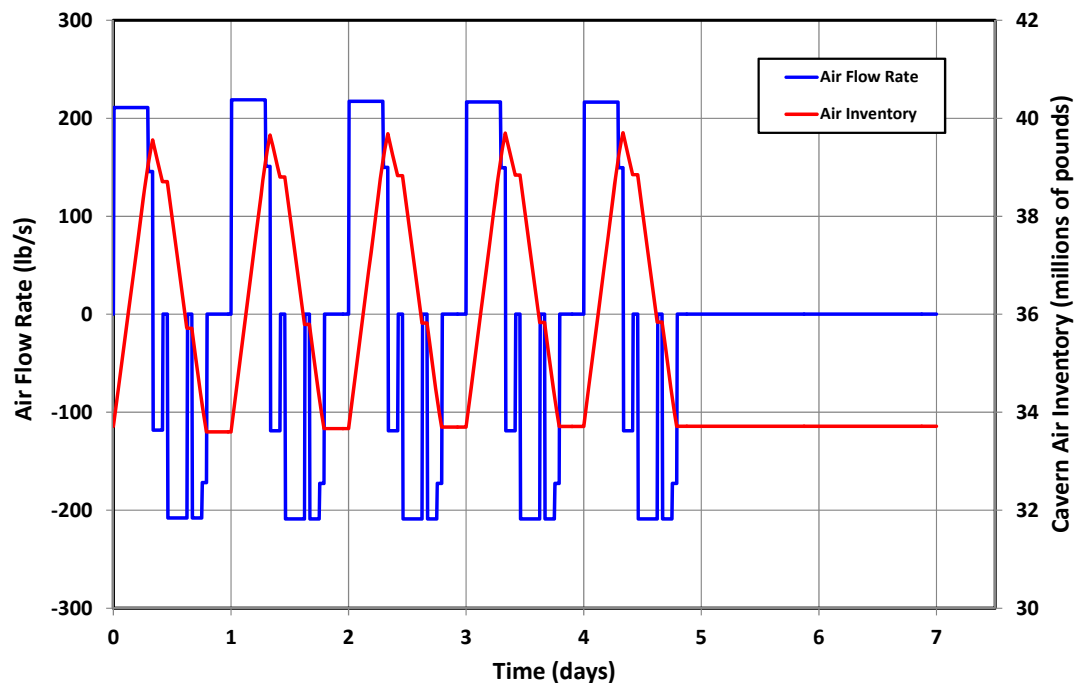


Figure 11. Air Flow Rate and Cavern Inventory of a Single Cavern (Assuming Three Caverns Operating in Parallel) During a 1-Week Period After 5 Years of Operations of Scaled Typical Daily Cycle.

RSI-2040-11-012

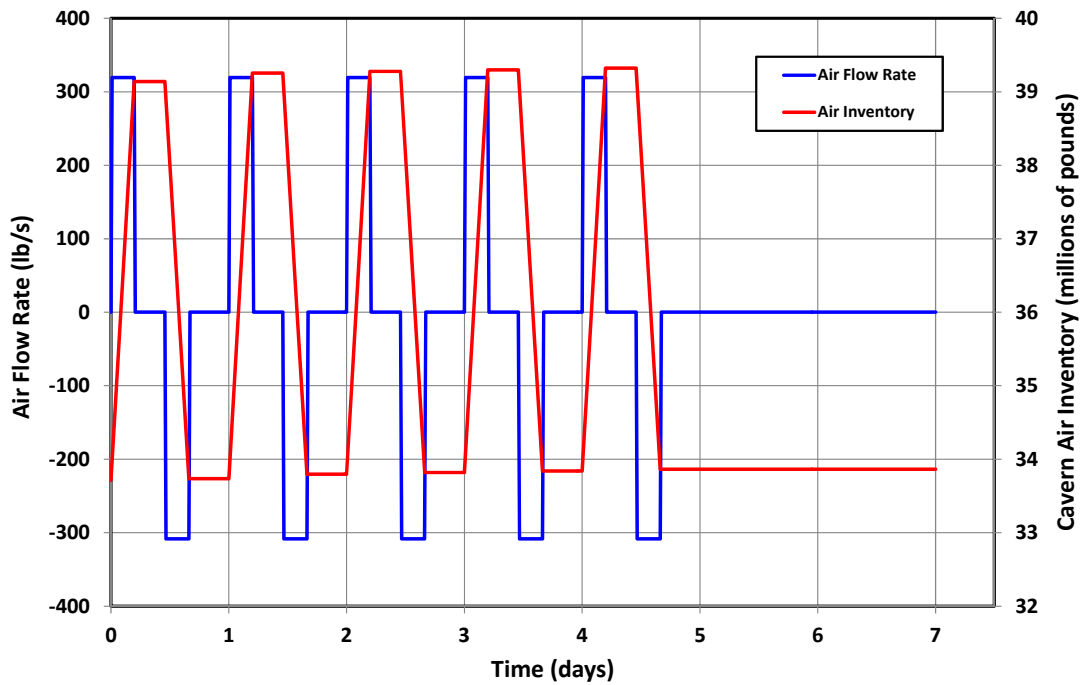


Figure 12. Air Flow Rate and Cavern Inventory for a Single Cavern During a 1-Week Period Assuming Two Caverns Operating in Parallel.

RSI-2040-11-013

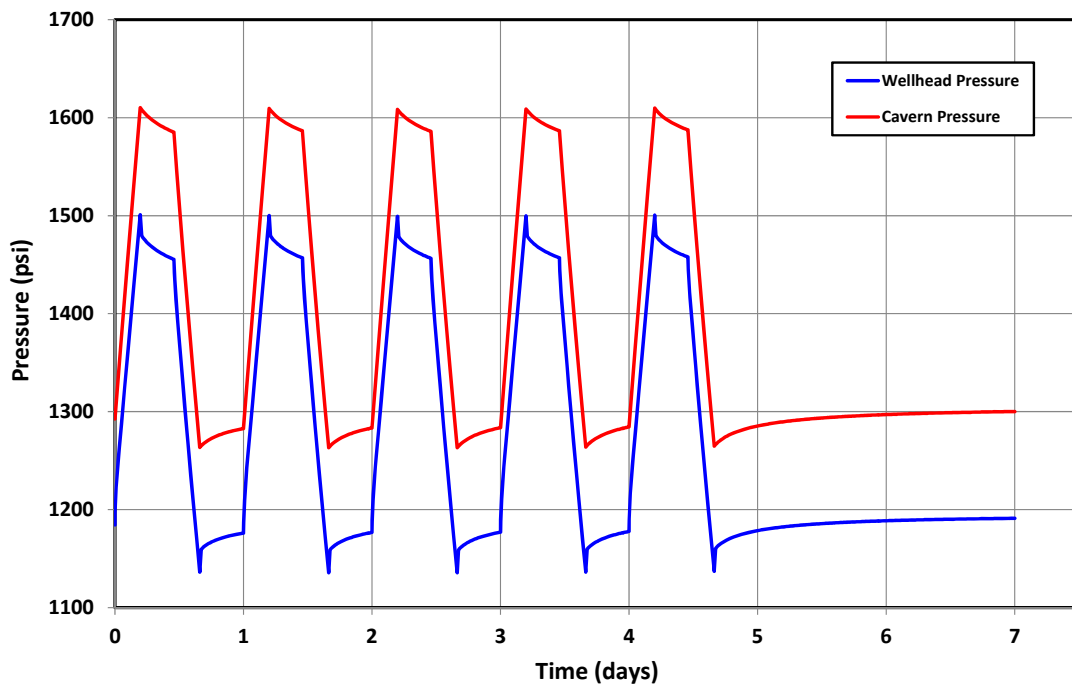


Figure 13. Wellhead and Cavern Pressure for a Single Cavern During a 1-Week Period Assuming Two Caverns Operating in Parallel.

617 lb/s), the pressure losses in the wellbore are reduced during filling; consequently, more air can be injected into the cavern before reaching the maximum wellhead pressure of 1,500 psi and the two-cavern capacity can be increased by about 5 percent.

RSI-2040-11-014

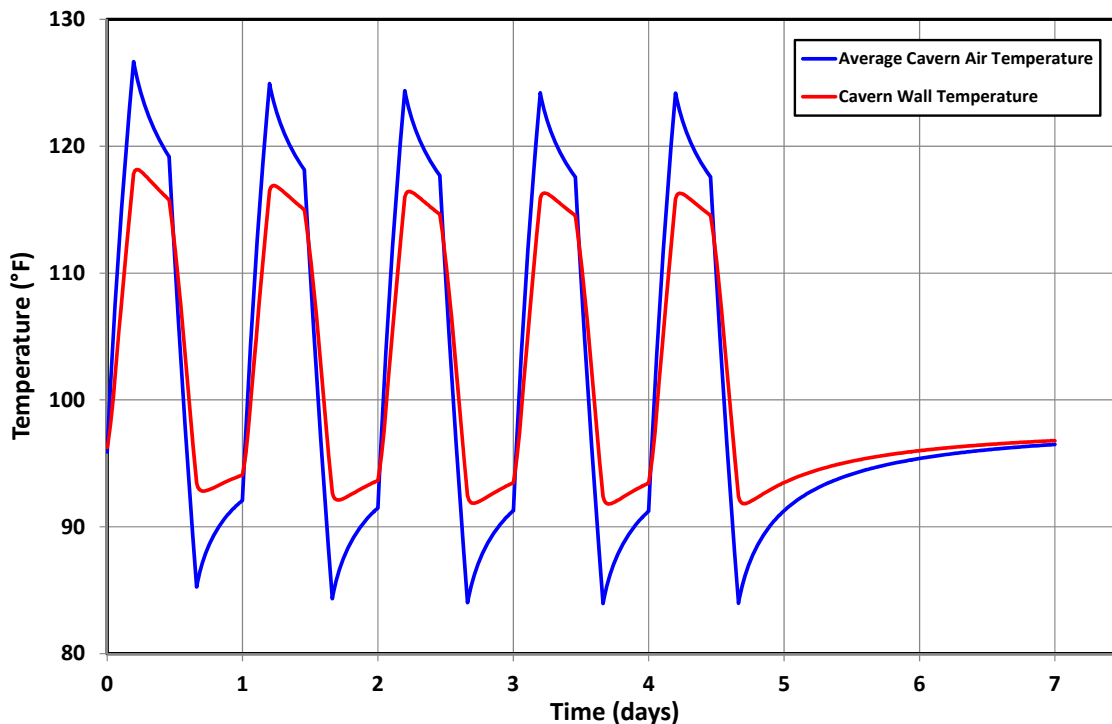


Figure 14. Average Cavern Air Temperature and Cavern Wall Temperature During a 1-Week Period Assuming Two Caverns Operating in Parallel.

The single-cavern operation simulation was conducted using a 20-inch liner. Figure 15 shows the air flow rate and cavern inventory in the single cavern during a 1-week period of single-cavern operation. Air was injected into the cavern at a rate of 639 lb/s for about 2.26 hours to fill the cavern and was withdrawn at a rate of 617 lb/s for about 2.33 hours to bring the cavern down to minimum pressure. This results in a daily withdrawal of about 5.2 million pounds of air—about 29 percent of full capacity. The pressure and temperature swings in the cavern, as shown in Figures 16 and 17, are comparable to those for the three-cavern operation. If single-cavern operation were performed with a 16-inch liner, the additional wellbore pressure losses would result in a decrease in air capacity of about 17 percent. For the 20-inch liner, the air storage capacity can be increased by about 10 percent by filling the cavern at a rate of 213 lb/s rather than 639 lb/s.

4.0 SUMMARY AND CONCLUSIONS

A study was conducted to evaluate the thermodynamic performance of the NYSEG CAES cavern design and to determine the appropriate liner sizes for the caverns. The main findings of the study include:

- Based on estimated wellbore pressure losses, it is recommended that a 20-inch liner be installed in the first cavern developed and that 16-inch liners be installed in the second and third caverns developed. This will allow interim operation (at reduced power generation) with the first and second caverns developed and allow for taking any one of the caverns off-line for maintenance after all three caverns are developed.
- The minimum wellbore liner sizes required to prevent erosion of the liner walls were less than or equal to those required to keep pressure losses at acceptable levels. Thus, the liner sizes were selected based on pressure losses, and the maximum air velocities expected (about 50 ft/s) are not expected to result in erosion of wellbore liners.
- The proposed cavern design will provide about 34 percent of the total storage capacity required for the anticipated power generation with a single cavern. Thus three caverns of this design will need to be developed to operate the typical daily cycle.
- Two-cavern operation will provide about 62 percent of full-power generation when operating at the maximum injection and withdrawal rates. This capacity can be increased by about 5 percent by reducing the injection rate from 639 lb/s to 213 lb/s.
- Single-cavern operation will provide about 29 percent of full-power generation when operating at the maximum injection and withdrawal rates. This capacity can be increased by about 10 percent by reducing the injection rate from 639 lb/s to 213 lb/s.
- The predicted conditions at minimum and maximum pressures for the three-cavern operation after 5 years are listed in Table 6.

RSI-2040-11-015

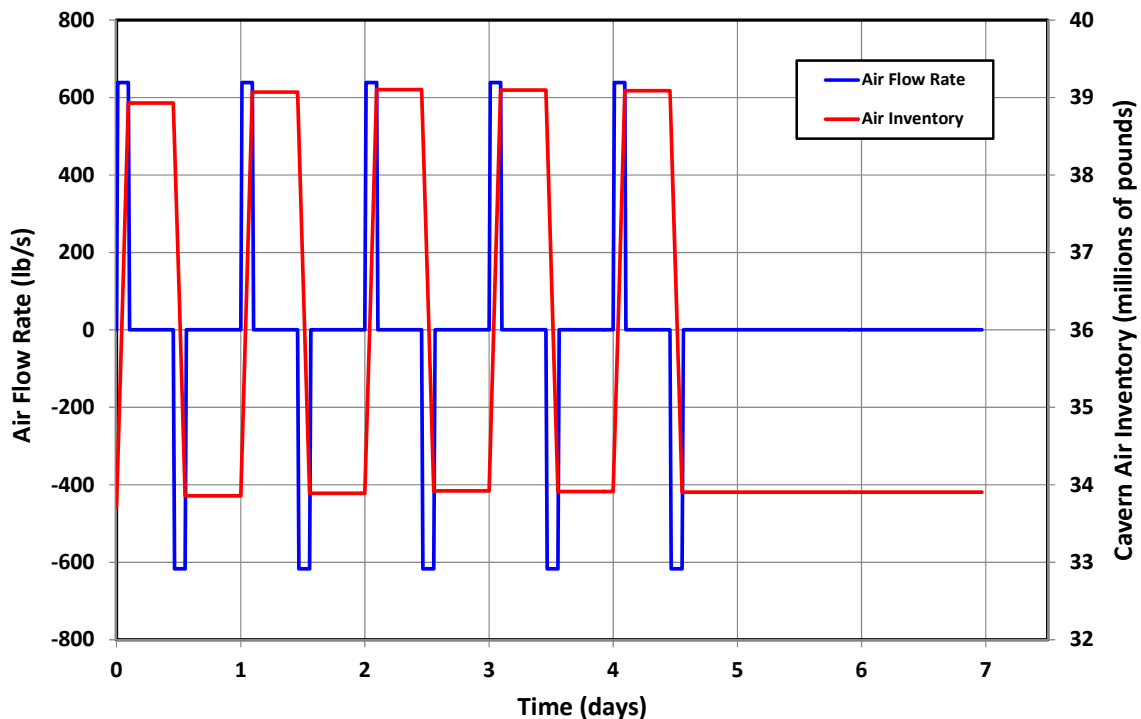


Figure 15. Air Flow Rate and Cavern Inventory During a 1-Week Period of Single-Cavern Operation.

RSI-2040-11-016

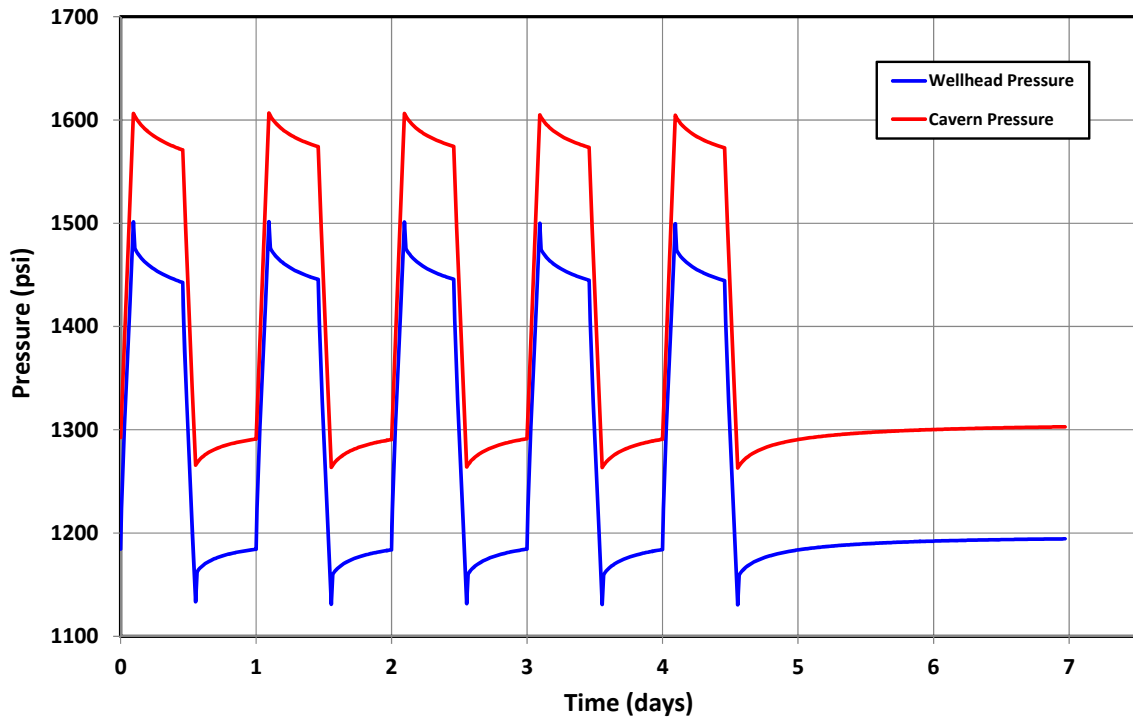


Figure 16. Wellhead and Cavern Pressure During a 1-Week Period of Single-Cavern Operation.

RSI-2040-11-017

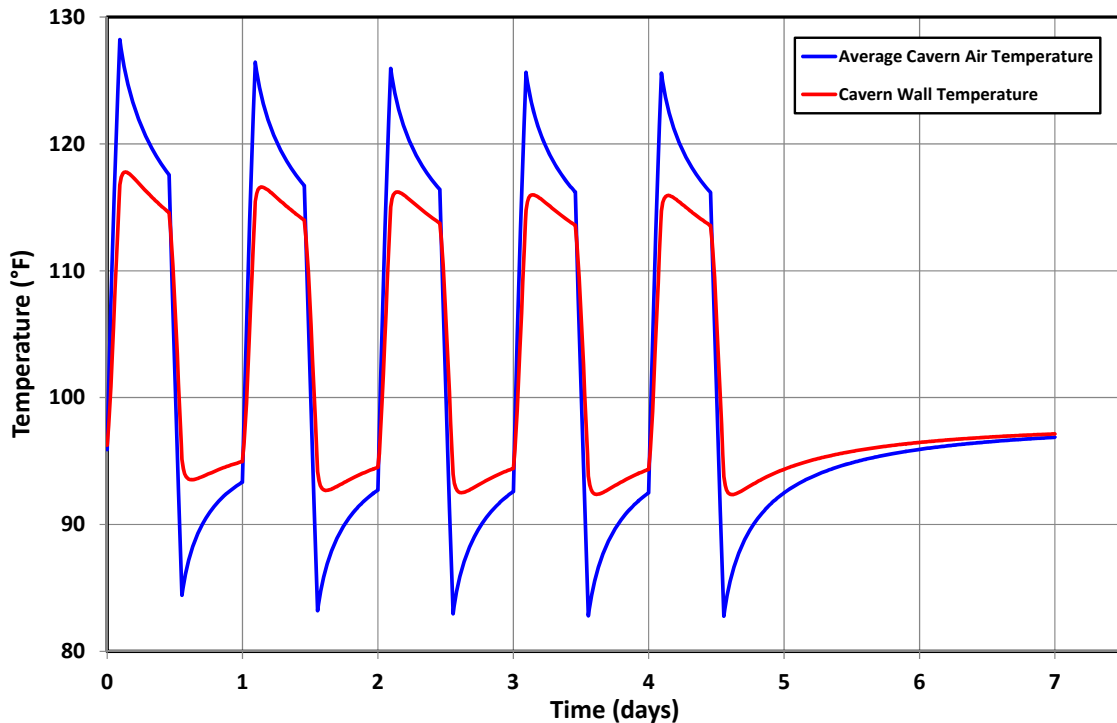


Figure 17. Average Cavern Air Temperature and Cavern Wall Temperature During a 1-Week Period of Single-Cavern Operation.

Table 6. Properties at Minimum and Maximum Pressure Conditions

Property	At Minimum Pressure	At Maximum Pressure
Wellhead Pressure	1,150 psi	1,500 psi
Cavern Pressure	1,267 psi	1,621 psi
Wellhead Temperature	71°F	101°F
Cavern Temperature	85°F	126°F
Cavern Wall Temperature	91°F	119°F

5.0 REFERENCES

American Petroleum Institute, 1991. *Recommended Practice for Design and Installation of offshore Production Platform Piping Systems*, API Recommended Practice 14E (RP 14E) Fifth Ed., American Petroleum Institute, Washington, DC, October.

Callahan, G. D., 1981. *Inelastic Thermomechanical Analysis of a Generic Bedded Salt Repository*, ONWI-125, prepared by RE/SPEC Inc., Rapid City, SD, for the Office of Nuclear Waste Isolation, Battelle Memorial Institute, Columbus, OH.

Croff, A. G., T. F. Lomenick, R. S. Lowrie, and S. H. Stow, 1985. *Evaluation of Five Sedimentary Rocks Other Than Salt for High-Level Waste Repository Siting Purposes*, prepared for Oak Ridge National Laboratory, Oak Ridge, TN.

Eyermann T. J., 2011a. *Conceptual Cavern for NYSEG Compressed Air Energy Storage at Watkins Glen, NY*, prepared by PB Energy Storage Services, Inc., Houston, TX (draft).

Eyermann T. J. 2011b. *Overview of Geology of the Area Around the US Salt Watkins Glen Refinery*, prepared for NYSEG, Binghamton, NY, by PB Energy Storage Services, Inc., Houston, TX.

Nieland, J. D., 2004. *Salt Cavern Thermal Simulator Version 2.0 User's Manual*, RSI-1760, prepared by RESPEC, Rapid City, SD, for Gas Technology Institute, Chicago, IL.

Osnes, J. D. and T. J. Eyermann, 1996. *Geomechanical Analyses of Compressed Natural Gas Storage in Gallery No. 1, Watkins Glen, New York*, RSI-0670, prepared by RE/SPEC Inc., Rapid City, SD, for PB-KBB Inc., Houston, TX.

WorleyParsons Group, Inc., 2011. Electronic communication between M. C. Holdridge, WorleyParsons Group, Inc., Reading, PA, and J. L. Ratigan, PB Energy Storage Services, Inc., Houston, TX, August 11.

JDN:krl

**GEOMECHANICAL EVALUATION OF THE
NEW YORK STATE ELECTRIC & GAS CORPORATION
COMPRESSED AIR ENERGY STORAGE CAVERN DESIGN**

Topical Report RSI-2240

prepared for

PB Energy Storage Services, Inc.
16285 Park Ten Place, Suite 400
Houston, Texas 77084

November 2011



**GEOMECHANICAL EVALUATION OF THE
NEW YORK STATE ELECTRIC & GAS CORPORATION
COMPRESSED AIR ENERGY STORAGE CAVERN DESIGN**

Topical Report RSI-2240

by

Joel D. Nieland

RESPEC

P.O. Box 725

Rapid City, South Dakota 57709

prepared for

PB Energy Storage Services, Inc.

16285 Park Ten Place, Suite 400

Houston, Texas 77084

November 2011

FOREWORD

This report addresses a proposed new cavern for Compressed Air Energy Storage (CAES) developed in the bedded salt formation at Seneca Lake, New York. The size (roof span and volume) of a solution-mined storage cavern in this geologic setting depends on the intended function of the cavern and the associated impact of the cavern pressures on the stability of the cavern. Solution-mined galleries have been developed for brine production with roof spans (along the “short” axis of the cavern) of approaching 400 feet. A natural gas storage cavern developed in the bedded salts at Seneca Lake has a maximum roof span of approximately 300 feet. The volume of these caverns depends to a large degree on the vertical extent of the solution-mining. Natural gas storage caverns necessarily require that a salt roof (that can be demonstrated to be stable) must remain in place; whereas, a solution-mined cavern for brine production need not necessarily require an intact salt roof to meet its function.

The internal cavern pressures in a brine production cavern and a natural gas storage cavern are typically significantly different—resulting in different allowable maximum cavern roof spans. The internal pressure in a brine production cavern is generally very close to about 0.52 psi/foot of depth to the cavern; whereas, the internal pressure in a natural gas storage cavern can be as little as half of that and as high as about 0.85 psi/foot of depth to the cavern.

The maximum diameter and volume of the CAES cavern and the associated minimum and maximum operating pressures evaluated in this report are not necessarily the “optimum,” as variations in cavern diameter and solution-mined (vertical) interval were not addressed in detail. Nonetheless, based on experience with other caverns at Seneca Lake operating over a range of internal cavern pressures, it is expected that an “optimum” cavern geometry is not dramatically different than the cavern geometry evaluated in this report.

Final design of the CAES caverns at Seneca Lake will depend on the in situ stress and temperature conditions and the thermomechanical properties of the salt and nonsalt rocks surrounding the proposed cavern. The in situ conditions will be best determined by open-hole logs and testing, and the salt and nonsalt rock properties will be best determined with the open-hole logging and a comprehensive laboratory testing program (see for example, Appendix B).

TABLE OF CONTENTS

1.0 INTRODUCTION	1
1.1 BACKGROUND.....	1
1.2 SCOPE AND OBJECTIVES	1
1.3 REPORT ORGANIZATION	1
2.0 PROPOSED COMPRESSED AIR ENERGY STORAGE FACILITY	2
3.0 TECHNICAL APPROACH	6
3.1 NUMERICAL MODELING	6
3.1.1 Cavern Thermodynamics Program	6
3.1.2 Heat Transfer Finite Element Program	6
3.1.3 Thermomechanical Finite Element Program	7
3.1.4 Constitutive Model for Salt	7
3.2 STRATIGRAPHY	9
3.3 MATERIAL PROPERTIES	10
3.3.1 Elastic and Thermal Properties	11
3.3.2 Creep Properties	14
3.3.3 Air Characteristics.....	15
3.3.4 Brine Characteristics.....	17
3.4 IN SITU CONDITIONS	17
3.4.1 Temperature Profile.....	17
3.4.2 In Situ Stress	19
3.5 FINITE ELEMENT MODEL	20
3.6 CRITERIA FOR EVALUATING STRUCTURAL STABILITY	23
3.6.1 Tensile Zones.....	23
3.6.2 Salt Dilation	23
3.6.3 Shear Failure Criterion for Nonsalt Strata	24
4.0 MODELING RESULTS	26
4.1 THERMAL MODELING	27
4.2 CAVERN STABILITY	31
4.3 POTENTIAL FOR HYDRAULIC FRACTURE DEVELOPMENT.....	37
4.4 CAVERN CLOSURE AND CASING STRAIN	42
5.0 SUMMARY AND CONCLUSIONS	45
6.0 REFERENCES	47
APPENDIX A. THERMODYNAMICS MEMORANDUM	A-1

TABLE OF CONTENTS
(Continued)

APPENDIX B. MECHANICAL ROCK PROPERTIES TESTS	B-1
B.1 QUASI-STATIC COMPRESSION TEST.....	B-2
B.2 CONSTANT MEAN STRESS TEST.....	B-2
B.3 BRAZILIAN INDIRECT TENSION TEST.....	B-5
B.4 CONFINED CREEP TEST	B-5

LIST OF TABLES

TABLE		PAGE
2-1	Flow Rates for Typical Daily Cycle.....	2
3-1	Stratigraphy Modeled in the NYSEG Compressed Air Energy Storage Simulations.....	10
3-2	Stratigraphy Within the Syracuse Formation	11
3-3	Elastic and Thermal Properties.....	13
3-4	Munson-Dawson Creep Parameters Used to Model Syracuse Formation Salt	15
3-5	Assumed Air Composition.....	17
3-6	Assumed In Situ Temperature Profile.....	19

LIST OF FIGURES

FIGURE	PAGE
2-1 Typical Daily Air Flow Cycle for the Compressed Air Energy Storage Facility	3
2-2 Weekly Wellhead Pressure for Typical Air Flow Cycle	3
2-3 Simulated Shape of Proposed Compressed Air Energy Storage Cavern Design	5
3-1 Measured and Predicted Axial Creep Strains for Creep Tests Performed on Salt From Well No. 58	16
3-2 Measured and Predicted Axial Creep Strains for Creep Tests Performed on Salt From Well No. 59	17
3-3 Measured and Fitted Temperatures in Well No. 59	19
3-4 Axisymmetric Finite Element Model of the NYSEG Compressed Air Energy Storage Cavern Design	22
3-5 Mohr-Coulomb Envelope for Triaxial Compression Tests on Camillus Formation Core From Well No. 59.....	25
4-1 Average Cavern Air Temperature and Cavern Wall Temperature During 30 Years of Compressed Air Energy Storage Operations	28
4-2 Temperature Contours at Various Times From Immediately Following Dewatering Through 30 Years of Compressed Air Energy Storage Operations	29
4-3 Salt Temperature as a Function of Distance From the Cavern Wall Before and After Air Withdrawal During the First Compressed Air Energy Storage Cycle and During a Cycle After 5 Years of Compressed Air Energy Storage Operations at a Depth of 2,448 Feet	30
4-4 Dilation Factor-of-Safety Contours in the Salt During the First Day of Compressed Air Energy Storage Operations	32
4-5 Dilation Factor-of-Safety Contours in the Salt During the Fourteenth Day of Compressed Air Energy Storage Operations	33
4-6 Dilation Factor-of-Safety Contours in the Salt After 5 Years of Compressed Air Energy Storage Operations.....	34
4-7 Shear Failure Factor-of-Safety Contours in the Nonsalt Units at Various Times From Immediately Following Dewatering Through 30 Years at a Wellhead Pressure of 1,150 psi (In-Plane Horizontal In Situ Stress Equals 0.95 Times the Vertical Stress, Out-of-Plane Horizontal In Situ Stress Equals 1.9 Times the Vertical Stress).....	35
4-8 Shear Failure Factor-of-Safety Contours in the Nonsalt Units at Various Times From Immediately Following Dewatering Through 30 Years at a Wellhead Pressure of 1,150 psi (In-Plane Horizontal In Situ Stress Equals 1.9 Times the Vertical Stress, Out-of-Plane Horizontal In Situ Stress Equals 0.95 Times the Vertical Stress).....	36

LIST OF FIGURES (Continued)

FIGURE	PAGE
4-9 Stresses and Temperature at the Center of the Cavern Roof During the First Week of Compressed Air Energy Storage Operations	38
4-10 Stresses and Temperature at the Center of the Cavern Roof After 5 Years of Compressed Air Energy Storage Operations	39
4-11 Maximum Principal Stress Contours (Compression Negative) Before and After First Withdrawal After Dewatering (In-Plane Horizontal In Situ Stress Equals 0.95 Times the Vertical Stress, Out-of-Plane Horizontal In Situ Stress Equals 1.9 Times the Vertical Stress)	40
4-12 Maximum Principal Stress Contours (Compression Negative) Before and After Withdrawal After 5 Years of Compressed Air Energy Storage Operations (In-Plane Horizontal In Situ Stress Equals 0.95 Times the Vertical Stress, Out-of-Plane Horizontal In Situ Stress Equals 1.9 Times the Vertical Stress).....	41
4-13 Predicted Cavern Closure Versus Time During 30 Years at a Wellhead Pressure of 1,150 psi.....	42
4-14 Predicted Vertical Casing Strain During 30 Years at a Wellhead Pressure of 1,150 psi.....	45
B-1 Schematic Illustration of (a) Confined Quasi-Static Compression Test and (b) Constant Mean Stress Test	B-3
B-2 Schematic Illustration of (a) Brazilian Indirect Tension Test and (b) Creep Test	B-4

1.0 INTRODUCTION

1.1 BACKGROUND

New York State Electric & Gas Corporation (NYSEG) is planning to develop a Compressed Air Energy Storage (CAES) plant at their facility at the southern end of Seneca Lake about 4 miles north of Watkins Glen, New York. Their plan is to develop air storage caverns in the bedded salt deposits of the Syracuse Formation at a depth of about 2,400 feet below the ground surface. RESPEC was engaged by PB Energy Storage Services, Inc. (PB ESS) to perform thermodynamic and geomechanics studies to evaluate the proposed CAES storage cavern. The results of the thermodynamic study were previously reported [Nieland, 2011] and are included in Appendix A of this report. This report presents the results of the geomechanics study that was conducted to ensure that the proposed operating conditions will not jeopardize the structural integrity of the proposed caverns.

During CAES operations, energy will be stored by compressing air into the cavern during off-peak periods when low-cost electricity is available. The compressed air will then be produced from the cavern to generate electricity during periods of peak demand. This mode of operation will likely require 250 or more injection/withdrawal cycles per year.

1.2 SCOPE AND OBJECTIVES

The scope of this study was to evaluate the proposed cavern design over the proposed storage pressure range using a typical storage cycle. The objective of this study was to perform thermo-mechanical calculations to evaluate the structural integrity of the proposed cavern design under the anticipated CAES operating conditions.

This objective was addressed in this study by numerical simulations of the proposed cavern design using software developed by RESPEC specifically for modeling excavations in salt. The assumptions associated with in situ conditions, geometric approximations, and material properties used in the models are described throughout the report.

1.3 REPORT ORGANIZATION

A description of the proposed NYSEG CAES facility is given in Chapter 2.0. Chapter 3.0 gives the technical approach used in this study, and Chapter 4.0 presents the numerical modeling results. Chapter 5.0 gives a summary of the modeling results and the study conclusions. Cited references are provided in Chapter 6.0. Appendix A contains a memorandum describing the thermodynamic analyses performed for the proposed cavern design. Appendix B contains a description of typical laboratory tests that can be conducted to determine the mechanical properties of salt and nonsalt rocks.

2.0 PROPOSED COMPRESSED AIR ENERGY STORAGE FACILITY

The proposed NYSEG CAES facility has a rated capacity between approximately 135 and 210 MW and will provide energy during peak periods in support of market needs. WorleyParsons Group, Inc. [2011] provided a typical daily air flow cycle that meets the power generation needs of the facility. The hourly flow rates for the typical cycle are listed in Table 2-1 and are shown graphically in Figure 2-1. Three caverns operating in parallel are planned for the facility. The flow rates for a single cavern are also shown in Table 2-1 and were used in this analyses to evaluate the cavern design. The cycle has air injected into the cavern during off-peak hours and air is withdrawn from the cavern to generate power during peak periods. An air injection temperature at the wellhead of 95°F is specified. The daily cycle requires a total working gas of 17.7 million pounds of air. It was assumed in this analyses that there will not be any flow during weekend hours. Figure 2-2 shows the weekly wellhead pressure for this cycle.

Table 2-1. Flow Rates for Typical Daily Cycle

Time of Day	Hours of Operation	Facility Flow Rate ^(a) (lb/s)	Single Cavern Flow Rate (lb/s)
12 a.m.–5 a.m.	5	639	217
5 a.m.–6 a.m.	1	441	150
6 a.m.–8 a.m.	2	–351	–119
8 a.m.–9 a.m.	1	0	0
9 a.m.–1 p.m.	4	–617	–210
1 p.m.–2 p.m.	1	0	0
2 p.m.–4 p.m.	2	–617	–210
4 p.m.–5 p.m.	1	–510	–173
5 p.m.–10 p.m.	5	0	0
10 p.m.–12 a.m.	2	639	217

(a) Positive values indicate injection into storage and negative values indicate withdrawal for power generation.

Preliminary geomechanical analyses determined that an operating wellhead pressure range of 1,150 psi to 1,500 psi (about 1,260 psi to 1,630 psi within the cavern) will result in a structurally stable cavern. Based on preliminary thermodynamic analyses, a cavern volume of roughly 3 million barrels (MMbbls) is required to provide the required working gas for this pressure range. The rate of cavern volume development is governed by a brine disposal rate of

RSI-2040-11-018

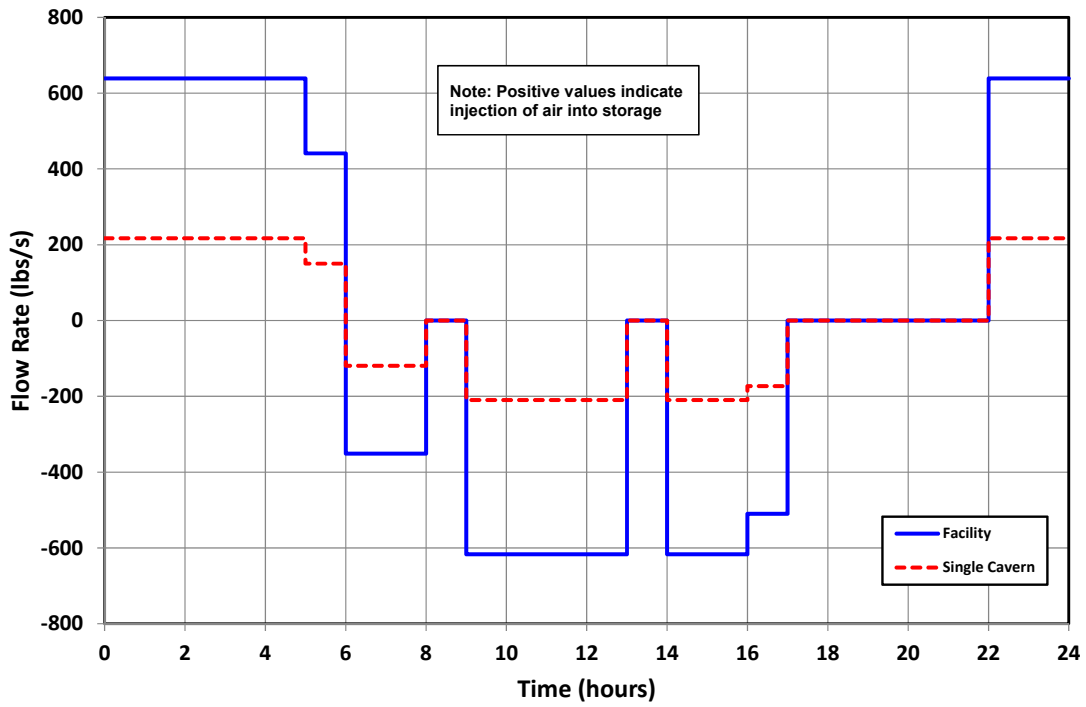


Figure 2-1. Typical Daily Air Flow Cycle for the Compressed Air Energy Storage Facility.

RSI-2040-11-019

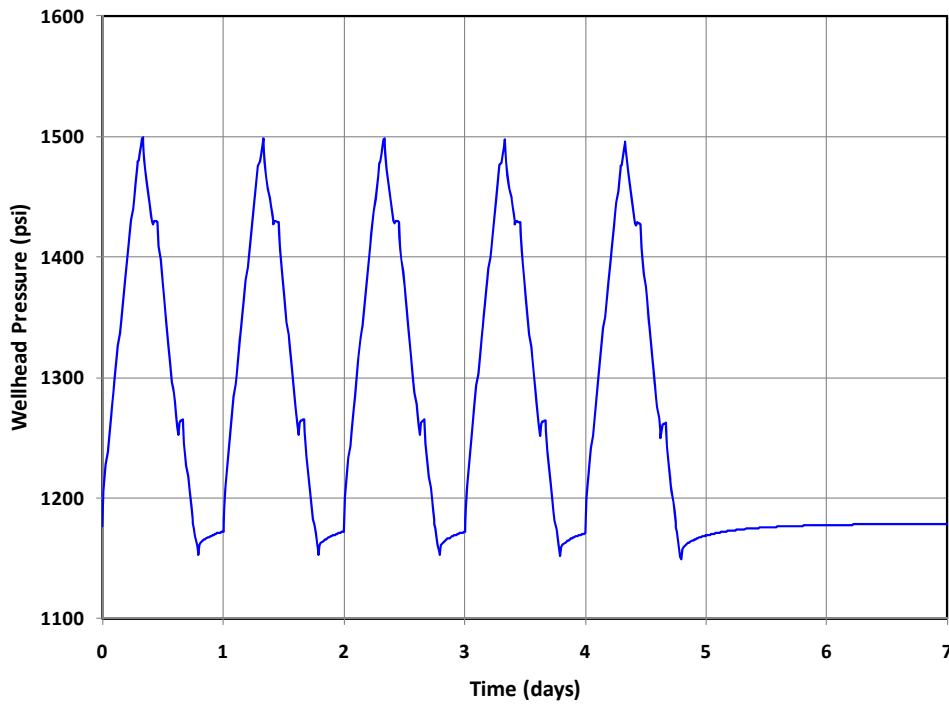


Figure 2-2. Weekly Wellhead Pressure for Typical Air Flow Cycle.

about 350 gallons per minute (gpm) and it is estimated that approximately 6 years will be required to develop a cavern volume of 3 MMbbls. Because of solution-mining limitations and also to provide partial interim operation, three caverns each having a volume of approximately 1 MMbbl will be developed.

The proposed cavern design analyzed in this study [Eyermann, 2011a] is based on solution-mining calculations performed following the preliminary analyses described above. The radius of the cavern design as a function of depth is shown in Figure 2-3. This cavern design has a mined volume of about 970,000 barrels (bbls) of which about 940,000 bbls can be dewatered and used for air storage. The roof of the cavern is at a depth of 2,402 feet (50 feet below the top of salt) and has a dewatered depth of about 2,525 feet. The casing seat is assumed to be at a depth of 2,360 feet, about 8 feet below the top of the salt¹.

¹ This selection for the casing seat depth is based on the following: (1) the casing seat needs to be set in the salt, (2) placing the casing seat too close to the cavern roof will make mechanical integrity testing difficult or impossible, and (3) increasing the distance between the cavern roof and casing seat results in a lower amount of casing strain.

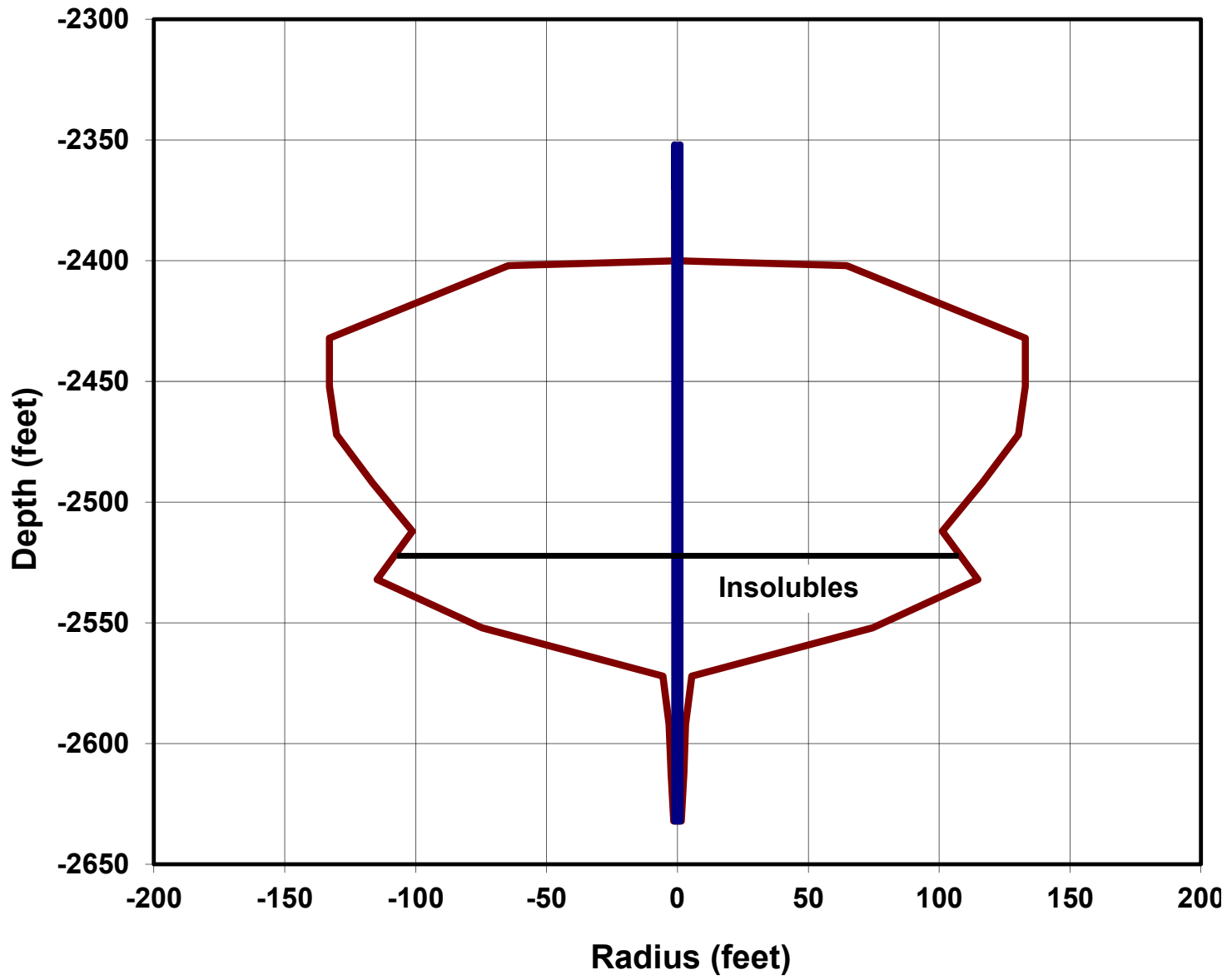


Figure 2-3. Simulated Shape of Proposed Compressed Air Energy Storage Cavern Design [Eyermann, 2011a].

3.0 TECHNICAL APPROACH

The geomechanics study was performed using numerical modeling. Thermomechanical finite element simulations of the NYSEG CAES cavern design were performed to evaluate stability of the rock surrounding and overlying the cavern and to estimate cavern closure and associated casing strain during CAES operations. The following sections describe the numerical modeling software, material properties, in situ conditions, and the finite element model used in this evaluation.

3.1 NUMERICAL MODELING

Numerical modeling software was used to model the thermodynamics and heat transfer in the cavern, the heat transfer in the salt surrounding the cavern, and the mechanical behavior of the salt surrounding the cavern. These specialized computer programs and the constitutive model used to define the viscoplastic deformation of the salt are described in the following subsections.

3.1.1 Cavern Thermodynamics Program

The Salt Cavern Thermal Simulator (SCTS) [Nieland, 2004] is a program developed by PB ESS and RESPEC for simulating the thermodynamics and heat transfer related to the storage of natural gas in underground salt caverns. It accounts for the thermal effects associated with gas compression and expansion; the mass transfer during injection and withdrawal; and the heat transfer between the gas and its surroundings, both in the wellbore and in the cavern. A modified version of SCTS that allows the simulation of air storage was used in this study.

SCTS was used to estimate the cavern temperatures during cavern development, dewatering, and throughout the simulated air storage operations. SCTS calculates a single bulk cavern temperature and a cavern wall temperature. The cavern wall temperatures as a function of time, determined from SCTS, were applied as a boundary condition to the thermal finite element model to estimate the temperature of the salt surrounding the cavern as a function of time.

3.1.2 Heat Transfer Finite Element Program

SPECTROM-41 [Svalstad, 1989] is a finite element heat transfer analysis program that was developed by RESPEC to analyze thermal problems in geologic formations. The primary transport process modeled by SPECTROM-41 is conductive heat transfer. SPECTROM-41 has the capability to model complex material properties (including temperature-dependent thermal conductivity) and boundary conditions. SPECTROM-41 was used in this study to simulate the heat transfer between the cavern and the surrounding salt. The results of these calculations were

then integrated into the thermomechanical analyses to account for the thermal stresses and strains that are a result of the temperature changes in the salt surrounding the cavern.

3.1.3 Thermomechanical Finite Element Program

SPECTROM-32 [Callahan et al., 1989] is a thermomechanical, finite element program that was developed by RESPEC for the solution of rock mechanics problems. It was designed specifically for the simulation of underground openings and structures. SPECTROM-32 not only has the capability to model the elastic-plastic response that is commonly associated with brittle rock types, but it also has the capability to simulate the viscoplastic behavior that is observed in rock salt. The features and capabilities of SPECTROM-32 that were required specifically for this investigation include:

- Option for axisymmetric geometries.
- Kinematic and traction boundary conditions.
- Munson-Dawson multimechanism constitutive model for viscoplastic behavior of salt.
- Capability to represent arbitrary in situ stress and temperature fields.
- Capability to simulate excavation operations.

3.1.4 Constitutive Model for Salt

The deformation rate of salt can be decomposed into thermal expansion, elastic deformation, and inelastic deformation. The inelastic deformation is stress-, temperature-, and rate-dependent. It is comprised of both viscoplastic (creep) and brittle components, with the viscoplastic component usually dominating in the range of stress and temperature expected in the salt surrounding the storage caverns.

Considerable research has been performed to determine a satisfactory constitutive law that characterizes the viscoplastic behavior of rock salt. The Munson-Dawson multimechanism constitutive model (M-D model) has been found to perform reasonably well in fitting data from laboratory constant-stress tests and in predicting the response of laboratory, field, and bench-scale tests performed on Avery Island salt [DeVries, 1988].

Two differential rate equations comprise the M-D model: (1) the strain-rate equations which give the viscoplastic strain rates (Equation 3-1) and (2) the evolutionary equation which gives the rate of change of an internal variable (Equation 3-2). The three-dimensional form of the M-D model is given below:

$$\dot{\epsilon}_{ij}^{vp} = \frac{\partial \sigma_e}{\partial \sigma_{ij}} F \dot{\epsilon}_s \quad (3-1)$$

$$\dot{\zeta} = (F - 1)\dot{\varepsilon}_s \quad (3-2)$$

where:

$$\dot{\varepsilon}_s = \sum_{i=1}^3 \dot{\varepsilon}_{s_i} \quad (3-3)$$

$$\dot{\varepsilon}_{s_i} = \text{steady-state strain rate for mechanism } i \quad (3-4)$$

$$\dot{\varepsilon}_{s_1} = A_1 \exp(-Q_1/RT)(\sigma_e/\mu)^{n_1} \quad (3-5)$$

$$\dot{\varepsilon}_{s_2} = A_2 \exp(-Q_2/RT)(\sigma_e/\mu)^{n_2} \quad (3-6)$$

$$\dot{\varepsilon}_{s_3} = [B_1 \exp(-Q_1/RT) + B_2 \exp(-Q_2/RT)] \cdot \sinh[q(\sigma_e - \sigma_o)/\mu] H(\sigma_e - \sigma_o) \quad (3-7)$$

$$F = \begin{cases} \exp\left[\Delta\left(1 - \frac{\zeta}{\varepsilon_t^*}\right)^2\right] & \text{for } \zeta < \varepsilon_t^* \\ 1 & \text{for } \zeta = \varepsilon_t^* \\ \exp\left[-\delta\left(1 - \frac{\zeta}{\varepsilon_t^*}\right)^2\right] & \text{for } \zeta > \varepsilon_t^* \end{cases} \quad (3-8)$$

$$\varepsilon_t^* = K_o \exp(cT)(\sigma_e/\mu)^m \quad (3-9)$$

$$\Delta = \alpha + \beta \log(\sigma_e/\mu) \quad (3-10)$$

and

$\dot{\varepsilon}_{ij}^{vp}$ = viscoplastic strain-rate tensor

$\sigma_e = \sqrt{3J_2}$ (effective stress)

$J_2 = \frac{1}{2} s_{ij} s_{ji}$

$s_{ij} = \sigma_{ij} - \delta_{ij} \sigma_m$ (deviatoric stress tensor)

$\sigma_m = \frac{1}{3} \sigma_{kk}$ (mean stress)

σ_{ij} = stress tensor

δ_{ij} = Kronecker delta

ζ = internal variable

T = absolute temperature

$H(x)$ = Heaviside function

$\mu = 1.7985(10^6)$ a normalizing constant

$A_1, A_2, B_1, B_2, Q_1/R,$

$Q_2/R, n_1, n_2, q, \sigma_o,$

$\delta, K_o, c, m, \alpha, \beta$ = experimentally determined parameters.

As indicated by Equation 3-3, the steady-state creep rate ($\dot{\epsilon}_s$) based on the M-D model is composed of three terms. Each term is associated with a different creep mechanism. The first and third mechanisms ($\dot{\epsilon}_{s_1}$ and $\dot{\epsilon}_{s_3}$) are dislocation climb and dislocation glide, respectively, and the second mechanism ($\dot{\epsilon}_{s_2}$) is referred to as the undefined mechanism. The undefined mechanism is well characterized but is not defined in a sense of classical dislocation motion. The relative contribution of each mechanism to the steady-state creep rate strongly depends on the effective stress and temperature.

When pressure conditions in a cavern are changed, the transient nature of the M-D model can be an important factor in the response of the cavern. According to Equation 3-1, the steady-state creep rate is multiplied by a transient factor (F) to obtain the viscoplastic strain rate. The value of the transient factor depends on whether the internal variable (ζ) is less than, equal to, or greater than the transient strain limit (ϵ_t^*), which is a function of the effective stress and temperature. When $\zeta < \epsilon_t^*$, the viscoplastic strain rate is greater than the steady-state creep rate ($F > 1$). This is the work-hardening branch of the M-D model. The work-hardening branch is commonly associated with an increase in loading, such as when a cavern is excavated or when the cavern pressure is decreased. When $\zeta > \epsilon_t^*$, the viscoplastic strain rate is less than the steady-state creep rate ($F < 1$). This is the recovery branch of the M-D model. This branch is commonly associated with a decrease in loading, such as when the cavern pressure is increased. Through the evolutionary equation, the value of the internal variable is always approaching the transient strain limit. In turn, the viscoplastic strain rate is always approaching the steady-state creep rate (i.e., F approaches unity as ζ approaches ϵ_t^*).

The Munson-Dawson model has 16 parameters that must be determined experimentally or estimated empirically. The parameter values used to represent the salt surrounding the NYSEG CAES caverns are presented in Section 3.3.2.

3.2 STRATIGRAPHY

The stratigraphy modeled in the NYSEG CAES simulations is based on the local stratigraphy described by Eyermann [2011b]. Eyermann estimates the thickness of the entire Syracuse Formation to be 850 feet and calls out the salt and nonsalt units in the F Unit (the upper 450 feet in the Syracuse Formation). The lower portion of the Syracuse Formation was modeled as salt, and the units below the Syracuse Formation were simply defined as

“Underlying Groups” and modeled as shale. Because these lower units are so distant from the region of interest around the cavern, their individual thicknesses and properties should not have a significant effect in the simulation results. The densities for each of the units are based on a density log conducted in Well No. 59 [Osnes and Eyermann, 1996]. The complete stratigraphic column modeled is listed in Table 3-1, and the salt and nonsalt layers modeled within the Syracuse Formation are listed in Table 3-2.

Table 3-1. Stratigraphy Modeled in the NYSEG Compressed Air Energy Storage Simulations

Unit-Lithology	Top Depth (ft)	Bottom Depth (ft)	Thickness (ft)
Genesee-Shale	0	830	830
Tully-Limestone	830	847	17
Hamilton-Shale	847	1,768	921
Marcellus-Shale	1,768	1,866	98
Onondaga-Limestone	1,866	1,911	45
Tristates Group-Sandstone	1,911	1,948	37
Oriskany-Sandstone	1,948	1,956	8
Helderberg Group-Limestone	1,956	2,106	150
Cobleskill/Akron-Dolostone	2,106	2,166	60
Bertie-Dolostone	2,166	2,255	89
Camillus-Shale	2,255	2,352	97
Syracuse-Salt/Nonsalt	2,352	3,202	850
Underlying Groups	3,202	—	—

3.3 MATERIAL PROPERTIES

Of the geologic units listed in Table 3-1, only the Syracuse Formation contains significant thicknesses of salt. The nonsalt units are assumed to deform elastically and are further assumed not to yield or fail in shear in response to the CAES operations. This assumption is subsequently checked in the geomechanical analyses by calculating factors of safety against shear failure. The material properties used in the simulations are described in the following sections.

Table 3-2. Stratigraphy Within the Syracuse Formation

Lithology	Top Depth (ft)	Bottom Depth (ft)	Thickness (ft)
Salt	2,352	2,361	9
Shale	2,361	2,363	2
Salt	2,363	2,415	52
Shale	2,415	2,418	3
Salt	2,418	2,433	15
Shale	2,433	2,441	8
Salt	2,441	2,454	13
Shale	2,454	2,462	8
Salt	2,462	2,466	4
Dolomite	2,466	2,469	3
Salt	2,469	2,477	8
Shale	2,477	2,482	5
Salt	2,482	2,534	52
Dolomite/Shale	2,534	2,567	33
Salt	2,567	2,618	51
Shale/Dolomite	2,618	2,651	33
Salt	2,651	2,675	24
Shale	2,675	2,708	33
Salt	2,708	2,743	35
Shale	2,743	2,750	7
Salt	2,750	2,795	45
Shale	2,795	2,802	7
Salt	2,802	3,202	400

3.3.1 Elastic and Thermal Properties

Table 3-3 lists the elastic and thermal properties used to represent the rock in the numerical models. Densities for the rock units are based on a density log conducted in Well No. 59 [Osnes

and Eyermann, 1996]. The elastic properties of the Camillus Formation and the salt from the

Table 3-3. Elastic and Thermal Properties

Unit-Lithology	Young's Modulus (psi)	Poisson's Ratio	Density (lb/ft³)	Coefficient of Thermal Expansion (°F⁻¹)	Thermal Conductivity (Btu/(hr-ft-°F))	Specific Heat (Btu/lb-°F)
Genesee-Shale	2.93×10^6	0.242	164	4.39×10^{-6}	0.804	0.190
Tully-Limestone	6.30×10^6	0.242	167	11.1×10^{-6}	1.775	0.123
Hamilton-Shale	3.11×10^6	0.242	165	4.39×10^{-6}	0.804	0.190
Marcellus-Shale	3.11×10^6	0.242	165	4.39×10^{-6}	0.804	0.190
Onondaga-Limestone	5.22×10^6	0.242	164	11.1×10^{-6}	1.775	0.123
Tristates Group-Sandstone	4.75×10^6	0.242	167	5.56×10^{-6}	1.966	0.170
Oriskany-Sandstone	4.75×10^6	0.242	167	5.56×10^{-6}	1.966	0.170
Helderberg Group-Limestone	7.47×10^6	0.242	168	11.1×10^{-6}	1.775	0.123
Cobleskill/Akron-Dolostone	7.20×10^6	0.242	169	11.1×10^{-6}	1.775	0.123
Bertie-Dolostone	7.03×10^6	0.242	175	11.1×10^{-6}	1.775	0.123
Camillus-Shale	5.02×10^6	0.242	170	4.39×10^{-6}	0.804	0.190
Syracuse-Salt	3.61×10^6	0.242	130	21.6×10^{-6}	3.000	0.200
Syracuse-Nonsalt	5.02×10^6	0.242	170	4.39×10^{-6}	0.804	0.190
Underlying Groups	5.02×10^6	0.242	170	4.39×10^{-6}	0.804	0.190

Syracuse Formation are based on laboratory testing of core recovered from Well No. 58 (salt only) and Well No. 59 [Pfeifle, 1996]. The elastic properties of the units above the Camillus Formation are based on sonic velocity logs of Well No. 59 [Osnes and Eyermann, 1996]. The elastic properties of the nonsalt units within the Syracuse Formation and underlying units were assumed to be the same as those for the Camillus Formation. Published values of the elastic properties of rock in and below the Vernon Formation [Carmichael, 1982] indicate these are reasonable assumptions. Because no testing has been conducted to determine thermal properties of the rock units, typical thermal and thermoelastic properties [Croff et al., 1985; Callahan, 1981; Senseny et al., 1992] for shale, sandstone, carbonates (limestone and dolomite), and salt were assigned to the units.

3.3.2 Creep Properties

The Munson-Dawson constitutive model parameters that were used to model the viscoplastic (creep) behavior of the Syracuse salt in this study were determined by fitting the model to creep tests conducted on salt from the Syracuse Formation in the Watkins Glen cavern field [Pfeifle, 1996]. Three tests were conducted on salt core obtained from Well No. 58 and three on salt core from Well No. 59. All of the creep tests were performed at a temperature of 86°F. The three tests from each well were run at stress differences (the axial stress minus confining pressure) of 1,000 psi, 2,000 psi, and 3,000 psi.

Although a set of parameters for the Munson-Dawson constitutive model was previously determined using these creep tests [Osnes and Eyermann, 1996], our increased experience in both parameter fitting and use of the Munson-Dawson model warranted refitting the data. Because of the limited number of creep tests, not all of the Munson-Dawson model parameters could be uniquely determined. Several Munson-Dawson model parameter values were assumed to be the same as those determined from an extensive study of eight Gulf Coast domal salts [Munson, 1998]. Munson classified the creep of domal salt as forming two distinct groups, either soft or hard, where the difference is roughly a factor of seven in the leading coefficients for each of the three deformation mechanisms (and thus the steady-state creep rate) between the two groups. The ratio of the leading coefficients to those of the soft salt provided by Munson were determined for Syracuse salt. Additionally, the transient parameters K_0 , m , α , and β were determined. The parameters were estimated through the use of a nonlinear least-squares fitting procedure.

The resulting Munson-Dawson parameter values used for Syracuse salt are shown in Table 3-4. The creep test data for Well No. 58 and Well No. 59 and the fits predicted using these estimated Munson-Dawson parameter values are shown in Figures 3-1 and 3-2, respectively. These figures indicate that the Munson-Dawson model with the fitted parameters adequately characterizes the creep behavior of the Syracuse salt.

Table 3-4. Munson-Dawson Creep Parameters Used to Model Syracuse Formation Salt

Parameters	Units	Value	Basis for Value
A_1	day ⁻¹	7.69(10 ²⁷)	Syracuse Salt
A_2	day ⁻¹	8.87(10 ¹⁷)	Syracuse Salt
B_1	day ⁻¹	5.58(10 ¹¹)	Syracuse Salt
B_2	day ⁻¹	2,780	Syracuse Salt
Q_1/R	R	22,700	Munson [1998]
Q_2/R	R	9,060	Munson [1998]
n_1	—	5.5	Munson [1998]
n_2	—	5.0	Munson [1998]
q	—	5,340	Munson [1998]
σ_o	psi	2,980	Munson [1998]
K_o	—	8,090	Syracuse Salt
m	—	2.43	Syracuse Salt
c	—	0.00511	Munson [1998]
α	—	-14.6	Syracuse Salt
β	—	-8.82	Syracuse Salt
δ	—	0.580	Munson [1998]

3.3.3 Air Characteristics

Air is modeled in SCTS as a real gas using the American Gas Association’s Detail Characterization Method as described by Starling and Savidge [1994]. The air composition used in the SCTS simulations is listed in Table 3-5.

In addition to the constituents listed above, the air in the cavern will likely contain a small amount of water vapor. However, the effects of the water vapor are expected to be extremely small and were not included in this study. Cavern air pressure was applied in the finite element model with tractions (applied pressure boundary conditions) on the cavern surface. A linear pressure gradient was assumed for the air in the cavern and is based on the casing seat pressures and cavern air densities estimated by SCTS.

RSI-2040-11-021

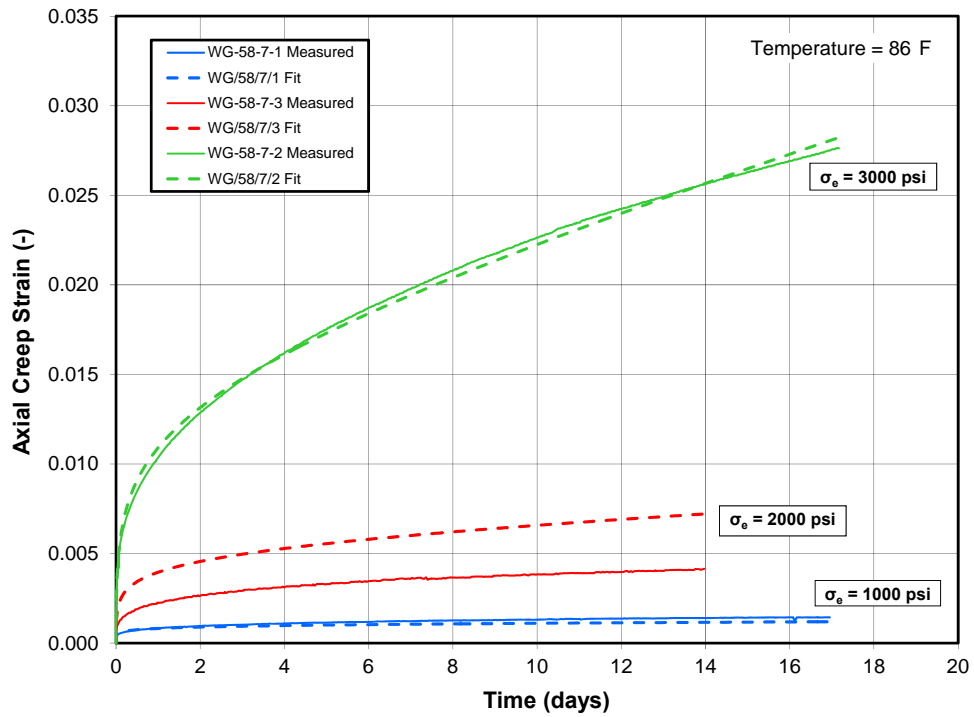


Figure 3-1. Measured and Predicted Axial Creep Strains for Creep Tests Performed on Salt From Well No. 58.

RSI-2040-11-022

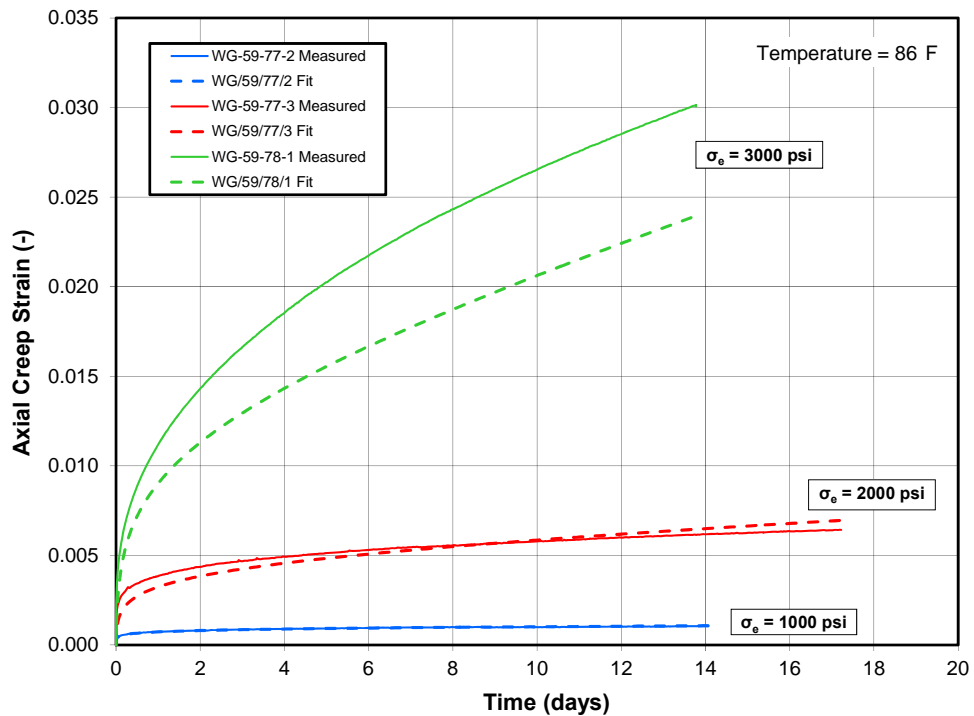


Figure 3-2. Measured and Predicted Axial Creep Strains for Creep Tests Performed on Salt From Well No. 59.

Table 3-5. Assumed Air Composition

Gas Component	Mole Percent
Nitrogen	78.0
Oxygen	21.0
Argon	1.0

3.3.4 Brine Characteristics

Brine pressure was applied in the finite element model with tractions on the cavern surface. Because of the very small compressibility of brine (approximately 1.9×10^{-6} /psi), the increase in brine density associated with the hydrostatic pressure increase over the height of a cavern is negligible (about 0.1 percent change per 1,000 feet). Consequently, the brine density was assumed to remain a constant 75 pcf, resulting in a vertical pressure gradient of 0.52 psi/foot.

In the simulations performed here, the cavern was dewatered to a depth of 2,525 feet. The thermal properties of the brine and insolubles modeled in the bottom portion of the cavern were assigned typical values for brine (specific heat = 0.76 BTU/lb_m-°F, thermal conductivity = 0.35 BTU/hr-ft-°F).

3.4 IN SITU CONDITIONS

Since the creep rate of salt is dependent on temperature and stress, it is important to model temperatures and stresses which are representative of those in the vicinity of the CAES storage cavern. The following two subsections describe the in situ temperature and stress distributions assumed in this analysis.

3.4.1 Temperature Profile

The initial in situ temperature assumed in this study is based on temperature logs conducted during mechanical integrity testing of Well No. 59 in May 1996. Figure 3-3 shows the measurements from the three temperature logs conducted and the fitted temperature profile. Because of the elevation difference between Well No. 59 (about 540 feet above mean sea level (amsl)) and the proposed CAES site location (about 1,000 feet amsl), the temperature gradient in the upper portion of Well No. 59 was projected upward an additional 460 feet to obtain the estimated surface temperature of 45.6°F at the CAES location. The entire temperature profile assumed for the CAES site is defined in Table 3-6. Based on this profile, the estimated in situ temperature of the rock at the midheight of the cavern is about 77°F.

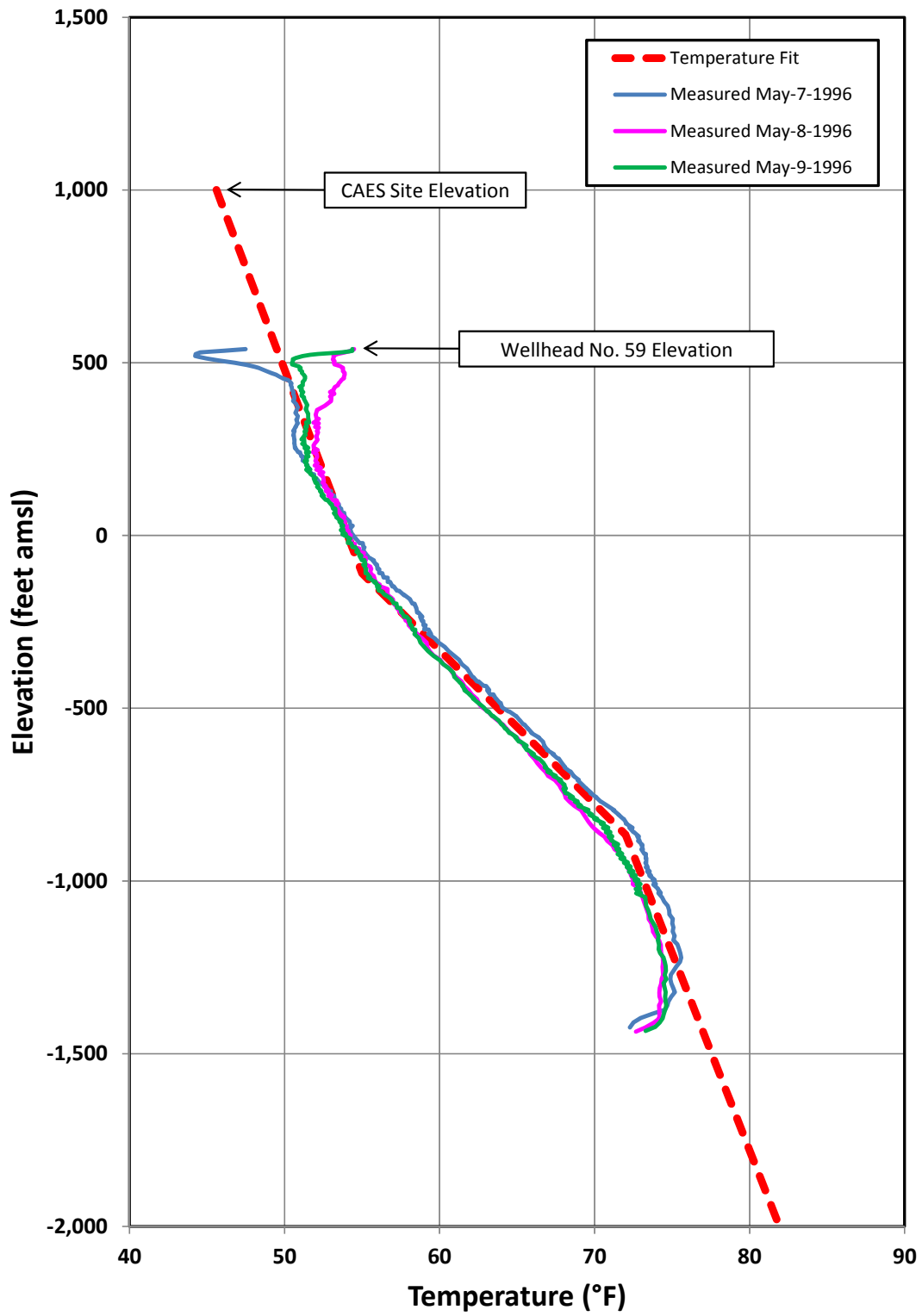


Figure 3-3. Measured and Fitted Temperatures in Well No. 59.
Table 3-6. Assumed In Situ Temperature Profile

Surface Temperature = 45.6°F		
CAES Site Depth Range (ft)	Elevation Range (ft amsl)	Temperature Gradient (°F/ft)
0 to 1,110	1,000 to -110	0.0085
1,110 to 1,866	-110 to -866	0.0225
Below 1,866	Below -866	0.0088

3.4.2 In Situ Stress

Principal in situ stresses are generally assumed to be aligned with an axis system that is vertical and horizontal. The magnitude of the vertical principal stress is typically assumed to be equal to the weight of the overburden. This assumption was made in the geomechanical analysis of the NYSEG CAES cavern design using the thicknesses (Tables 3-1 and 3-2) and densities (Table 3-3) of the geologic units in the stratigraphic model. In salt deposits, it is generally accepted that the horizontal components of in situ stress are nominally equal to the vertical component (i.e., the stress state is isotropic) because any differences between the horizontal and vertical components introduce shear stress components that are relieved by creep over geologic time frames. Consequently, it is reasonable to assume that the horizontal components of in situ stress in the Syracuse salt units are equal to the vertical stress determined by the weight of the overlying units.

In nonsalt rock that does not creep appreciably even over geologic time frames, differences between the two principal components of horizontal stress and the vertical stress can be sustained, and the in situ stress state is not necessarily isotropic. The inequality of the principal stresses in most regions is reflected in the regional faulting. The faulting in western New York State suggests that the in situ stresses are not equal in magnitude in the nonsalt strata. A literature review performed in the 1996 study of Gallery No. 1 revealed that the in situ stress state in western New York State is one in which the principal stress components are not equal [Osnes and Eyermann, 1996]. The two principal horizontal stresses are different from the vertical stress and are also different from each other. Based on regional stress measurements, it appears likely that the minimum horizontal stress at the Watkins Glen site is slightly lower than the vertical stress, with a ratio of about 0.95. Based on the same regional measurements, the maximum horizontal stress would be about 1.9 times the vertical stress.

The in situ stress state used in the 1996 modeling of Gallery No. 1 was adopted for this study. Because an axisymmetric model was used in this analysis, it was necessary to conduct each of the simulations twice to evaluate the anisotropic stress state. First, the simulations

were with the in-plane horizontal stresses in the nonsalt units at 1.9 times the vertical stress and the tangential or out-of-plane horizontal stresses in the nonsalt units at 0.95 times the vertical stress. The simulations were then repeated with the in-plane horizontal stresses in the nonsalt units at 0.95 times the vertical stress and the out-of-plane horizontal stresses in the nonsalt units at 1.9 times the vertical. The horizontal stresses in the salt units were assumed to be equal to the vertical stress in all simulations.

3.5 FINITE ELEMENT MODEL

Figure 3-4 shows the axisymmetric finite element model of the cavern used in the NYSEG CAES simulations. The modeled cavern radii as a function of depth were estimated by placing a smoothed curve through the estimated solution-mining geometry provided by Eyermann [2011a]. The small sump below a depth of 2,572 feet will have no impact on cavern stability and was not included in the model. The region immediately outside the walls of the cavern is very finely subdivided. This extremely fine subdivision was used to accurately represent the high stress and temperature gradients that were anticipated near the cavern periphery. The extents of the model were selected to isolate the response of the cavern from the influences of the radial and bottom boundaries which are artificial truncations of the actual horizontal and vertical extents of the stratigraphy.

In simulating CAES operations, the cavern was dewatered to a depth of 2,525 feet. The elements below this level (dark blue elements in Figure 3-4) represent the brine and insolubles left in the cavern after dewatering and were represented as brine in the simulations.

During heat transfer simulations, the outer boundaries of the model are insulated, and thus, no heat is transferred across these boundaries. The cavern wall temperature histories from the SCTS simulations were applied to the cavern boundary in the finite element model to calculate temperatures in the salt surrounding the cavern for each of the simulations in SPECTROM-41. These temporal temperature distributions were subsequently used in the thermomechanical simulations to account for thermal stresses.

During thermomechanical simulations, the kinematic boundary conditions specified along the sides of the axisymmetric model were:

- No radial displacement along the centerline.
- No radial displacement along the outer radius.
- No vertical displacement along the bottom surface.

The upper surface of the model is free to move in the vertical direction.

In the thermomechanical simulations, after excavation of the salt, normal tractions are specified along the surfaces of the cavern to simulate the fluid and air pressure inside the

cavern. The magnitudes of these tractions are equal to the hydrostatic pressure based on the

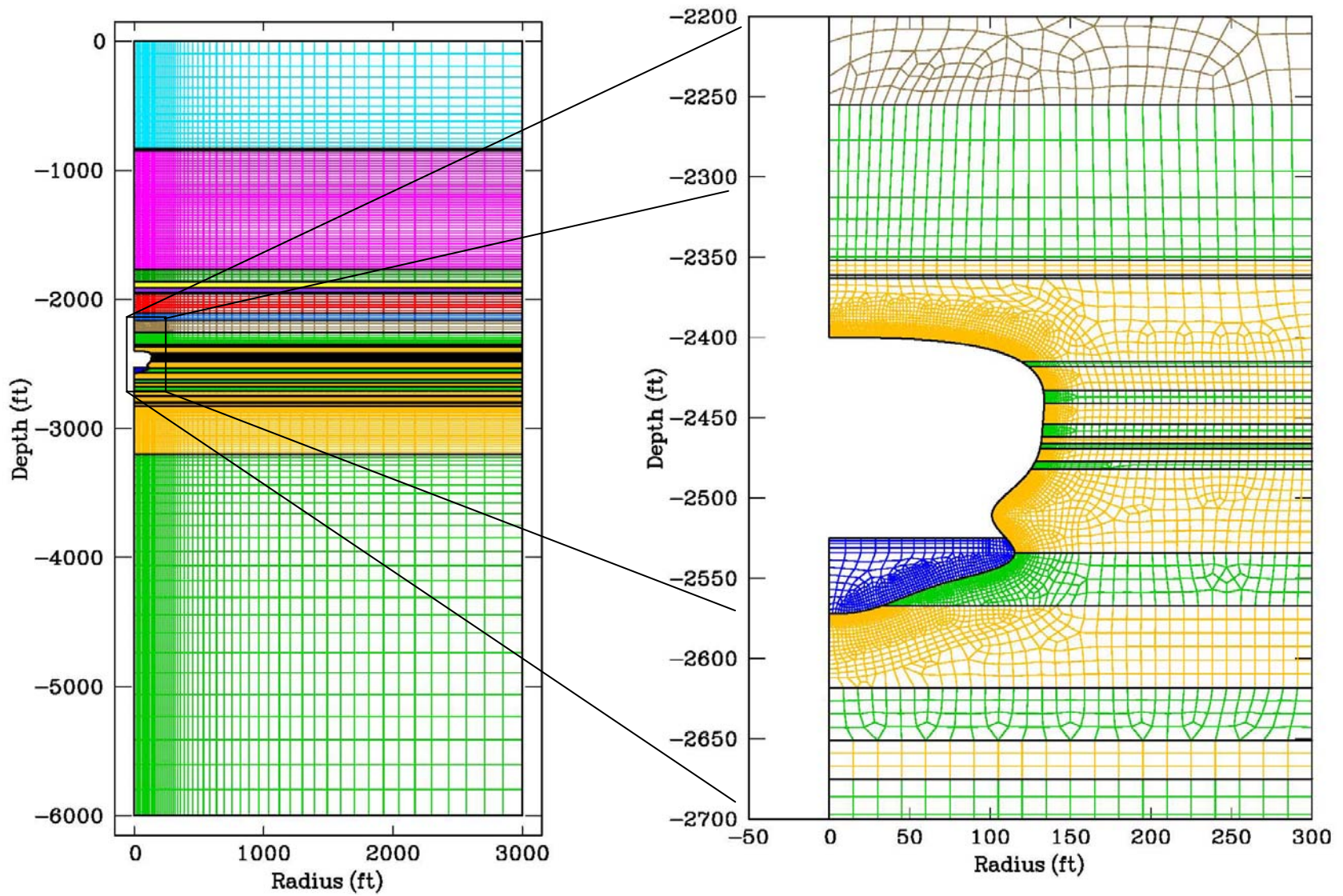


Figure 3-4. Axisymmetric Finite Element Model of the NYSEG Compressed Air Energy Storage Cavern Design.

density of brine during the solution-mining portion of the simulation and based on the respective casing seat pressure and the average air density during the CAES portion of the simulations.

3.6 CRITERIA FOR EVALUATING STRUCTURAL STABILITY

Cavern stability was evaluated by examining the stress states in the salt surrounding the cavern. Stress states that result in extensive salt dilation in the upper portion of the cavern can lead to spalling of the roof and/or walls of the cavern and subsequent damage to the casing seat or well. Tensile stresses around the cavern periphery that may result from temperature fluctuations in the cavern can also result in spalling of the salt. Thus the anticipated CAES operating cycles were evaluated and a minimum pressure was determined to ensure that no tensile zones or extensive regions of salt dilation occur.

3.6.1 Tensile Zones

Geologic materials are much stronger in compression than in tension. The unconfined compressive strength of most rocks is generally about ten times greater than the tensile strength. Therefore, tensile stresses in rocks surrounding storage caverns are to be avoided whenever possible through appropriate design of the cavern or through specification of operating pressures.

Laboratory testing of salt core from Wells No. 58 and No. 59 indicates the tensile strength of the bedded salts in the region is as high or higher than many other bedded salts. The average tensile strength of the salt is 205 psi and 328 psi for the core from wells No. 58 and No. 59, respectively [Pfeifle, 1996]. Laboratory testing of Camillus Formation core from Well No. 59 indicates that the tensile strength of this geologic unit, which overlies the roof of the proposed CAES cavern, is variable with an average value of 1,149 psi [Pfeifle, 1996] and ranges from 729 psi to 1,530 psi. The material models used in this analysis do not provide for tensile failure. Postprocessing of the modeling results was used to determine whether or not tensile stresses and fracturing have occurred.

3.6.2 Salt Dilation

The viscoplastic deformation of salt is isovolumetric, which means that the volume of the salt remains constant during creep deformation. An increase in salt volume, a phenomenon referred to as dilation, indicates the formation of microfractures within the salt. A criterion used to determine whether or not a stress state is one that results in salt dilation has been previously developed based on laboratory testing of Avery Island domal salt and Waste Isolation Pilot Plant (WIPP) bedded salt [Van Sambeek et al., 1993]. Two stress measures are used in defining the dilation criterion: the first invariant of the stress tensor (I_1) and the second invariant of the deviatoric stress tensor (J_2). These two stress measures are defined as follows:

$$I_1 = \sigma_1 + \sigma_2 + \sigma_3 \quad (3-11)$$

$$J_2 = \frac{1}{6} \left[(\sigma_1 - \sigma_2)^2 + (\sigma_2 - \sigma_3)^2 + (\sigma_3 - \sigma_1)^2 \right] \quad (3-12)$$

where:

$\sigma_1, \sigma_2, \sigma_3$ = principal stress components.

Van Sambeek et al. [1993] concluded that stress states satisfying the following inequality generally did not result in dilation of salt test specimens:

$$\sqrt{J_2} \leq 0.27 I_1 \quad (3-13)$$

The testing to determine the dilation properties of Syracuse salt included six multistage creep tests and five constant mean stress tests (eleven individual specimens) on salt core from Well No. 58 and Well No. 59 [Pfeifle, 1996]. Osnes and Eyer mann [1996] concluded that based on these tests, Syracuse salt exhibits a dilation limit similar to that described by Equation 3-13.

The above criterion is based on triaxial compression testing of salt. Like all other rocks, salt is known to be weaker in triaxial extension than in triaxial compression. The stress state in the salt surrounding a cavern varies between triaxial compression and triaxial extension. As the cavern pressure is lowered, the stresses move closer to triaxial extension. To account for extensile stress states, the dilation limit described above was reduced conservatively to:

$$\sqrt{J_2} \leq 0.18 I_1 \quad (3-14)$$

Factors of safety were used to quantify the potential for dilation in the salt around the proposed CAES cavern design. The factor of safety (at constant I_1) is defined as:

$$\text{Factor of Safety} = \frac{0.18 I_1}{\sqrt{J_2}} \quad (3-15)$$

3.6.3 Shear Failure Criterion for Nonsalt Strata

The criterion used to determine whether or not a stress state is one that results in shear failure of the nonsalt strata is based on laboratory testing of Camillus Formation core from Well No. 59 [Pfeifle, 1996]. Six constant strain rate tests, each on an individual specimen, were performed. In these tests, the confining pressure is held constant at nominally 0, 500, or 1,000 psi while an axial strain rate of 10^{-4} s^{-1} is imposed until the specimen fails.

The Mohr-Coulomb failure criterion has been shown to adequately predict shear failure in brittle (nonsalt) rock types. The Mohr-Coulomb failure envelope is represented in shear (τ)

versus normal (σ_n) stress space by Equation 3-16 and is described by two parameters, the cohesion (S_0) and friction angle (ϕ). The Mohr-Coulomb failure criterion simply states that if the shear stress along any plane in the rock exceeds the shear strength along that same plane, failure will occur. The Mohr-Coulomb failure envelope is defined as:

$$\tau = S_0 + \sigma_n \tan \phi \quad (3-16)$$

Plotted in Figure 3-5 are the Mohr's circles for each of the tests at their failure point along with the fitted Mohr-Coulomb failure envelope. The resulting parameters for the failure envelope are a cohesion (S_0) of 735 psi and a friction angle (ϕ) of 59.0 degrees. Factors of safety were then used to quantify the potential for shear failure in the nonsalt strata, which is defined as the ratio between the shear strength, τ , as defined by Equation 3-16 above, divided by the actual shear stress. Failure is expected to occur when the factor of safety is less than 1.

RSI-2040-11-025

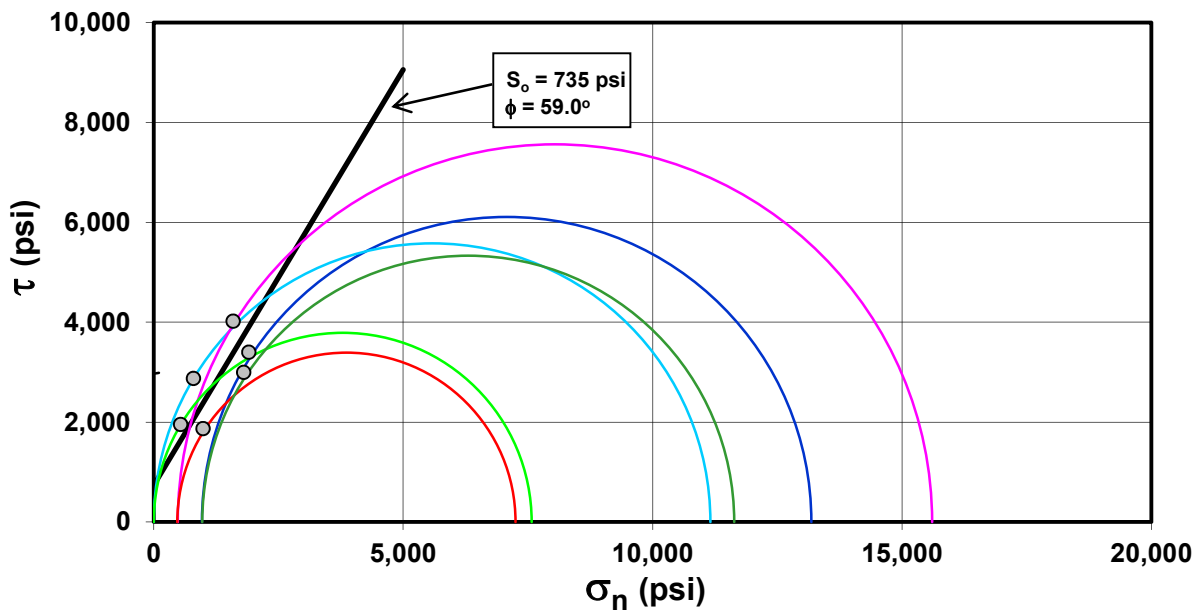


Figure 3-5. Mohr-Coulomb Envelope for Triaxial Compression Tests on Camillus Formation Core From Well No. 59.

4.0 MODELING RESULTS

Thermal and thermomechanical finite element simulations were conducted to evaluate the cavern design during CAES operations. Long-term simulations of a single cavern were conducted using the typical weekly CAES pressure cycle shown in Figure 2-2 with an air injection temperature of 95°F. The cavern wall temperature versus time obtained from the thermodynamic simulations (see Appendix A) was used as a boundary condition in the thermal finite element simulations to estimate the temperature distribution around the cavern as a function of time. These temporal temperature distributions were then used in the thermomechanical finite element simulations along with the daily pressure cycle to evaluate cavern stability and estimate cavern closure during CAES operations.

The stability of a solution-mined cavern is dependent upon the state of stress in the salt surrounding the cavern. The stress state around a cavern is used to determine the structural stability of the cavern roof and walls. The stress state in the salt around the cavern is dependent on (1) the original in situ state of stress, (2) the fluid pressure in the cavern, (3) cavern geometry, (4) salt creep, and (5) temperature changes in the salt. Because salt has a relatively high coefficient of thermal expansion, temperature changes in the salt can have a significant effect on stresses surrounding the cavern during air injection and withdrawal.

In all of the thermomechanical finite element simulations of the CAES cavern design, the cavern was instantaneously excavated and allowed to creep for 2 years under a brine pressure gradient (0.52 psi/foot) with a wellhead pressure of 30 psi. This pressure condition is representative of the pressure the cavern will experience during its development. After 2 years at brine pressure conditions, dewatering of the cavern with air was simulated. The stress and temperature conditions at the end of dewatering are the starting conditions for the simulations used in evaluating cavern stability. The simulations performed to evaluate cavern stability include:

- A single 30-year thermal simulation to estimate the thermal response of the rock surrounding the cavern. To make this simulation, SCTS was used to estimate the cavern wall temperature as a function of time while repeating the typical CAES cycle for 30 years. The cavern wall temperature as a function of time was used as a boundary condition on the cavern surface in the thermal model. The thermal response of this simulation was used in all of the thermomechanical simulations.
- A 5-year thermomechanical simulation of the typical CAES cycle. This model was used to evaluate the potential for salt dilation and to evaluate the potential for hydraulic fracture development.
- A 30-year thermomechanical simulation with the cavern at the minimum wellhead pressure of 1,150 psi. Maintaining the pressure at the minimum pressure provides a

conservative estimate of the creep closure that the cavern will experience. In turn, it also provides conservative estimates of all factors affected by creep closure, including shear failure of the nonsalt units and of casing strain.

As discussed in Section 3.4.2, all of the thermomechanical simulations were conducted with two scenarios for the in situ stress in the nonsalt units. The following sections presents the results of the models.

4.1 THERMAL MODELING

Figure 4-1 shows the average cavern air temperature and cavern wall temperature as a function of time during 30 years of cycling predicted with SCTS. As seen in the figure, the cavern temperatures increase significantly during the first couple of years, then only very gradually increases throughout the 30-year simulation. The predicted cavern wall temperature as a function of time was used as a boundary condition on the cavern surface in the thermal finite element simulation to predict temperatures in the rock surrounding the cavern as a function of time.

The rock surrounding the CAES cavern is expected to experience both short-term and long-term temperature changes. Figure 4-1 shows the long-term thermal changes expected in the rock around the cavern. During cavern development, a large volume of rock around the cavern will gradually cool because the assumed freshwater injection temperature of 52°F is cooler than the in situ rock temperature at the cavern elevation (77°F) and because the dissolution of salt is an endothermic process. The contours at a time of 0 years in Figure 4-2 show the temperatures expected at the end of dewatering. During CAES operations, air is injected at the wellhead at a temperature of 95°F and enters the cavern at around 105°F because of compression and friction in the wellbore. Continuous cycling with this injection temperature will gradually warm the rock around the cavern to temperatures well above the in situ rock temperature.

The daily injection and withdrawal of air from the cavern will also result in short-term temperature changes in the rock very near the cavern surface. Figure 4-3 shows the salt temperature as a function of radial distance from the cavern wall at a depth of 2,448 feet at minimum and maximum pressure for the first cycle after dewatering and for a cycle after 5 years of cycling. Note that although the magnitudes of the temperature profiles are higher after 5 years of cycling, the temperature changes that occur between minimum and maximum pressure are nearly the same. The temperature difference between minimum and maximum pressure is about 25°F at the cavern wall. The temperature changes between about 0.75 foot and 5 feet from the wall are less than 5°F over a single daily cycle. Temperature fluctuations related to the daily cycle are nearly nonexistent beyond a distance of 5 feet from the cavern wall.

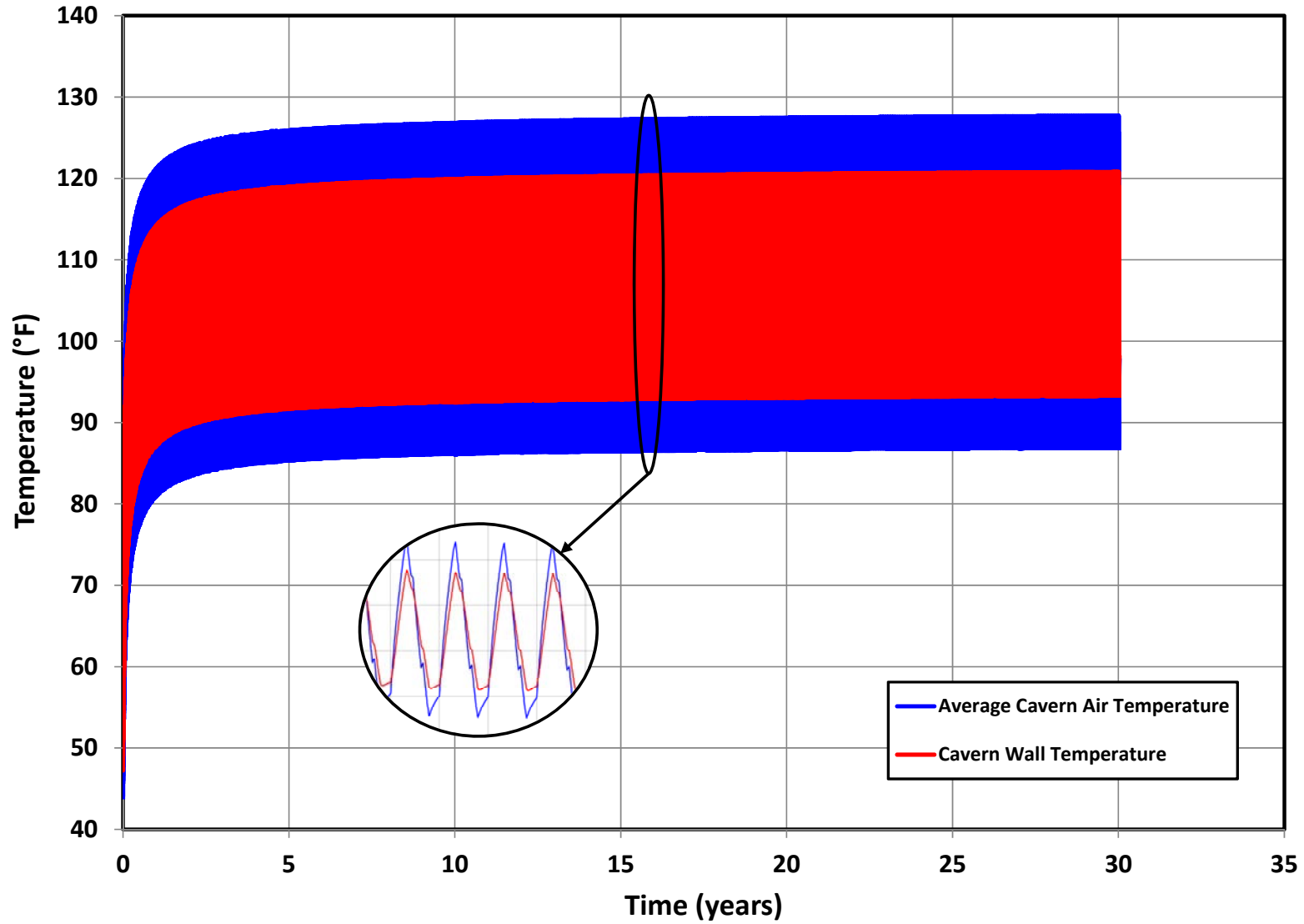


Figure 4-1. Average Cavern Air Temperature and Cavern Wall Temperature During 30 Years of Compressed Air Energy Storage Operations.

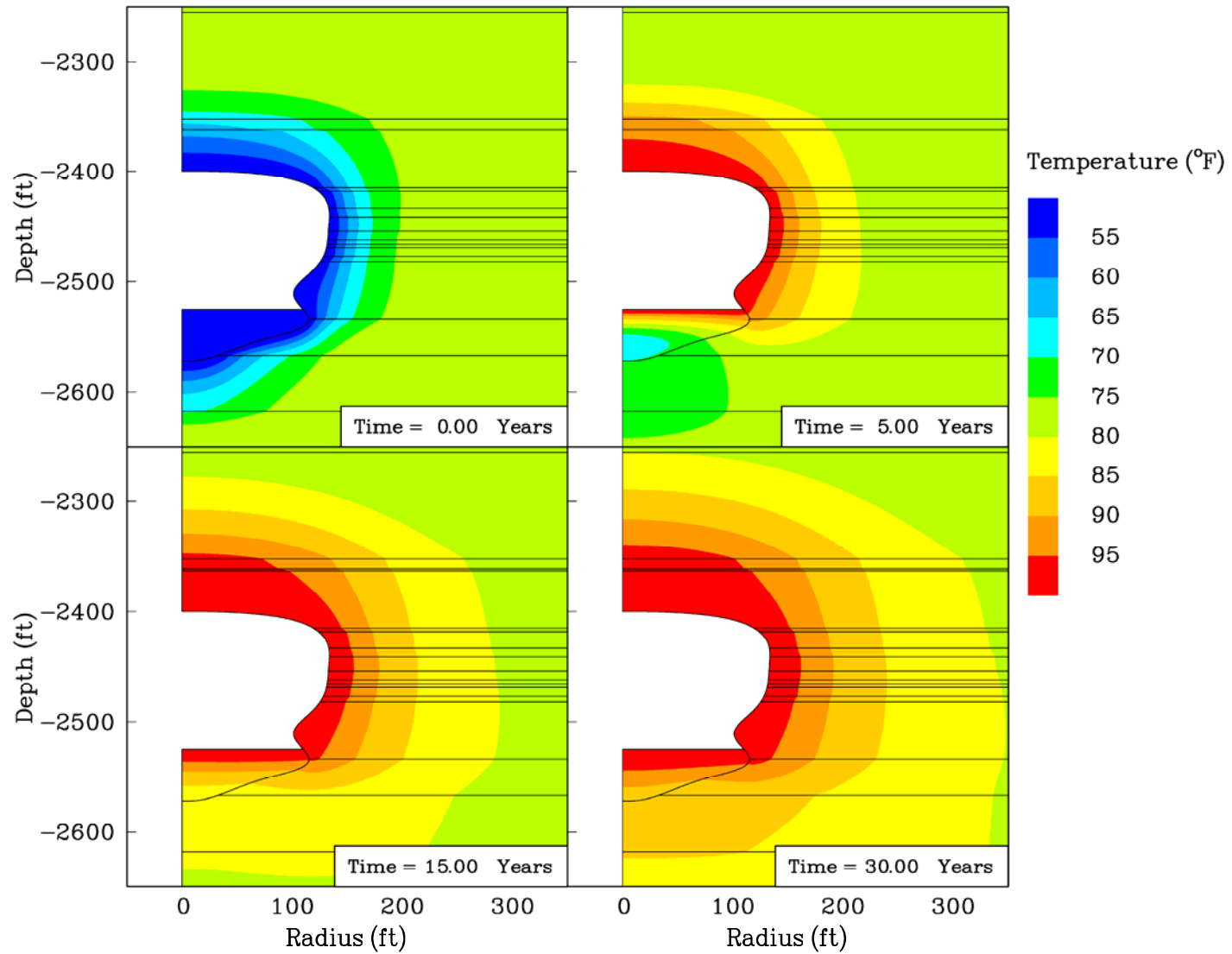


Figure 4-2. Temperature Contours at Various Times From Immediately Following Dewatering Through 30 Years of Compressed Air Energy Storage Operations.

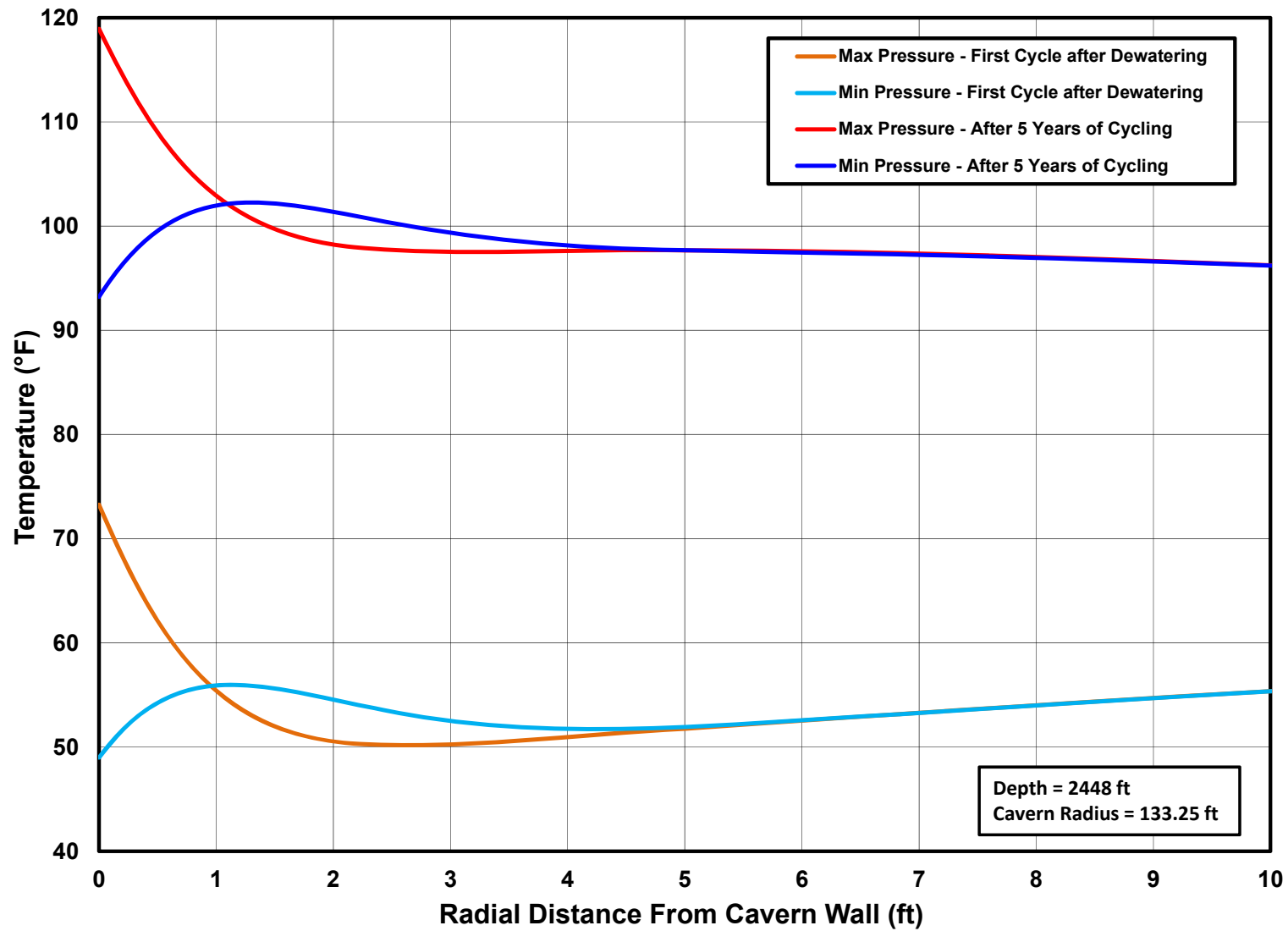


Figure 4-3. Salt Temperature as a Function of Distance From the Cavern Wall Before and After Air Withdrawal During the First Compressed Air Energy Storage Cycle and During a Cycle After 5 Years of Compressed Air Energy Storage Operations at a Depth of 2,448 Feet.

4.2 CAVERN STABILITY

Cavern stability was evaluated by examining the factors of safety with respect to dilation in the salt surrounding the cavern and with respect to shear failure in the nonsalt units intersecting and overlying the cavern. The effects of creep closure on the stability of the salt around a cavern are generally opposite to its effects on the stability of the nonsalt rocks. Because salt has the ability to redistribute the stresses to a more stable condition as it creeps, the stability of the salt around a cavern generally increases with time. However, the nonsalt units are not able to redistribute the stresses that develop because of creep closure and shear stresses tend to increase until brittle failure eventually occurs.

Figure 4-4 shows dilation factor-of-safety contours in the salt just before and just after the withdrawal from maximum pressure (1,500 psi at the wellhead) down to minimum pressure (1,150 psi at the wellhead) on the first day of CAES operations. At maximum pressure, dilation is predicted (factor-of-safety values less than 1) in the upper corner of the cavern and also in the floor of the cavern, and a large portion of the roof is predicted to have factor-of-safety values between 1 and 1.5. At minimum pressure, only a small amount of dilation is predicted below the upper nonsalt bed that intersects the cavern. These generally low factors of safety, especially those at higher pressure, are related to the cooling of the salt around the cavern during cavern development. After 2 weeks of operations (Figure 4-5), some warming of the salt has occurred and no dilation is predicted at maximum pressure, and the factor-of-safety values in the roof have increased significantly. At minimum pressure, there is a thin skin of dilating salt on the lower lobe of salt between the bottom two nonsalt beds. Although there may be some sloughing of salt in the area, it is in the lower portion of the cavern and is not expected to affect stability. After 5 years (Figure 4-6) of CAES operations, most of the dilation factor-of-safety values are greater than 3 when the cavern is at maximum pressure and greater than 2 at minimum pressure. The thin skin of dilating salt in the lower portion of the cavern is still predicted at minimum pressure after 5 years of operations. Based on these results, salt dilation is not expected to affect cavern stability for the pressure range evaluated.

Figures 4-7 and 4-8 show shear failure factor-of-safety contours in the nonsalt units assuming in situ horizontal stresses in the plane of the model of 0.95 and 1.9 times the vertical stress, respectively. In the thin overlying nonsalt unit within the Syracuse Formation, the factors of safety are greater than 1. In the Camillus Formation and other overlying formations, the factors of safety are greater than 1.5 and do not change significantly with time because the creep closure of the cavern is relatively low. The thin nonsalt units that intersect the cavern do have regions with factor-of-safety values less than 1 and the extent of the regions increases with time. These regions of failure are the result of tensile stresses that develop because these units will be continually pulled on by the salt as it creeps toward the cavern. As such, the failures are expected to result in vertical tensile fractures parallel to the cavern wall and are not expected to result in cavern instability or provide a pathway for leakage.

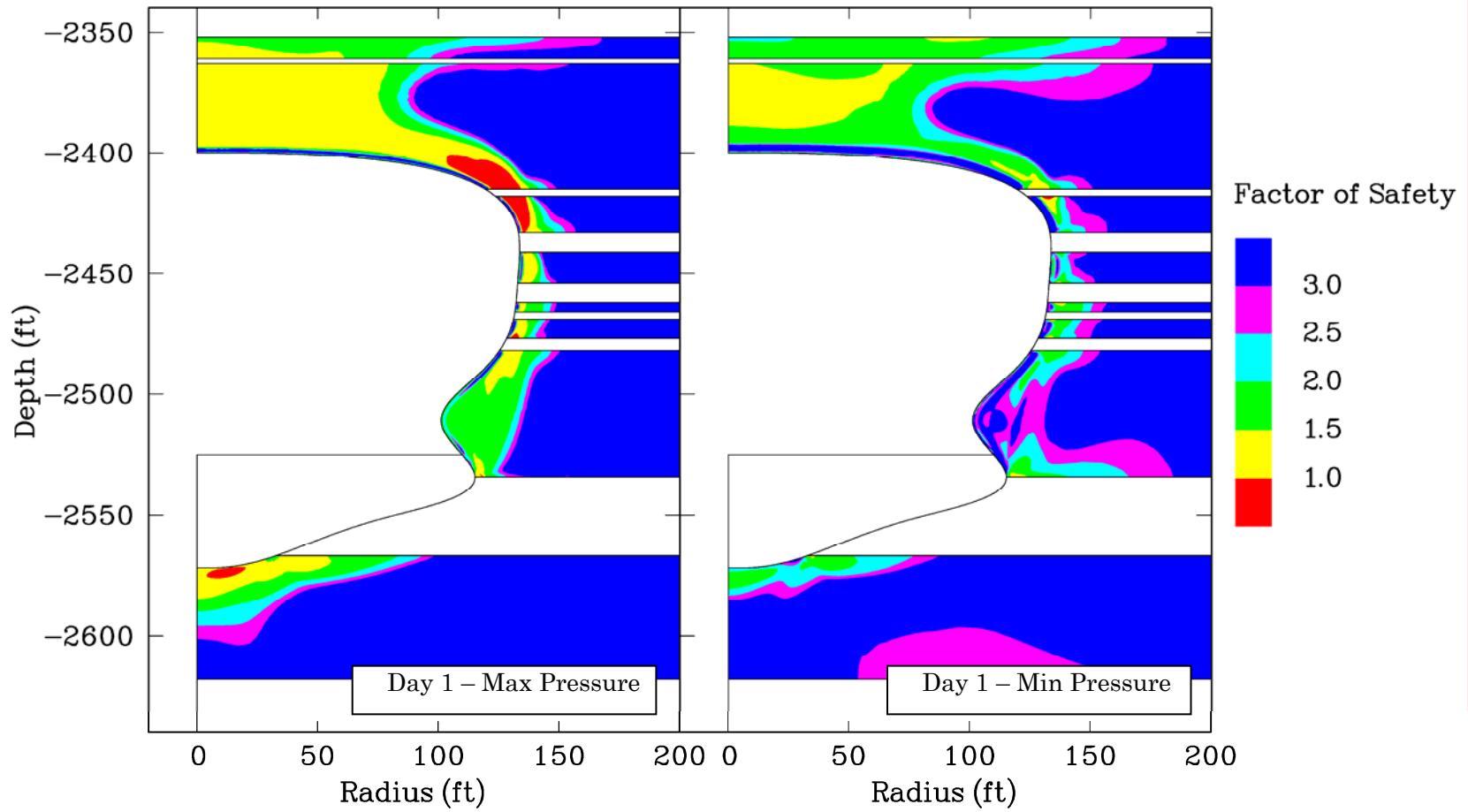


Figure 4-4. Dilation Factor-of-Safety Contours in the Salt During the First Day of Compressed Air Energy Storage Operations.

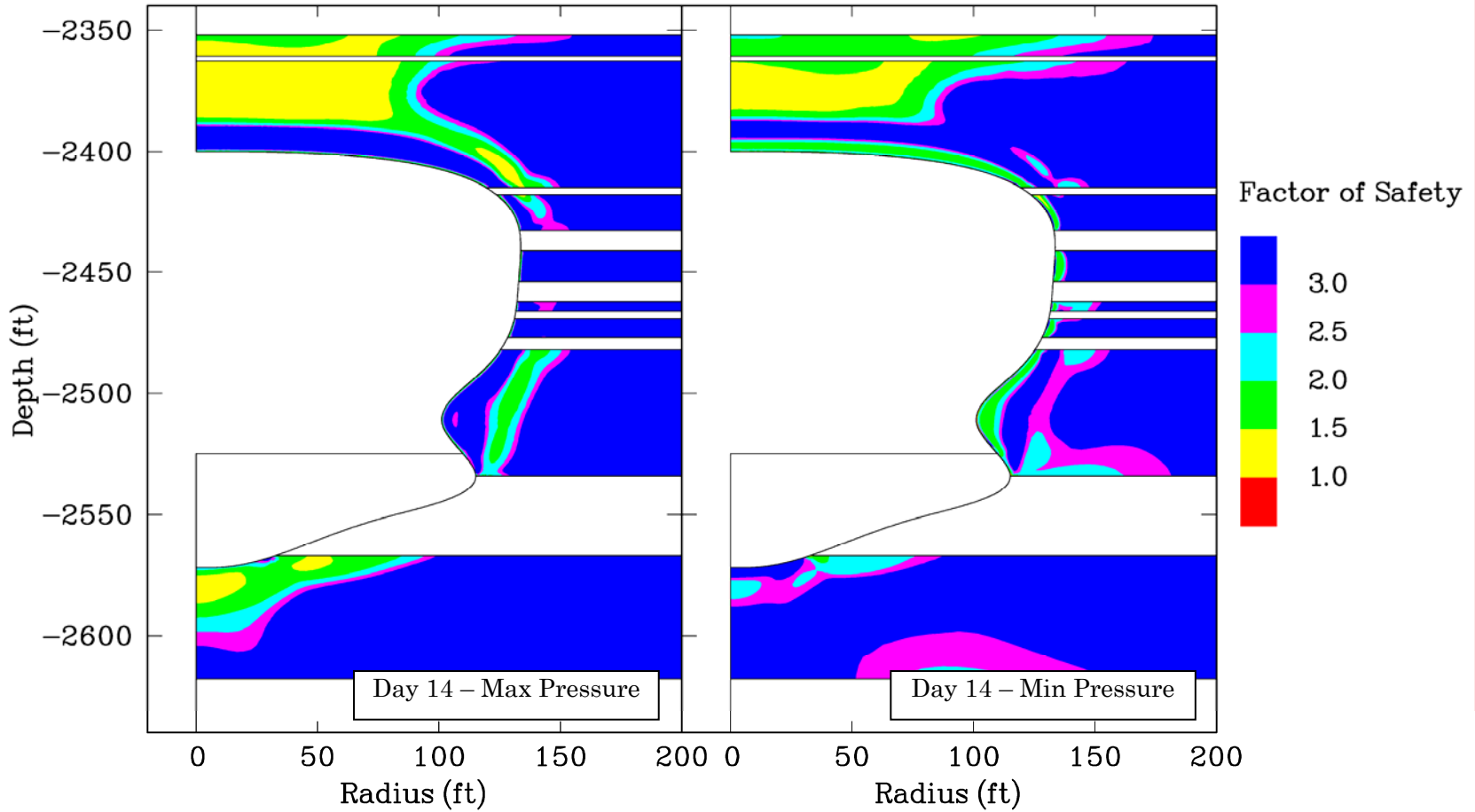


Figure 4-5. Dilation Factor-of-Safety Contours in the Salt During the Fourteenth Day of Compressed Air Energy Storage Operations.

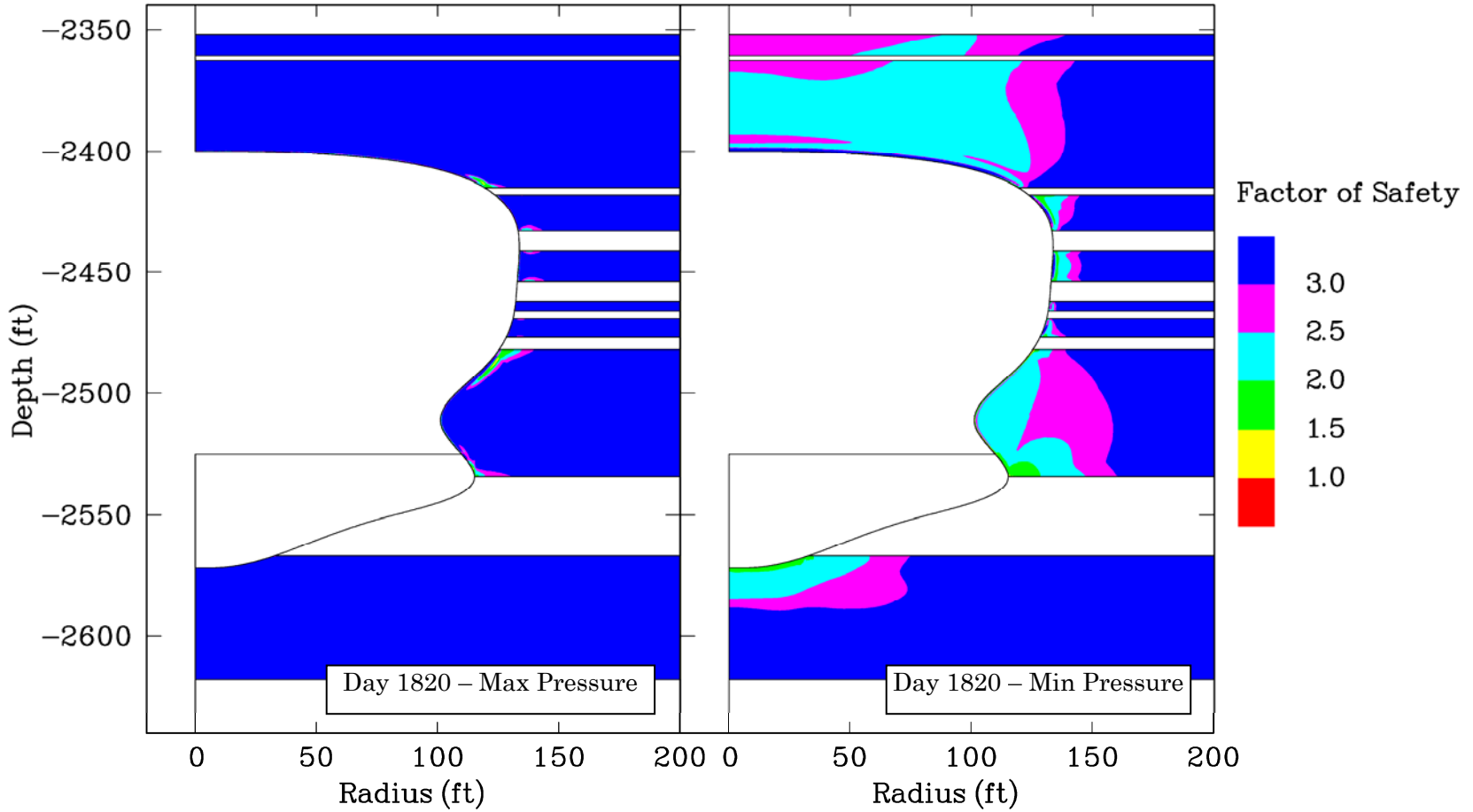


Figure 4-6. Dilation Factor-of-Safety Contours in the Salt After 5 Years of Compressed Air Energy Storage Operations.

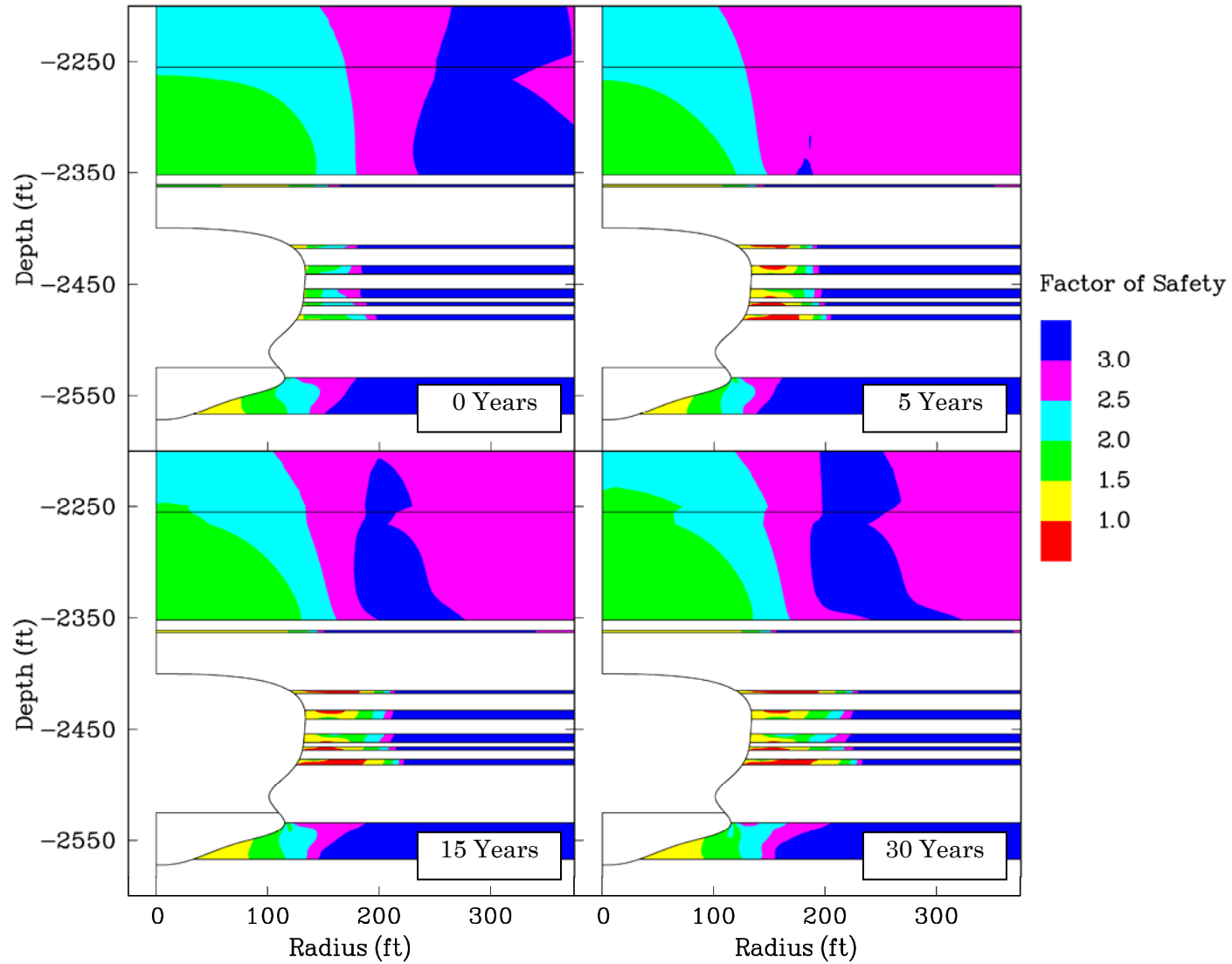


Figure 4-7. Shear Failure Factor-of-Safety Contours in the Nonsalt Units at Various Times From Immediately Following Dewatering Through 30 Years at a Wellhead Pressure of 1,150 psi (In-Plane Horizontal In Situ Stress Equals 0.95 Times the Vertical Stress, Out-of-Plane Horizontal In Situ Stress Equals 1.9 Times the Vertical Stress).

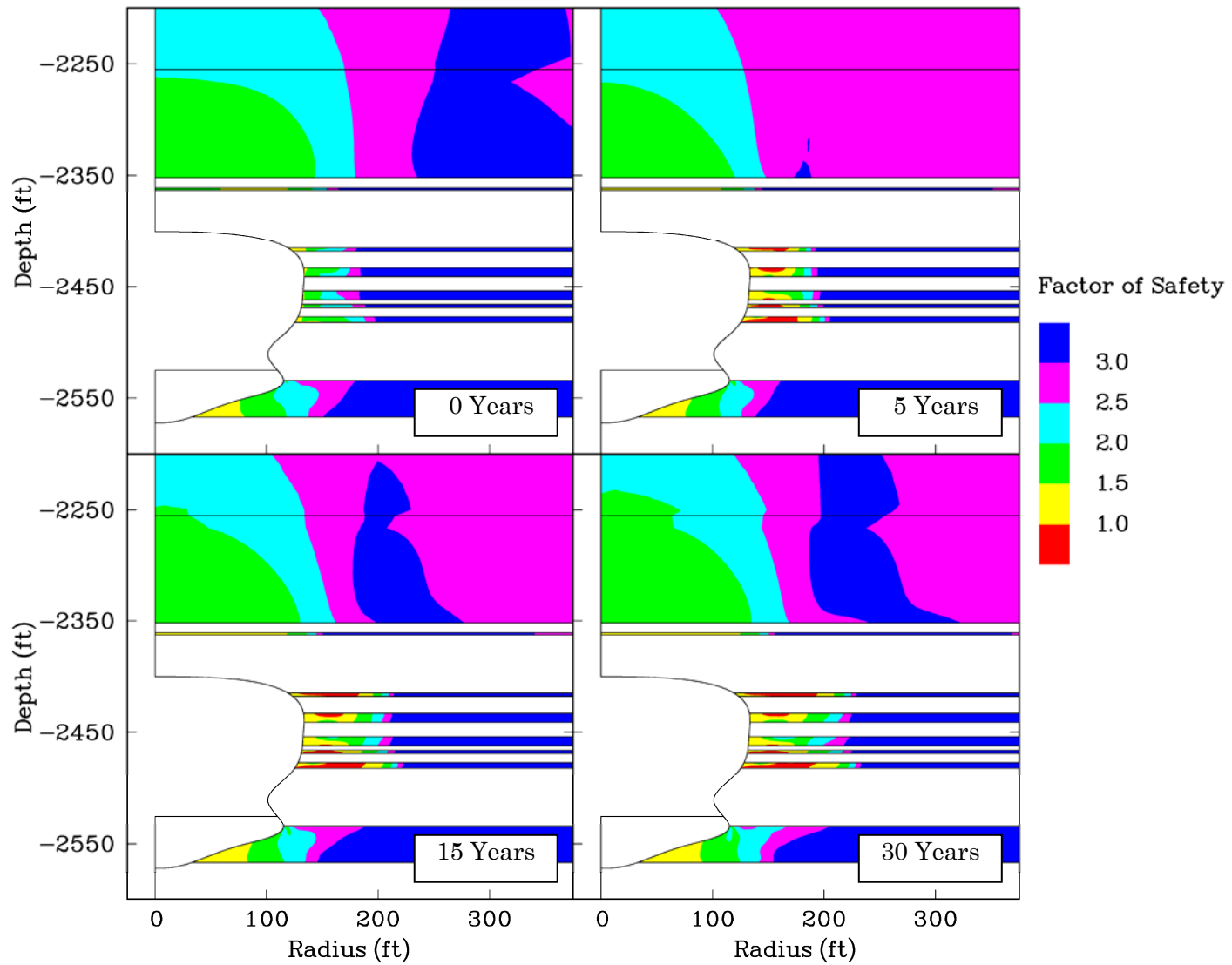


Figure 4-8. Shear Failure Factor-of-Safety Contours in the Nonsalt Units at Various Times From Immediately Following Dewatering Through 30 Years at a Wellhead Pressure of 1,150 psi (In-Plane Horizontal In Situ Stress Equals 1.9 Times the Vertical Stress, Out-of-Plane Horizontal In Situ Stress Equals 0.95 Times the Vertical Stress).

4.3 POTENTIAL FOR HYDRAULIC FRACTURE DEVELOPMENT

One of the main concerns with high-frequency pressure cycling in a CAES storage cavern is that the temperature fluctuations caused by the compression and decompression of the air will result in thermally induced tensile fractures perpendicular to the cavern surface. Such fractures in the roof or walls of a CAES cavern could result in instability of the cavern roof or walls or in the loss of air containment.

Figures 4-9 and 4-10 show the effect of pressure cycling on the stresses in the center of the roof during the first week after dewatering the cavern and after 5 years of CAES operations, respectively. With the sign convention of compressive stresses being negative, the normal stress is the negative of the internal cavern pressure and is perpendicular to the cavern surface. The tangential stress is horizontal (i.e., parallel to the cavern surface). As the cavern pressure increases, the temperature increases and both the normal and tangential stresses become more compressive. When the cavern pressure decreases, the opposite is true. This is contrary to the isothermal pressurization or depressurization where the changes in tangential stress are generally in the opposite direction of the normal stress. During the first week of CAES operations, the maximum tangential stress is expected to remain compressive by more than 500 psi. After 5 years, when the temperature fluctuations in the cavern have essentially attained a steady-state value, the tangential stress is expected to remain compressive by about 200 psi.

Figures 4-11 and 4-12 show the maximum principal stress² (the least-compressive or most-tensile stress) contours around the cavern at minimum and maximum pressure for the first cycle after dewatering and after 5 years of CAES operations for the case where the nonsalt units have an in situ stress of 0.95 times the vertical stress. The stresses in the nonsalt units are slightly more compressive for the case where the horizontal stresses in the plane of the model are 1.9 times the vertical stress. After withdrawal to minimum pressure during the first CAES cycle, the stresses in the salt around the cavern are all more than 500 psi in compression. As discussed in the previous section, some of the stresses in the nonsalt units intersecting the cavern are in tension because salt creep drags the nonsalt units toward the cavern. After 5 years of cycling, all of the stresses in the salt remain in compression and, as expected, the regions of tensile stress in the intersecting nonsalt units have increased. It should be noted that the elastic material model used for the nonsalt units does not fail the material in the simulations. In reality, these units will fail when the tensile stresses are larger than the tensile strength. The orientation of these fractures will be vertical and parallel to the cavern surface and thus are not expected to jeopardize cavern stability or air containment. Because all other stresses remain compressive, no development of tensile fractures perpendicular to the cavern surface is expected.

² Compressive stresses are negative.

RSI-2040-11-034

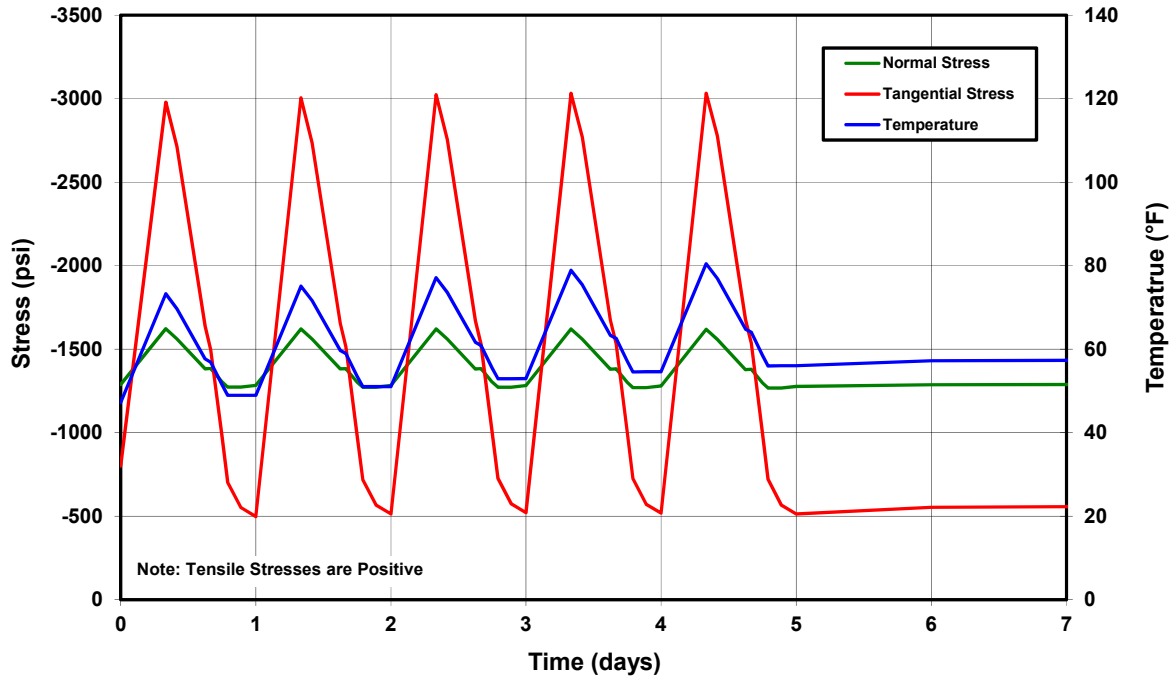


Figure 4-9. Stresses and Temperature at the Center of the Cavern Roof During the First Week of Compressed Air Energy Storage Operations.

RSI-2040-11-035

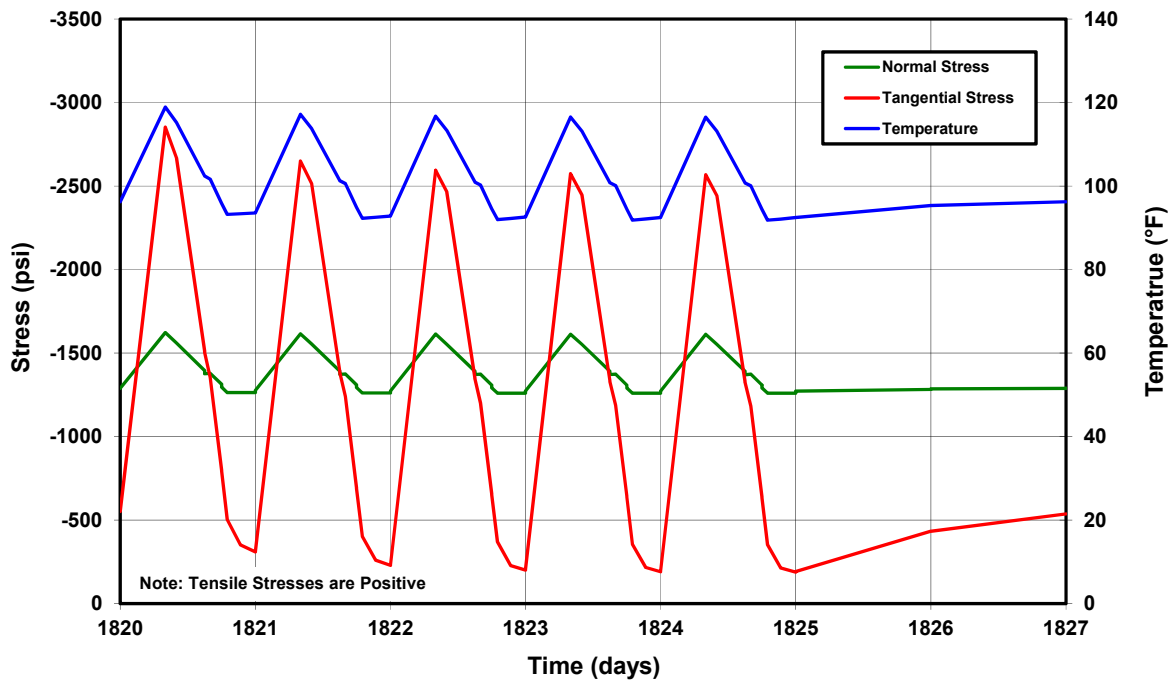


Figure 4-10. Stresses and Temperature at the Center of the Cavern Roof After 5 Years of Compressed Air Energy Storage Operations.

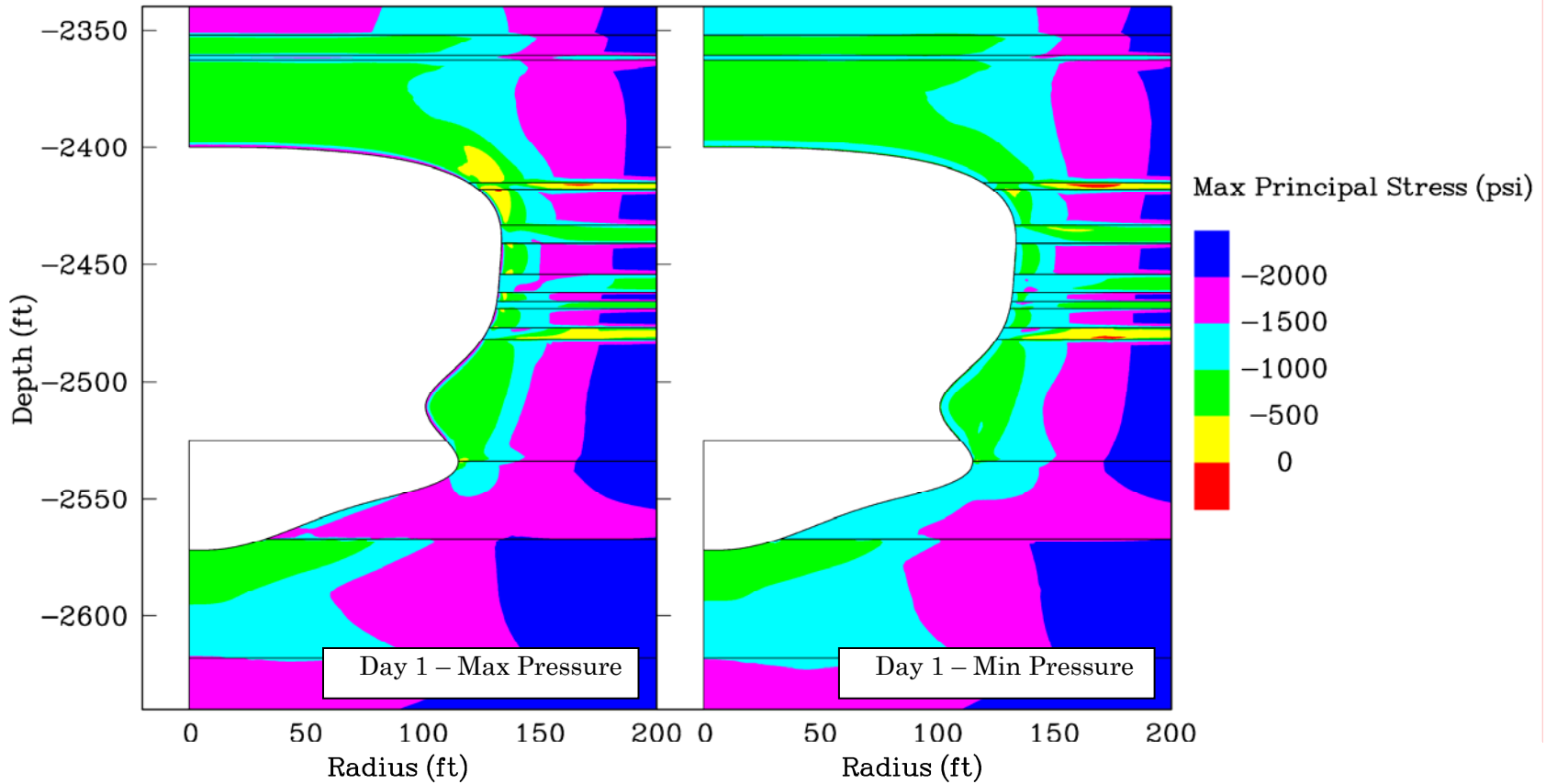


Figure 4-11. Maximum Principal Stress Contours (Compression Negative) Before and After First Withdrawal After Dewatering (In-Plane Horizontal In Situ Stress Equals 0.95 Times the Vertical Stress, Out-of-Plane Horizontal In Situ Stress Equals 1.9 Times the Vertical Stress).

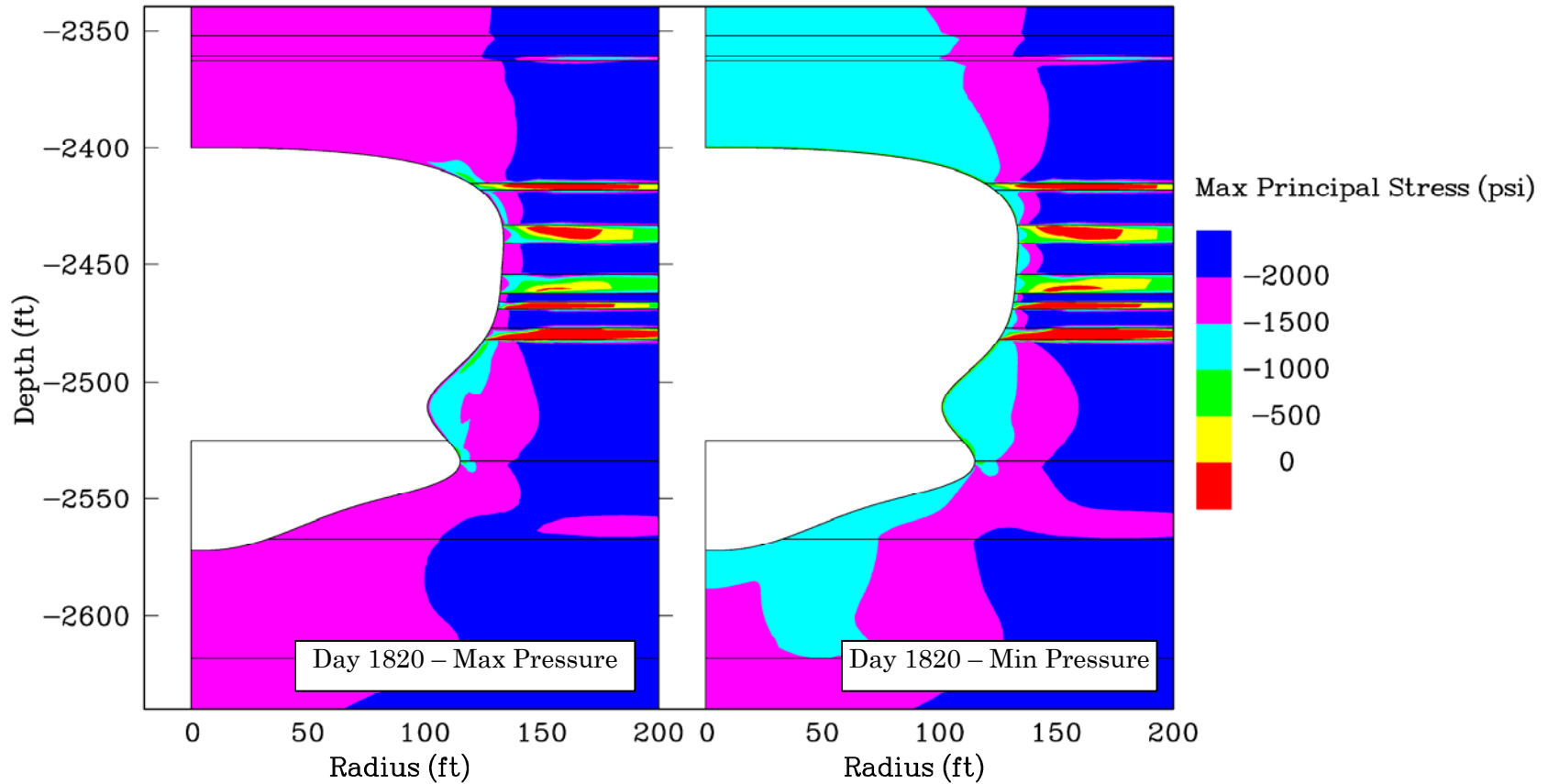


Figure 4-12. Maximum Principal Stress Contours (Compression Negative) Before and After Withdrawal After 5 Years of Compressed Air Energy Storage Operations (In-Plane Horizontal In Situ Stress Equals 0.95 Times the Vertical Stress, Out-of-Plane Horizontal In Situ Stress Equals 1.9 Times the Vertical Stress).

4.4 CAVERN CLOSURE AND CASING STRAIN

Cavern closure occurs because the internal cavern pressure is lower than the stress in the salt surrounding the cavern. This stress difference results in continuous creep movement of the salt toward and into the cavern. The creep closure rate of the cavern during CAES operations will depend mostly on the internal air pressure and the temperature of the surrounding salt. However, because of the transient effects of pressure changes on work hardening and recovery, they will also depend on the pressurization and depressurization rates of the cavern.

Cavern closure was estimated during the 30-year simulation with the wellhead pressure at the minimum value of 1,150 psi. Figure 4-13 shows the estimated closure as a function of time for this simulation. The in situ stress assumption in the nonsalt units has no effect on the predicted cavern closure. Even at the minimum wellhead pressure of 1,150 psi, the predicted cavern closure is small. A total cavern closure of 0.48 percent was predicted after 30 years. The annual closure rate at the end of the 30 years is about 0.004 percent per year. This closure rate is considered quite small for a storage cavern.

RSI-2040-11-038

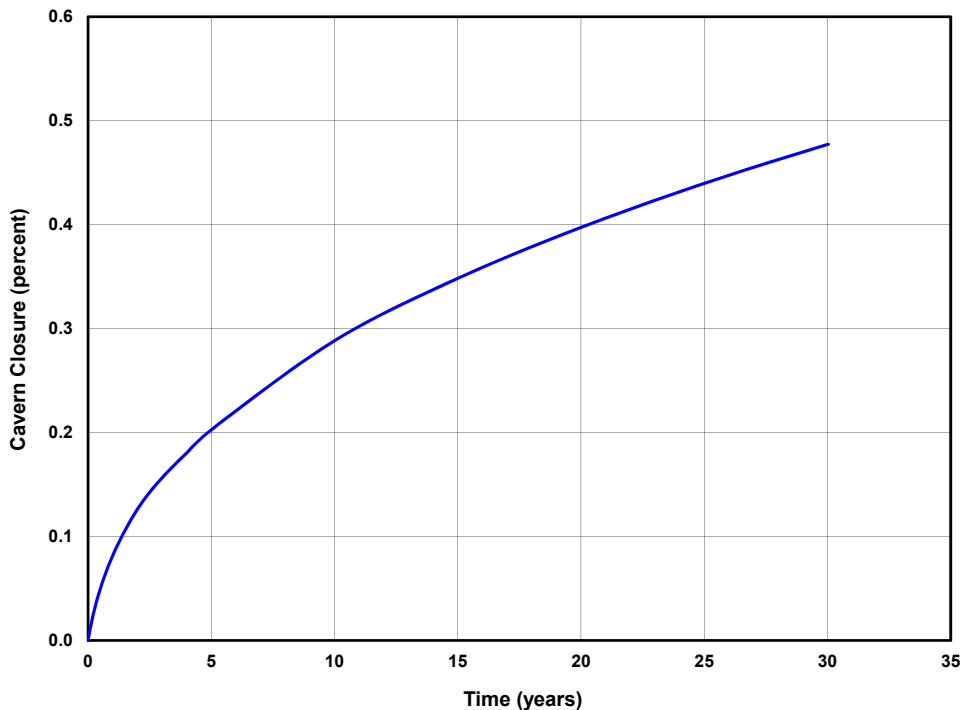


Figure 4-13. Predicted Cavern Closure Versus Time During 30 Years at a Wellhead Pressure of 1,150 psi.

As a cavern experiences creep closure, the salt flowing into the cavern can drag the casing string toward the cavern, resulting in casing string strain. This stretching of the casing results in axial tensions. Assuming that the salt/cement and cement/casing interfaces remain perfectly

bonded, elongation of the casing will continue until the tensile limit of the casing and/or connection is exceeded, compromising the integrity of the casing.

The steel casing strings were not modeled in this study. However, the predicted strains along the axis of symmetry above the cavern provide a conservative estimate for casing string strains because the salt at this location is free to move vertically in the model in response to cavern closure caused by salt creep. Figure 4-14 shows the predicted vertical strain near the bottom of the casing string. Assuming typical values for the Young's modulus (30×10^6 psi), yield strength (55×10^6 psi), and ultimate strength of steel³ (95×10^6 psi), the casing will begin to yield at a strain of 0.0018 with ultimate failure occurring at 0.0032 strain. As shown in the figure, it is predicted that the casing will begin to yield in about 15 years. However, because the strain rate is so low (about 7 microstrain per year), ultimate failure is not predicted for about 200 years. Based on these estimates, casing strain because of creep closure will not be a problem for the life of the cavern.

³ The yield and ultimate tensile strengths for K-55 grade casing are 55,000 and 95,000 psi, respectively [American Petroleum Institute, 1987].

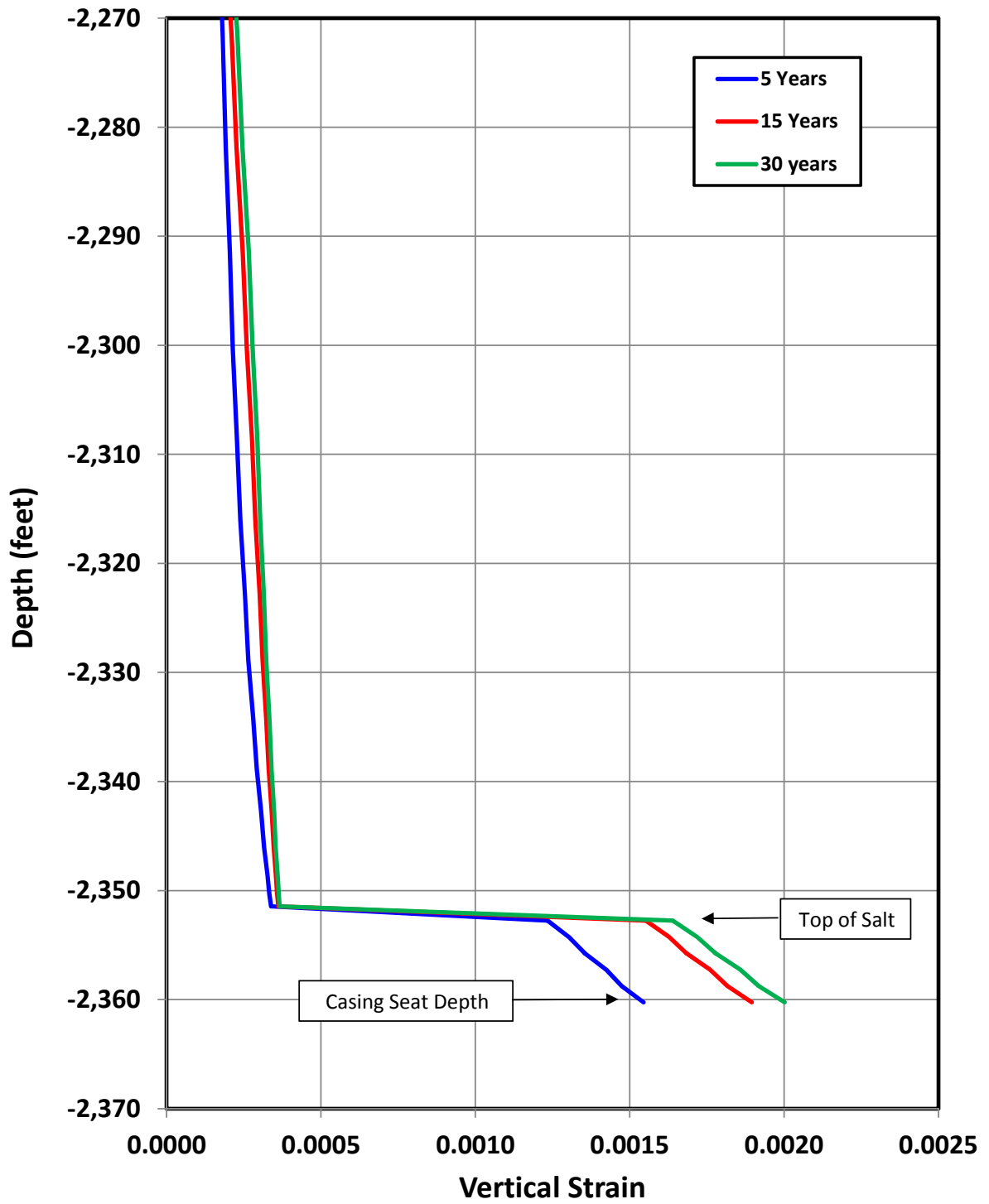


Figure 4-14. Predicted Vertical Casing Strain During 30 Years at a Wellhead Pressure of 1,150 psi.

5.0 SUMMARY AND CONCLUSIONS

A study was completed to assess the performance of the proposed NYSEG CAES cavern design. The objective of this study was to perform a geomechanical analysis to evaluate cavern stability, cavern closure, and casing strain under the proposed CAES operations. This was achieved through the use of thermomechanical finite element simulations.

Because temperature and salt creep are history dependent, the entire history of the cavern was modeled. The history includes 2 years of cavern development; dewatering of the cavern; and finally, CAES operation using a typical pressure cycle. The typical CAES cycle used in the simulations includes daily injections and withdrawals and operates between wellhead pressures of 1,150 and 1,500 psi. The daily cycle was repeated for 5 years to allow the cavern to nearly reach a steady-state thermal condition. To provide conservative results for creep closure and creep-related factors, including stability of the nonsalts units and casing strain, a 30-year simulation was conducted at the minimum wellhead pressure of 1,150 psi.

Cavern stability was evaluated by examining the stress states in the salt and nonsalt units surrounding the cavern. Stress states that result in extensive salt dilation in the upper portion of the cavern or in shear failure of the nonsalt units overlying the cavern can lead to roof falls, resulting in loss of containment and/or damage to the casing seat or well.

During the first 2 weeks of CAES operations, some salt dilation is predicted in the upper corner of the cavern and also in the floor of the cavern. This is related to the cooling of the salt around the cavern during cavern development, and the dilating stresses dissipate within a couple of weeks as the salt warms up. Throughout the simulation, a small amount of dilation is predicted in the lower portion of the cavern. Although there may be some sloughing of salt in this area, it is not expected to affect stability. Based on these results, salt dilation is not expected to affect cavern stability for the typical CAES cycle that was evaluated.

No shear failure is predicted in the nonsalt units overlying the cavern. In the Camillus Formation and other overlying formations, the factors of safety are greater than 1.5 and do not change significantly with time because the creep closure rate of the cavern is relatively low. Factors of safety in the overlying nonsalt units do not vary significantly with respect to the in situ stress orientation. The thin nonsalt units that intersect the cavern do have regions with factor-of-safety values less than 1 and the extent of the regions increases with time. These regions of failure are the result of tensile stresses that develop because these units will be continually pulled on by the salt as it creeps toward the cavern. As such, the failures are expected to result in vertical tensile fractures parallel to the cavern wall and are not expected to result in cavern instability or provide a pathway for leakage.

One of the main concerns with high-frequency pressure cycling in a CAES storage cavern is that the temperature fluctuations caused by the compression and decompression of the air will result in thermally induced tensile fractures perpendicular to the cavern surface. Such fractures in the roof or walls of a CAES cavern could result in instability of the cavern roof or walls or in the loss of air containment. The stresses in the salt surrounding the cavern remained compressive throughout the 5-year simulation of CAES operations. Thus no thermally induced fractures perpendicular to the cavern surface are expected to develop during CAES operations. As mentioned above, some tensile fracturing of thinner nonsalt units intersecting the cavern is expected but is not expected to result in cavern instability or loss of containment. The extent of these tensile fractures is expected to be larger in the direction of the minimum horizontal in situ stress.

Cavern closure and the associated casing strain were estimated during the 30-year simulation at the minimum wellhead pressure of 1,150 psi. A total cavern closure of about 0.48 percent was predicted over the 30-year simulation. The annual cavern closure rate at the end of the 30-year simulation is about 0.004 percent per year. These closure rates are considered to be quite small for a salt storage cavern. In conjunction with the small closure rates predicted, the predicted casing strain rates are also quite small (about 7 microstrain per year) and are not expected to be a problem for the life of the cavern.

6.0 REFERENCES

American Petroleum Institute, 1987. *API Specifications for Casing, Tubing and Drill Pipe*, API Specification 5A, Thirty-Ninth Edition, American Petroleum Institute, Washington, DC, May 31.

Callahan, G. D., 1981. *Inelastic Thermomechanical Analysis of a Generic Bedded Salt Repository*, ONWI-125, prepared by RE/SPEC Inc., Rapid City, SD, for the Office of Nuclear Waste Isolation, Battelle Memorial Institute, Columbus, OH.

Callahan, G. D., A. F. Fossum, and D. K. Svalstad, 1989. *Documentation of SPECTROM-32: A Finite Element Thermomechanical Stress Analysis Program*, DOE/CH/10378-2, prepared by RE/SPEC Inc., Rapid City, SD, for the U. S. Department of Energy, Chicago Operations Office, Argonne, IL, Vols. I and II.

Carmichael, R. S. (ed.), 1982. *Handbook of Physical Properties of Rocks, Volume II*, CRC Press, Inc., Boca Raton, FL.

Croff, A. G., T. F. Lomenick, R. S. Lowrie, and S. H. Stow, 1985. *Evaluation of Five Sedimentary Rocks Other Than Salt for High-Level Waste Repository Siting Purposes*, prepared for Oak Ridge National Laboratory, Oak Ridge, TN.

DeVries, K. L., 1988. *Viscoplastic Laws for Avery Island Salt*, RSI-0333, prepared by RE/SPEC Inc., Rapid City, SD, for Stone & Webster Engineering Corporation, Boston, MA.

Eyermann T. J., 2011a. *Conceptual Cavern for NYSEG Compressed Air Energy Storage at Watkins Glen, NY*, prepared by PB Energy Storage Services, Inc., Houston, TX (draft).

Eyermann T. J. 2011b. *Overview of Geology of the Area Around the US Salt Watkins Glen Refinery*, prepared for NYSEG, Binghamton, NY, by PB Energy Storage Services, Inc., Houston, TX.

Munson, 1998. *Analysis of Multistage and Other Creep Data for Domal Salts*, SAND98-2276, Sandia National Laboratories, Albuquerque, NM.

Nieland, J. D., 2004. *Salt Cavern Thermal Simulator Version 2.0 User's Manual*, RSI-1760, prepared by RESPEC, Rapid City, SD, for Gas Technology Institute, Chicago, IL.

Nieland, J. D., 2011. *Thermodynamic Evaluation of Proposed New York State Electric & Gas Corporation Compressed Air Energy Storage Cavern Design*, Memorandum RSI(RCO)-2040/9-11/9, prepared by RESPEC, Rapid City, SD, for J. M. McHenry, PB Energy Storage Services, Inc., Houston, TX, September 22.

Osnes, J. D. and T. J. Eyermann, 1996. *Geomechanical Analyses of Compressed Natural Gas Storage in Gallery No. 1, Watkins Glen, New York*, RSI-0670, prepared by RE/SPEC Inc., Rapid City, SD, for PB-KBB Inc., Houston, TX.

Pfeifle, T. W., 1996. *Mechanical Properties of Salt and Dolostone From Akzo Nobel Salt Inc. Well No. 58 and NYSEG Well No. 59, Seneca Lake Storage Project, Watkins Glen, New York*, RSI-0668, prepared by RE/SPEC Inc., Rapid City, SD, for PB-KBB, Houston, TX.

Senseny, P. E., F. D. Hansen, J. E. Russell, N. L. Carter, and J. W. Handin, 1992. “Mechanical Behaviour of Rock Salt: Phenomenology and Micromechanisms,” *International Journal of Rock Mechanics and Mining Sciences & Geomechanics Abstracts*, Vol. 29, No. 4, pp. 363–378.

Starling, K. E. and J. L. Savidge, 1994. *Compressibility of Natural Gas and Other Related Hydrocarbon Gases*, Report No. 8, 2nd Edition, Catalog No. XQ9212, prepared for American Gas Association.

Svalstad, D. K., 1989. *Documentation of SPECTROM-41: A Finite Element Heat Transfer Analysis Program*, DOE/CH/10378-1, prepared by RE/SPEC Inc., Rapid City, SD, for the U.S. Department of Energy, Chicago Operations Office, Argonne, IL.

WorleyParsons Group, Inc., 2011. Electronic communication between M. C. Holdridge, WorleyParsons Group, Inc., Reading, PA, and J. L. Ratigan, PB Energy Storage Services, Inc., Houston, TX, August 11.

Van Sambeek, L. L., J. L. Ratigan, and F. D. Hansen, 1993. “Dilatancy of Rock Salt in Laboratory Tests,” *Proceedings, 34th U.S. Symposium on Rock Mechanics*, University of Wisconsin–Madison, Madison, WI, June 27–30, B. C. Haimson (ed.), *International Journal of Rock Mechanics and Mining Sciences & Geomechanics Abstracts*, Pergamon Press, Vol. 30, No. 7, pp. 735–738.

APPENDIX A
THERMODYNAMICS MEMORANDUM

APPENDIX B

MECHANICAL ROCK PROPERTIES TESTS

APPENDIX B

MECHANICAL ROCK PROPERTIES TESTS

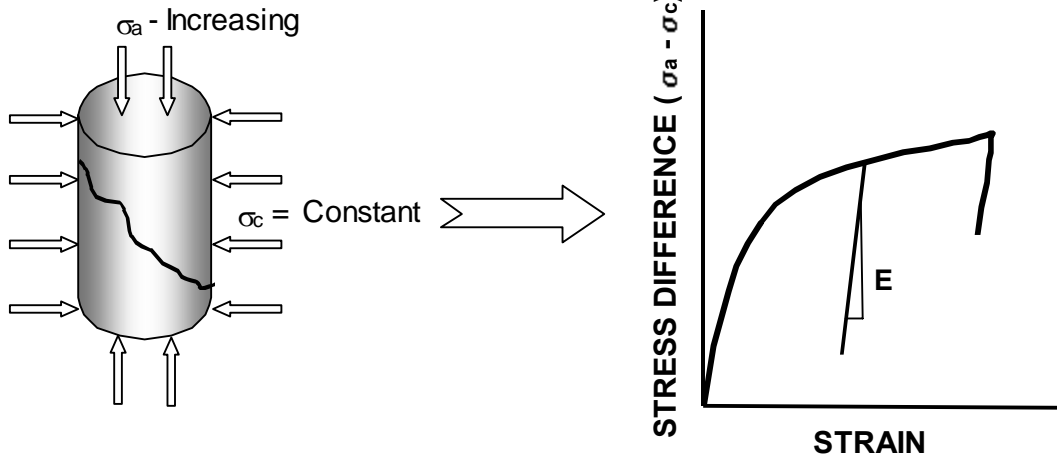
There are four types of mechanical properties tests generally used for characterization of the strength and deformational behavior of salt and nonsalt rocks. These tests are schematically illustrated in Figures B-1 and B-2. The four test types are the (1) quasi-static compression test, (2) constant mean stress test, (3) Brazilian indirect tension test, and (4) confined creep test. Each of these tests is performed in our laboratory to standards that meet or exceed all applicable American Society for Testing and Materials (ASTM) or International Society of Rock Mechanics (ISRM) specifications. Because of the relatively large grain size of most salts, the cylindrical test specimens need to have a minimum diameter of 4 inches. Nonsalt rocks generally have a smaller grain size and smaller test specimens can be used. The quasi-static compression test, constant mean stress test, and confined creep test are performed on specimens that have a length-to-diameter ratio (L:D) of at least 2, while the L:D of the indirect tension specimens is 0.5. Each of the four test types is briefly described below.

B.1 QUASI-STATIC COMPRESSION TEST

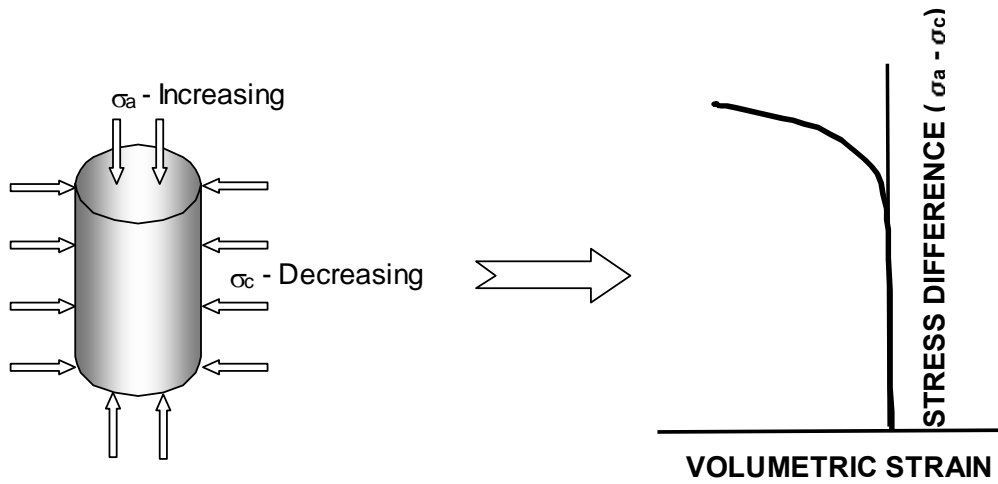
The quasi-static compression test is shown in Figure B-1(a). The test is used to determine (1) the compressive strength; (2) Young's modulus, E ; and (3) Poisson's ratio, ν . For nonsalt rocks, the strength data from these tests are used to determine a Mohr-Coulomb strength model (cohesion and friction angle), which is then used in modeling to determine factors of safety with respect to shear strength. A variation of the quasi-static compression test in which the confining pressure is zero is typically known as the unconfined compression test. The unconfined strength is used as an index property for comparisons between rock types and for examining variations in the same rock type recovered from different locations. The deformation properties (Young's modulus and Poisson's ratio) are used directly in modeling and design of underground structures.

B.2 CONSTANT MEAN STRESS TEST

The constant mean stress (CMS) test (Figure B-1(b)) is also a variation of the confined quasi-static compression test and is used to characterize the dilational behavior of the salt. In this test, a hydrostatic stress or uniform pressure is applied to all surfaces of the specimen. Then, the axial stress (σ_a) is increased/decreased and the confining pressure (σ_c) is simultaneously decreased/increased in a manner that maintains the mean stress ($\sigma_m - (\sigma_a + 2\sigma_c)/3$) constant. The volumetric strain is monitored during the test and is used to determine the stress state that induces salt dilation (volume expansion caused by microfracturing). Not shown in Figure B-1(b) is the small stress difference applied at the initial hydrostatic confining pressure to obtain data

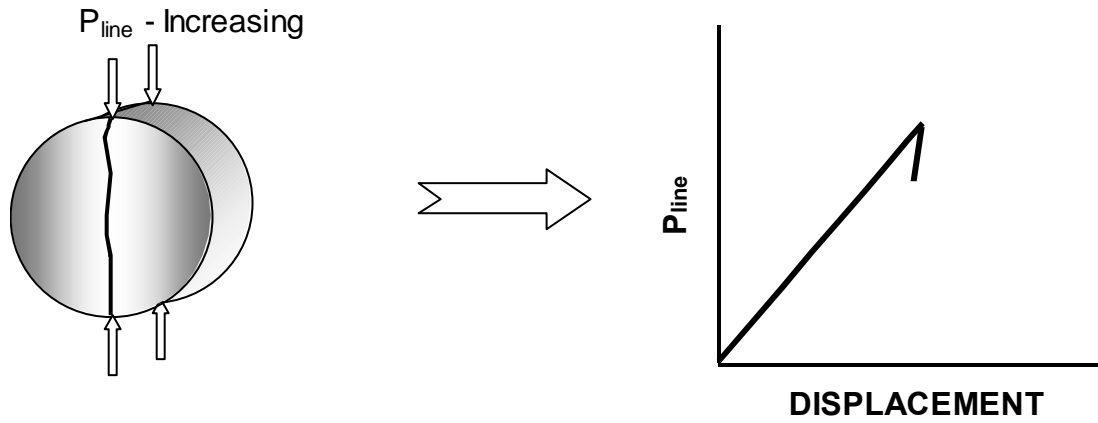


(a) QUASI-STATIC COMPRESSION

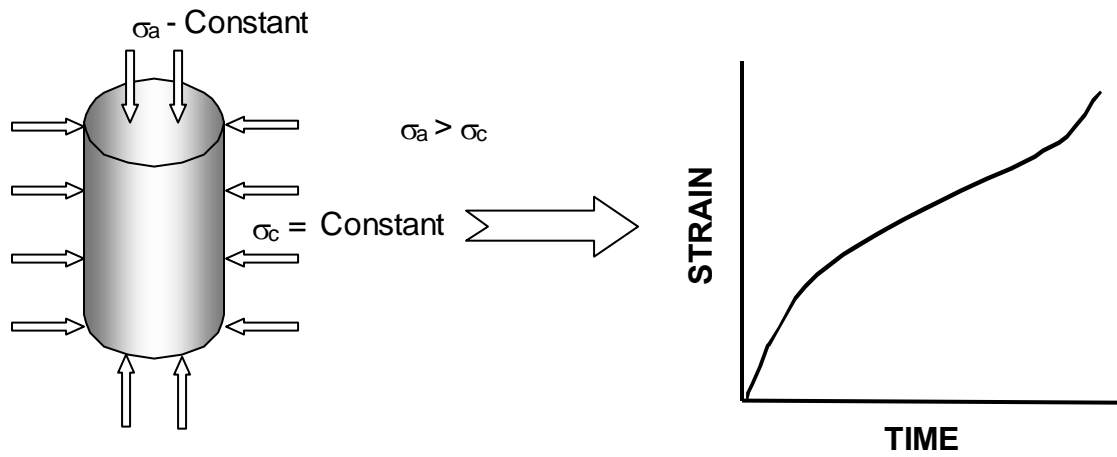


(b) CONSTANT MEAN STRESS COMPRESSION

Figure B-1. Schematic Illustration of (a) Confined Quasi-Static Compression Test and (b) Constant Mean Stress Test.



(a) BRAZILIAN INDIRECT TENSION



(b) CREEP

Figure B-2. Schematic Illustration of (a) Brazilian Indirect Tension Test and (b) Creep Test.

for estimating elastic constants (E and ν) under confined conditions. This is an inexpensive approach to obtaining elastic constants from nearly every specimen that gets tested.

RESPEC has developed and used two different load paths to complete CMS tests. The stress state in the conventional CMS test is generally termed triaxial compression (CMC), and the test is performed by simultaneously increasing the axial stress and decreasing the confining pressure. An alternative load path imposes a state of stress termed triaxial extension (CMX), and the test is performed by simultaneously decreasing the axial stress and increasing the confining pressure. Both the CMC and CMX tests impose the same difference between the maximum and minimum compressive principal stresses, but the intermediate principal stress is different between the two tests. In the CMC test, the intermediate principal stress equals the minimum compressive principal stress, while in the CMX test, the intermediate principal stress equals the maximum compressive principal stress. Dilational strength observed in CMX tests can be significantly lower than the dilation strength observed in CMC tests.

The dilational characteristics of the salt are used directly in the design of caverns in salt. Because the intermediate principal stresses around a cavern can range from a state of triaxial compression to a state of triaxial extension, both CMC and CMX constant mean stress tests are useful for establishing dilation criteria that are used for determining the minimum pressure in the cavern.

B.3 BRAZILIAN INDIRECT TENSION TEST

The Brazilian indirect tension test (Figure B-2(a)) is used to determine the apparent tensile strength of rocks. While the tensile strength is not generally used directly in any analysis (other than when damage accumulation or fracture is of concern), it is a useful measure for comparisons between rock types and for comparing variations in rock strength from one location to another. If tensile stresses are generated in an underground structural model, the apparent tensile strength can be used to estimate the propensity for rock tensile failure. The apparent tensile strength can also be used to estimate the intercept (dilation limit at zero mean stress) for the salt dilation criterion.

B.4 CONFINED CREEP TEST

The creep test (Figure B-2(b)) is used to determine the deformation of salt that occurs through time when a constant stress difference (axial stress minus confining pressure) is applied to the specimen. Although the test may be performed confined or unconfined, it is usually performed with confining pressure. Creep is the principal deformation mechanism in salt surrounding a storage cavern and leads to the closure or volume reduction of the cavern with time. Brittle (cracking) deformation mechanisms are suppressed when the test is “confined;” that is, when a pressure is applied to the external surface of the salt core being

tested. This test is useful for comparing different salts, for comparing variations in salt response from one location to another, and for numerical modeling of salt excavations. Salt creep is very dependent on the stress difference applied to the core specimen and the applied temperature. Typically, tests with at least three different stress differences are necessary to characterize the creep response of a particular salt.



**WELL CASING AND TUBULARS
WATKINS GLEN CAES**

Revision 1

Watkins Glen, New York

Prepared for

NYSEG

Binghamton, NY

Prepared by

James McHenry



PB ENERGY STORAGE SERVICES, INC.

Houston, TX

Project No. 50756B
November 2011

TABLE OF CONTENTS

SECTION	PAGE
1 INTRODUCTION	4
2 CASING SELECTION RATIONALE	4
2.1 Brine String Selection	4
2.1.1 Brine String Hydraulic Calculations	4
2.2 Production Liner Selection	6
2.2.1 Production Liner Hydraulics	7
2.3 Cemented Casing Selection	8
3 CASING PERFORMANCE	8
4 REFERENCES	9

LIST OF FIGURES

SECTION	PAGE
Figure 1 - Water Injection Pressure Direct Circulation	5
Figure 2 - Raw Water Pressure - Reverse Circulation	6
Figure 3 - Casing Program Cavern No. 1 - Leaching Configuration	11
Figure 4 - Casing Program Cavern No. 2 / 3 - Leaching Configuration	12
Figure 5 – Casing Program Cavern 1 - Storage Configuration	14
Figure 6 - Casing Program Caverns 2 & 3 - Storage Configuration	15
Figure 7 - Conductor Pipe Calculations Cavern No. 1	16
Figure 8 - Surface Casing Calculations Cavern No. 1	17
Figure 9 - Production Casing Calculations Cavern No. 1	18

Figure 10 - Outer Leach String Calculations Cavern No. 119

Figure 11 - Inner Leach String Calculations Cavern No. 1.....20

Figure 12 - Stainless Steel Production Liner Calculations Cavern No. 121

Figure 13 - Conductor Pipe Calculations Caverns No. 2 & 3.....22

Figure 14 - Surface Casing Calculations Caverns No. 2 & 3.....23

Figure 15 - Production Casing Calculations Caverns No. 2 & 324

Figure 16 - Outer Leach String Calculations Caverns No. 2 & 325

Figure 17 - Inner Leach String Calculations Caverns No. 2 & 3.....26

Figure 18 - Stainless Steel Production Liner Calculations Caverns No. 2 & 327

LIST OF TABLES

TABLE	PAGE
Table 1 - Calculation Input Assumptions.....	5
Table 2 - Calculated Pressures (Direct and Reverse Circulation).....	6
Table 3 - Slip Crushing Calculation Well No. 1	28
Table 4 - Slip Crushing Calculation Well Nos. 2 & 3	29

1 INTRODUCTION

NYEG has proposed to build a 170 MW CAES peak shaving facility on property owned by Inergy near Watkins Glen, NY. The maximum design air flow rate required is approximately 639 lb/sec during compression. Inergy will develop the required cavern space, provide water, and dispose of brine to the Watkins Glen brinefield. Inergy will provide water at a rate of 350 gpm for development of the cavern.

To meet the anticipated electrical duty cycle approximately 3 MMB (million barrels) of dewatered cavern volume will be required.¹ Based upon a review of local geology² a preliminary cavern development program³ was developed which indicated that three nominal 1 MMB caverns would be required. NYSEG directed PB ESS to develop casing specifications which will allow an air flow rate of 639 lb/sec for the first cavern and 320 lb/s for Caverns 2 and 3.

2 CASING SELECTION RATIONALE

2.1 BRINE STRING SELECTION

The inner leach string for NYSEG was sized to accommodate a modern sonar surveying tool. Modern sonar tools require a tubular with a minimum inside diameter of 4 inches. The minimum acceptable size for the inner solution mining string is 5.5 inch OD. A 5.5 inch diameter, 15.5 lb/ft, API J-55 tubular was selected for the inner string. Coupling diameters for the inner string require that the outside solution mining string no smaller than 7 inches. PB ESS selected an API 8-5/8 inch, 32 lb/ft, J-55 well casing for the outer solution mining casing to equalize velocities in both the inner string and the annulus.

2.1.1 Brine String Hydraulic Calculations

Hydraulic calculations across the wellbore were performed using a workbook specifically designed by PB ESS for solution mining calculations. Friction loss estimates are performed using the Darcy method, using the Colebrook Transition formula. Input parameters for calculations are given in Table 1.

Figure 1 (direct circulation) and Figure 2 (reverse circulation) show the wellhead water pressure for friction factor ratios ranging from 1 to 10 times the calculated friction factor. Typical wellbore performance is consistent with a friction factor ratio of about 4. Calculated pressures for a friction factor ratio of 4, and flow rates ranging from 100 gpm to 900 gpm are given in Table 2. As can be seen, the wellhead water pressure expected is 421 psi (assuming that the outlet pressure from the well is 50 psi) and the blanket pressure at the start of solution mining is 1,307 psi while circulating in direct mode. The calculated water pressure in reverse mode is 420 psi and the blanket pressure is 1,289 psi.

Table 1 - Calculation Input Assumptions

1.0 INPUT	Raw water roughness - 1 x brine roughness		10/24/11 9:19:19
PROJECT:	NYSEG - Seneca Lake CAES Cavern 1		
Qmin	100 gpm	minimum flow rate	
dQ	50 gpm	delta flow rate	
pprod	50 psi	brine production pressure	Assumes saturation by injection into second cavern.
di	4.825 in	inner diameter (inner pipe)	5.5" 15.5#/ft J-55 Collapse = 4040 psi & Yield = 4810 psi
do	5.500 in	outer diameter (inner pipe)	
dco	6.050 in	inner pipe coupling outer diameter	
cl	0.667 ft	inner pipe coupling length	
jl	40.000 ft	inner pipe joint length	
li	2.630 ft	length of inner pipe	
nj	64 -	number of couplings	
Di	7.921 in	inner diameter (outer pipe)	8.625" 32#/ft J-55 Collapse = 2530 psi & Burst = 3930 psi
lo	2,530 ft	length of outer pipe	
lcs	2,360 ft	length of final cemented casing	
lpad	2,520 ft	depth of pad	
epsbr	0.018 in	roughness of pipe (brine side)	
epsrw	0.018 in	roughness of pipe (raw water side)	
peff	0.75 -	pump & motor efficiency	
temp	51 F	average raw water / brine temperature	
gravrw	1.000 -	specific gravity (raw water)	
etarw	0.000 %	salinity (raw water)	
gravbr	1.130 cP	dynamic viscosity (raw water)	
gravbr	1.198 -	specific gravity (brine)	
etabr	97.242 %	salinity (brine)	
gravpad	1.600 cP	dynamic viscosity (brine)	
gravpad	-	specific gravity (pad) or Gas Constant if Nitrogen	Nitrogen R=55.16 ft lb/lbm/R
grad	0.700 psi/ft	permissible pressure gradient at casing shoe	
equiv. dia.	1	$0 = (Di-do)/CF$ and $1 = (Di-do)$	

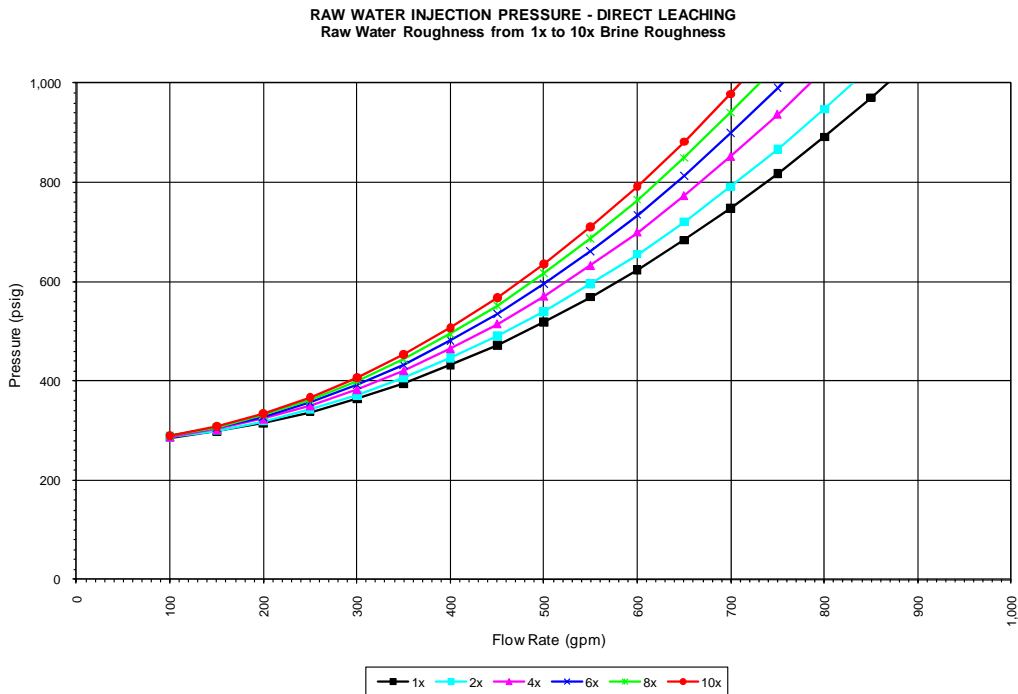


Figure 1 - Water Injection Pressure Direct Circulation

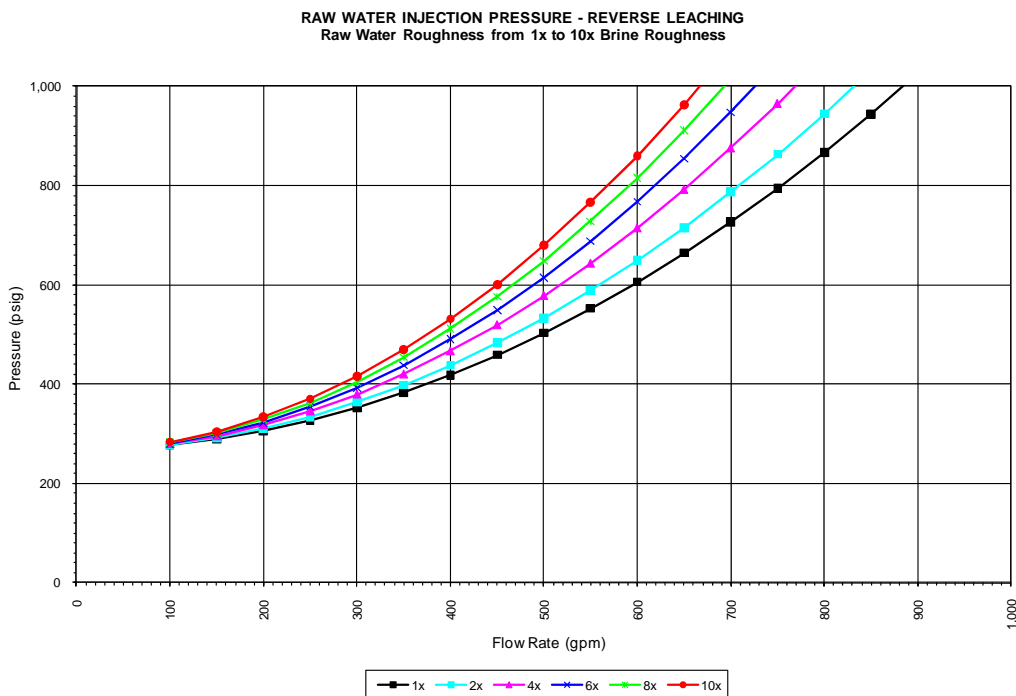


Figure 2 - Raw Water Pressure - Reverse Circulation

Table 2 - Calculated Pressures (Direct and Reverse Circulation)

Raw Water		Brine		Direct Leaching				Reverse Leaching				p cs max (psi)	pprod (psi)
Q rw (gpm)	Q rw (bpd)	Q br (gpm)	Q br (bpd)	p rw (psi)	p pad (psi)	p cs (psi)	Pump (bhp)	p rw (psi)	p pad (psi)	p cs (psi)	Pump (bhp)		
100	3,429	96	3,304	288	1,246	1,355	22	280	1,245	1,354	22	1,652	50
150	5,143	145	4,956	303	1,253	1,363	35	295	1,250	1,359	34	1,652	50
200	6,857	193	6,607	324	1,263	1,373	50	317	1,257	1,367	49	1,652	50
250	8,571	241	8,259	350	1,275	1,386	68	345	1,266	1,376	67	1,652	50
300	10,286	289	9,911	383	1,290	1,402	89	380	1,276	1,388	89	1,652	50
350	12,000	337	11,563	421	1,307	1,421	115	420	1,289	1,402	114	1,652	50
400	13,714	385	13,215	465	1,327	1,443	145	467	1,304	1,418	145	1,652	50
450	15,429	434	14,867	515	1,350	1,468	180	519	1,320	1,435	182	1,652	50
500	17,143	482	16,518	571	1,375	1,495	222	578	1,339	1,455	225	1,652	50
550	18,857	530	18,170	632	1,403	1,525	271	643	1,359	1,477	275	1,652	50
600	20,571	578	19,822	700	1,433	1,558	327	714	1,381	1,502	333	1,652	50
650	22,286	626	21,474	773	1,466	1,594	391	792	1,405	1,528	400	1,652	50
700	24,000	675	23,126	852	1,502	1,633	464	875	1,431	1,556	477	1,652	50
750	25,714	723	24,778	936	1,540	1,675	546	965	1,459	1,587	563	1,652	50
800	27,429	771	26,429	1,027	1,581	1,719	639	1,061	1,489	1,619	660	1,652	50
850	29,143	819	28,081	1,123	1,625	1,767	743	1,163	1,521	1,654	769	1,652	50
900	30,857	867	29,733	1,225	1,671	1,817	858	1,271	1,555	1,690	890	1,652	50

2.2 PRODUCTION LINER SELECTION

Carbon steel undergoes rapid corrosion in the presence of air and water. Huntorf, the site of the first commercial CAES facility in Germany, was initially built with carbon steel, however, severe corrosion took place within the first few months of operation⁴ and a fiberglass liner was installed to protect the carbon steel cemented casing string. Crotogino⁴ reported that the fiberglass casing liner used at Huntorf began exhibiting failure after approximately 20 years of operation. McIntosh, the site of the only commercial CAES facility in the US, was originally

designed to use fiberglass casing liners. The cavern was ultimately built using a 316L stainless steel casing liner suspended from the surface. Due to the high corrosion potential for this project PB ESS recommends the use of a corrosion resistant alloy or a fiberglass casing liner for the NYSEG CAES cavern.

The liner is designed to be suspended from a wellhead casing hanger to a depth approximately 5 feet below the cavern roof. A continuous flow of dry air or nitrogen will be injected down the annulus between the liner and the production casing to limit corrosion of the cemented casing. The liner is not equipped with a downhole packer to isolate the interval between the liner and the cemented casing. Due to the low collapse resistance of the liner and the pressure changes in the well during operation a packed off liner interval would be subject to collapse.

Fiberglass well casing with an outside diameter of 20” (largest diameter located)⁵ has a coupling diameter of 30” and an axial tension rating of 245,000 lb, or 136,000 lb using the design factors given in API-6A. The pipe weight suspended from the hanger liner would be 178,000 lb, which exceeds the recommended axial tension rating of the pipe. Further, the coupling diameter would require increasing the hole size to a minimum of 36”, with consequent increases in drilling and casing costs. The 36” cemented casing would require wall thickness of greater than 1.5” in the salt section of the hole to prevent collapse, which in our experience is not possible to weld on the rig floor.

Stainless steel was used for a production liner in CAES service at both Huntorf and McIntosh. No definitive information on the corrosion levels of the stainless steel tubulars in CAES service has been located during our review of appropriate materials. The most commonly available stainless steel exhibiting corrosion resistance to salt water and marine environments is Type 316 stainless steel.⁶ Type 316L stainless steel is an extra low carbon version of Type 316 which was developed for improved weldability.⁷

PB ESS recommends that stainless steel be used for the production liner since erosion velocities in CAES service are high and the potential for severe corrosion exists. Due to its corrosion resistant properties, high erosion resistance⁸, use at McIntosh and Huntorf, high strength, and weldability PB ESS recommends that a suspended liner fabricated from 316L stainless steel be used by NYSEG at Watkins Glen.

2.2.1 Production Liner Hydraulics

The Salt Cavern Thermal Simulator (SCTS)⁹ was used to determine the size of the air production liner. The analyses performed are thoroughly described in the Thermodynamic Evaluation Report.¹ Casing diameter was modeled to determine the air velocity, relative to erosion velocity limits recommended in API-14E¹⁰. The results of this assessment were that air erosion velocity is not the limiting factor in selecting the liner diameter for this application.

Friction loss due to airflow was simulated for casing diameters between 6.6 in. and 24 in. Friction loss in the liner affects the working gas volume of a storage cavern. The higher the friction loss, the lower the working gas volume of the cavern is, and the larger the amount of gas that must be left in the cavern once the minimum operating pressure is reached. The SCTS

analyses indicated that a liner diameter of 20” would be required for 639 lb/s flow rate and 16” liner diameter would be required for a flow rate of 320 lb/s.

2.3 CEMENTED CASING SELECTION

Generally, cemented casing for bedded salt caverns includes conductor pipe, surface casing, and the final cemented casing. This philosophy is used for the NYSEG casing program.

The outermost well casing is the conductor casing. Conductor casing is a short string of pipe (175’ in this case) that provides a channel for the flow of drilling fluids, provides a secure attachment point for blowout prevention equipment during drilling of the surface hole, and prevents washout from occurring under the base of the drilling rig. For all wells a 42” steel conductor pipe was selected.

Inside the conductor casing is the surface casing. The surface casing protects the upper formations from possible contamination by salt saturated drilling and completion fluids. At Watkins Glen there are no significant fresh water aquifers¹¹, with bedrock encountered no deeper than 157 feet below ground surface. A significant review of groundwater resources was done during 1995 as a part of permitting the Akzo Gallery No. 1 for natural gas storage. Consequently, protection of groundwater can be accomplished by isolating the surface sediments and the Genesee formation. Based upon the anticipated geology of the cavern location a depth of approximately 850 ft is suggested. To provide adequate surface for cementing a 24” OD steel production casing inside a 30” OD steel casing was selected for the surface pipe for Cavern No. 1 and 26” OD steel casing for the surface pipe for caverns 2 & 3.

Inside the surface casing is the production casing. The purpose of the production casing is to provide a positive seal, anchored in relatively impermeable salt, for air storage. In bedded salt it is commonly not possible, or necessary, to place two final casing strings into salt. The final cemented casing depth was selected based upon site geology and the nominal depth for the 24” production casing is 2,360 ft below ground level. Since the cavern roof is planned for 2,402 ft and the top of salt is projected to be at 2,352 ft the shoe was placed just into the Syracuse Salt to allow development of the cavern to the largest reasonable volume.

Figure 3 shows the proposed casing program for Cavern No. 1, while the program for Caverns 2 & 3 is provided in Figure 4. These figures show the well in leaching configuration. Figures 5 and 6 show the casings in storage configuration (with the stainless steel liner in place).

3 CASING PERFORMANCE

PB ESS evaluates casing performance in accordance with API 5C3¹⁰ to determine the appropriate wall thickness. All casing strings were evaluated for collapse, pipe body yield, joint strength (where applicable) and internal pressure resistance. All cemented casings are cemented to the surface. Casing grades and thicknesses were selected to obtain an economic casing program. Usually, a lower grade or thin walled casing costs less than a higher grade or thick

walled casing. Consequently, the most economic program is achieved by selecting lower grade, thinner walled casing, and taking into account relative availability.

Figures 7- 12 provide basic casing program calculations for the casing proposed for Well No. 1 while Figures 13-19 provide program calculations for Wells No. 2 & 3, respectively.

Selection of the Stainless Steel Liners required an additional consideration. When installing casing, slips are commonly used to hold the casing while another section is being welded in place. On thin tubulars and on very deep completions the slips can crush the tubing. PB ESS used a method used for deep water landing design¹² to determine minimum thickness for the stainless steel hanging strings. Calculations based on this technique are provided in Table 3 and 4, respectively for Wells 1 and 2 & 3.

4 REFERENCES

1. Nieland, Joel, External Memorandum, *Thermodynamic Evaluation of Proposed New York State Electric & Gas Corporation Compressed Air Energy Storage Cavern Design*, RESPEC Inc, September 14, 2011.
2. Eyer mann, Thomas, *Overview of Geology of the Area Around the US Salt Watkins Glen Refinery*, PB ESS, 2011.
3. Eyer mann, Thomas, *Conceptual Cavern For NYSEG Compressed Storage at Watkins Glen*, NY, PB ESS 2011.
4. Crotogino, Fritz, *Huntorf CAES: More Than 20 Years of Successful Operation*, KBB Inc, Solution Mining Research Institute April 2001.
5. Future Pipe Industries. *High Pressure Epoxy Pipe Systems*. 2007.
6. American Society for Metals. *ASM Metals Reference Book*. 1983.
7. AK Steel. *Product Data Bulletin 316/316L Stainless Steel*. 2007.
8. Salama and Ventatesh. *Evaluation of API RP 14E Erosion Velocity Limitations for Offshore Gas Wells*. OTC 4485. Offshore Technology Conference. 1983.
9. Nieland, J. D., 2002, *Salt Cavern Thermal Simulator Version 1.5 User's Manual*, Revision 1, RSI-1650, prepared by RESPEC, Rapid City, SD, for Gas Technology Institute, Chicago, IL.
10. American Petroleum Institute, API Recommended Practice 14E, *Recommended Practice for Design and Installation of Offshore Production Platform Piping Systems*, March 2007.
11. Russell, Bruce, *Ground Water Review – Akzo Cavern Gallery No. 1*, Fenix and Scisson, July 1995.
12. American Petroleum Institute, *Bulletin on Formulas and Calculations for Casing, Tubing, Drill Pipe, and Line Pipe*, 1994.

13. Adams, Richard J., *Deepwater Landing String Design*, American Association of Drilling Engineers, AADE 01-NC-HO-05, 2001.

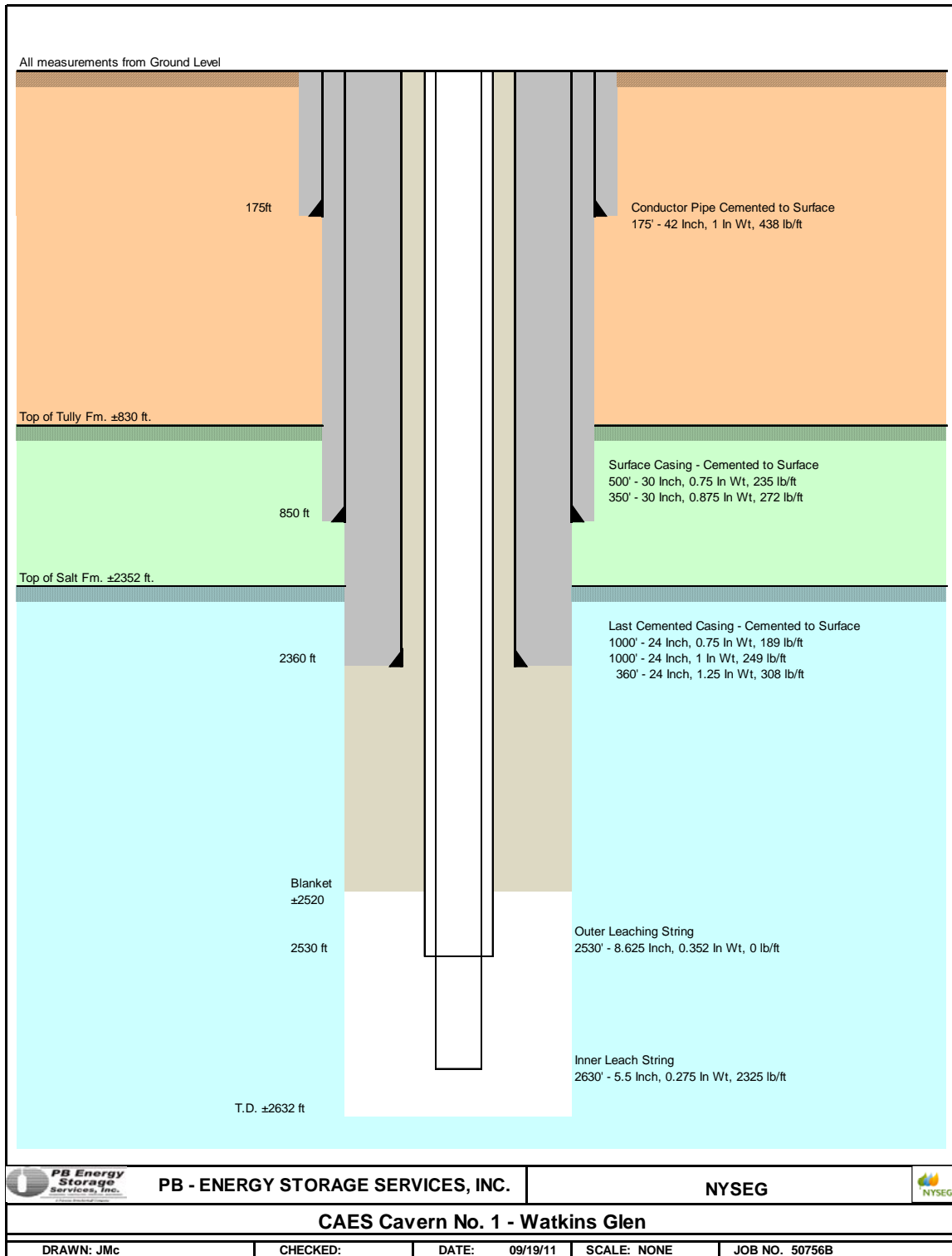


Figure 3 - Casing Program Cavern No. 1 - Leaching Configuration

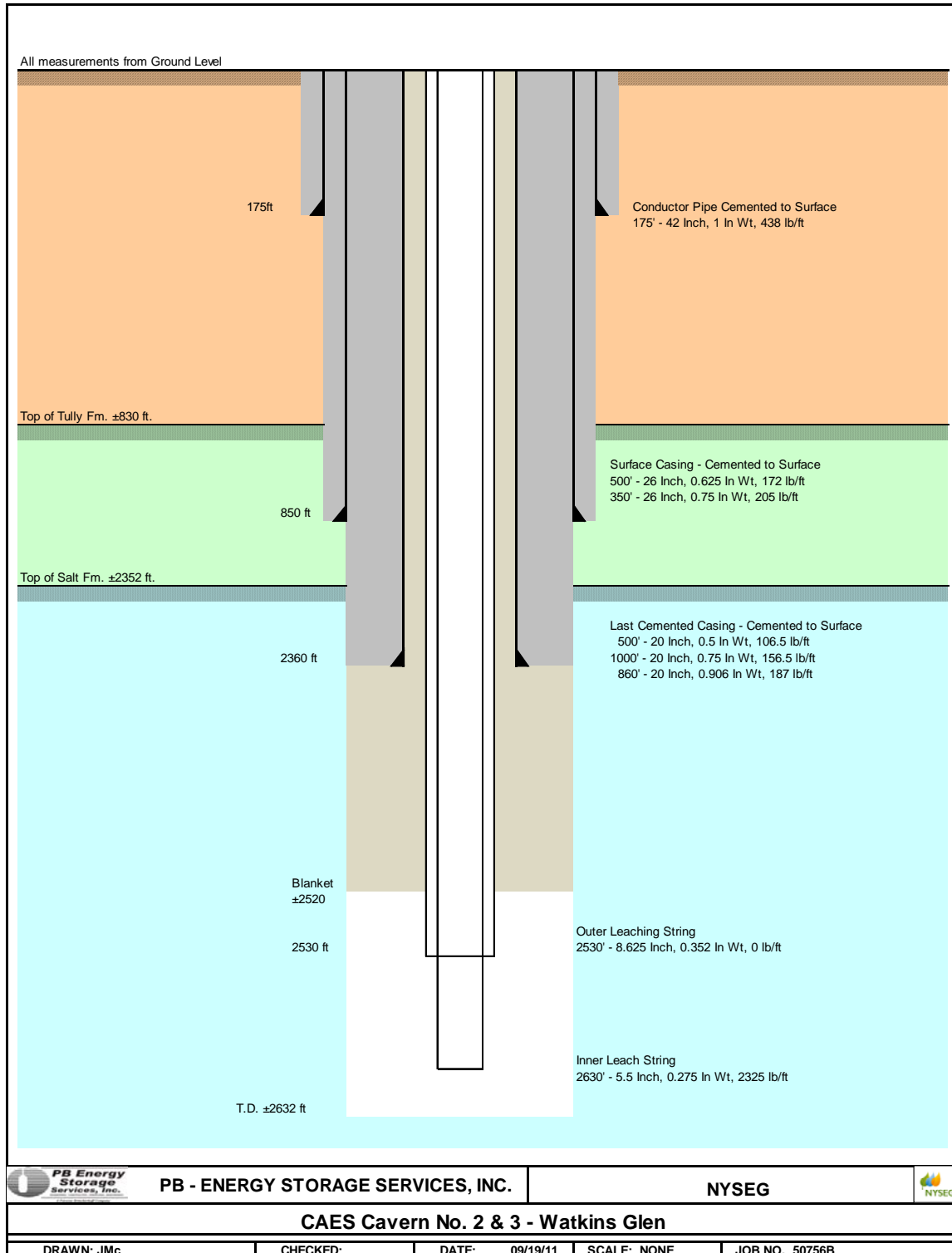


Figure 4 - Casing Program Cavern No. 2 / 3 - Leaching Configuration

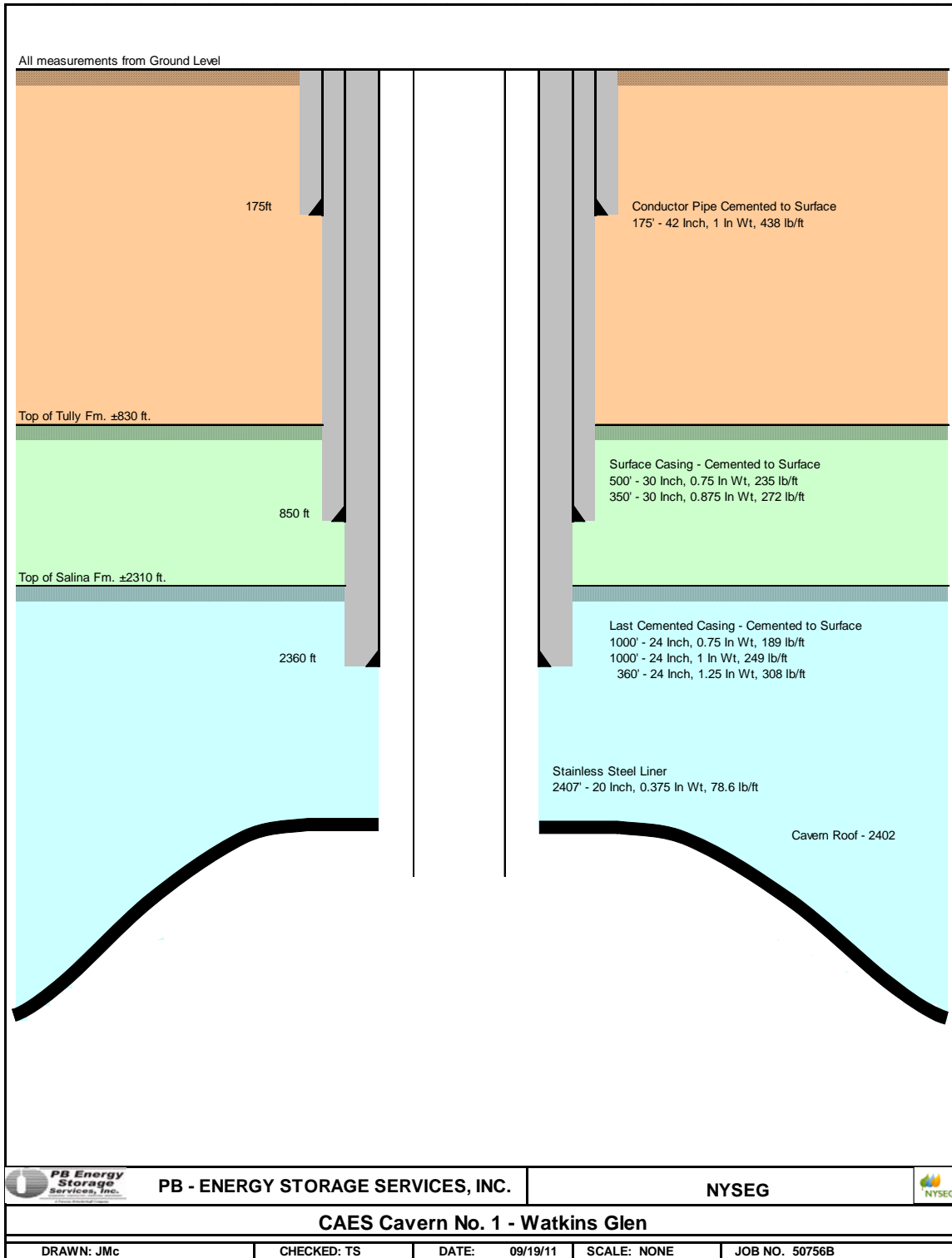


Figure 5 – Casing Program Cavern 1 - Storage Configuration

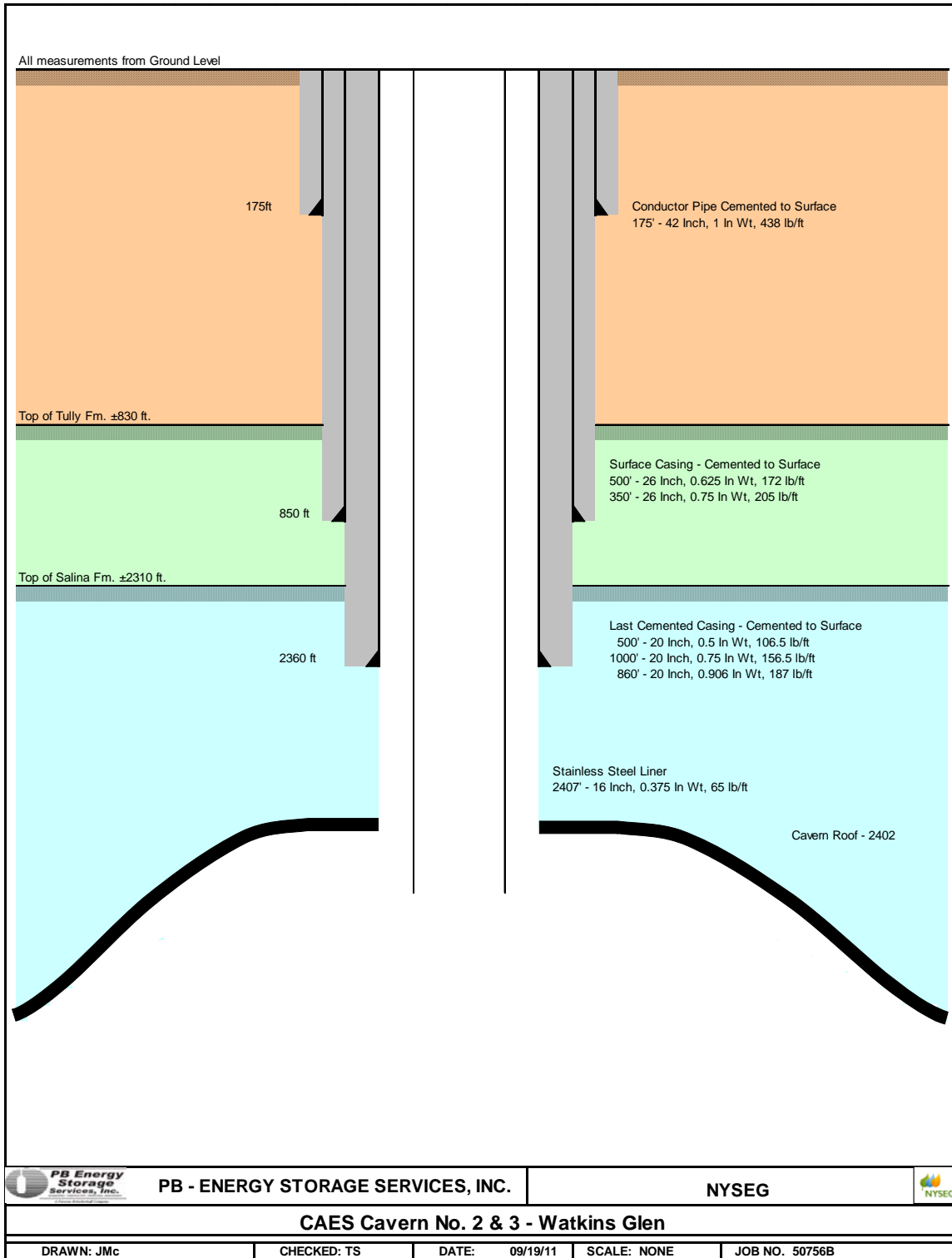


Figure 6 - Casing Program Caverns 2 & 3 - Storage Configuration

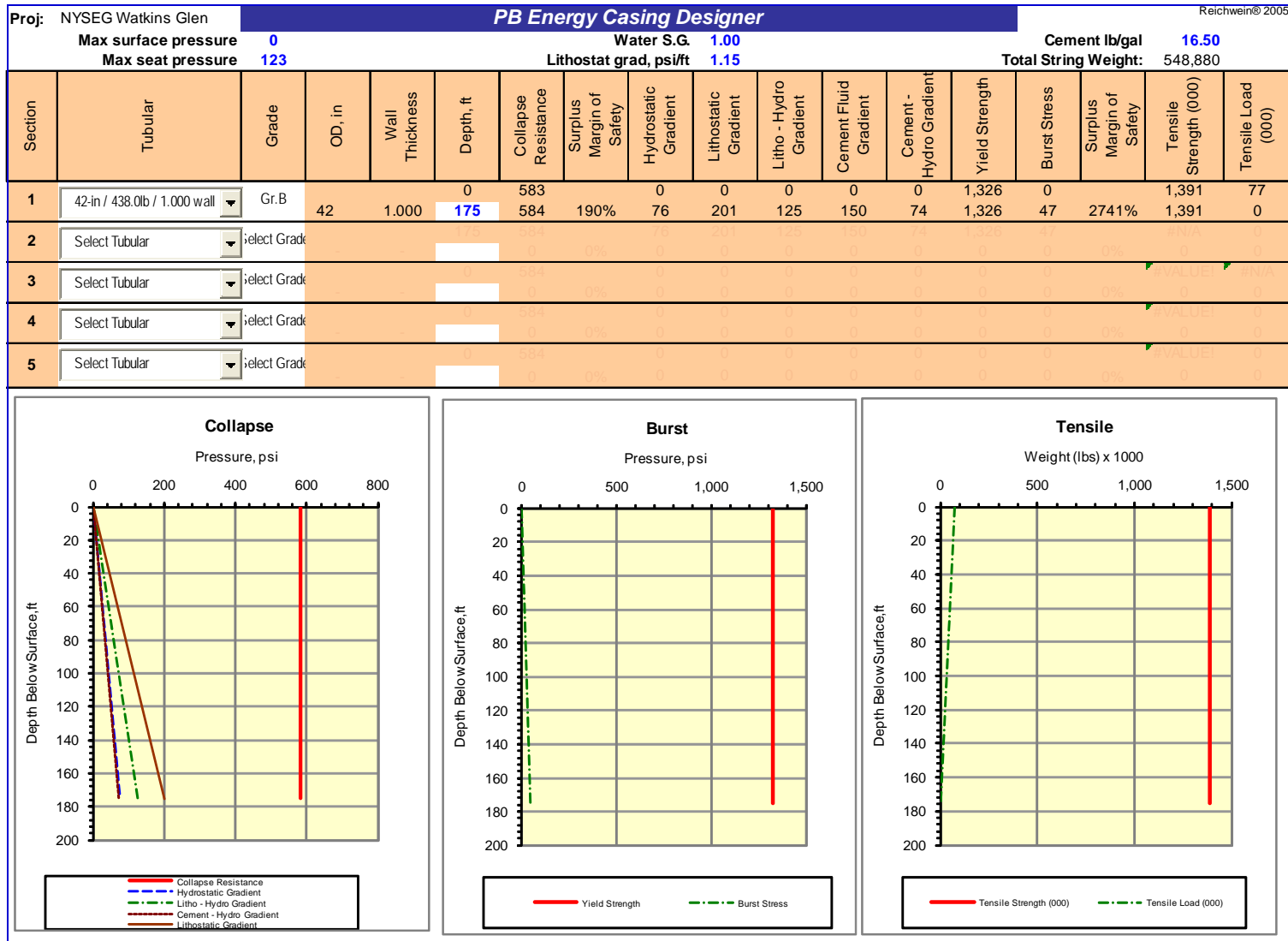


Figure 7 - Conductor Pipe Calculations Cavern No. 1



Figure 8 - Surface Casing Calculations Cavern No. 1

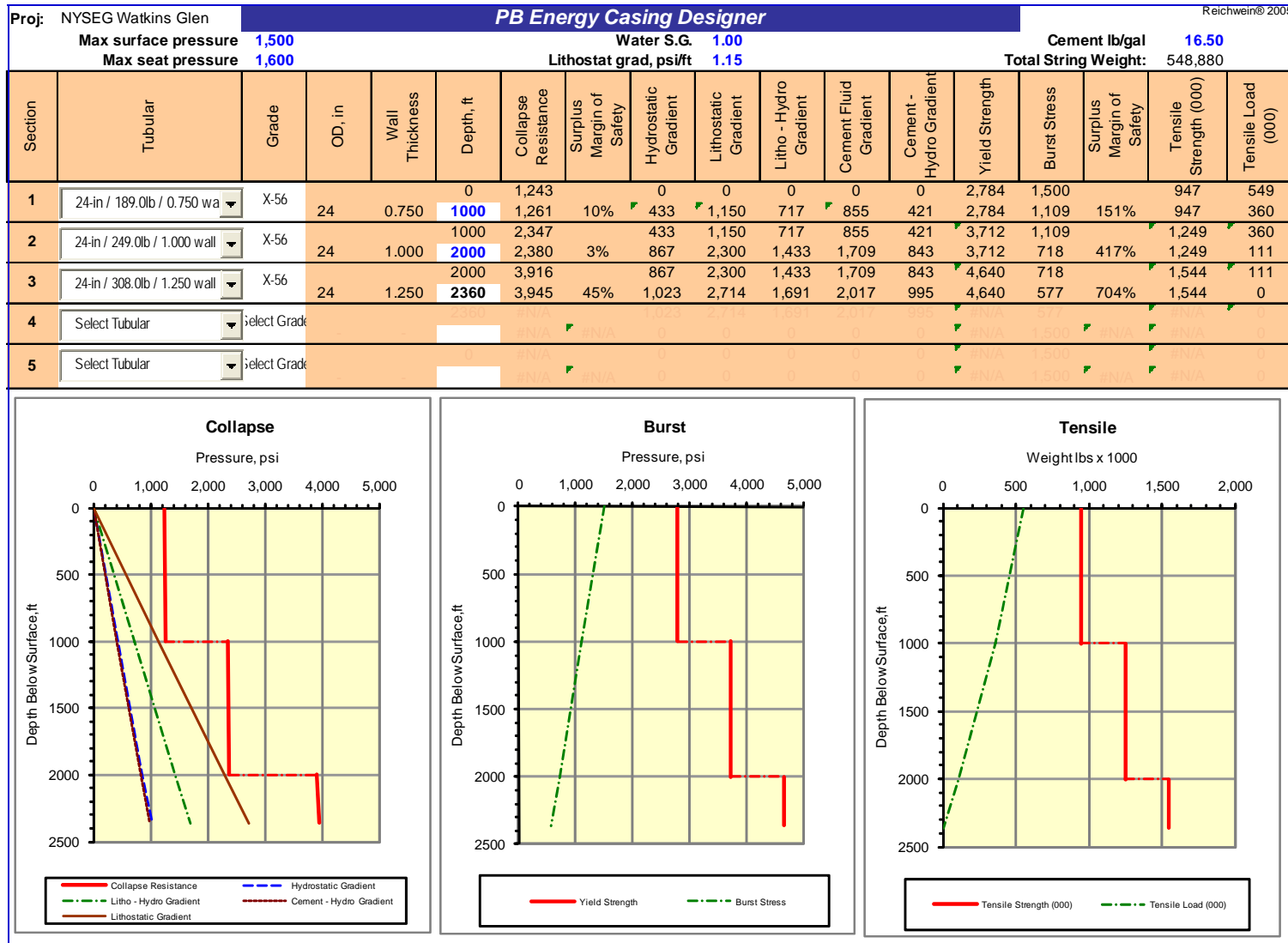


Figure 9 - Production Casing Calculations Cavern No. 1

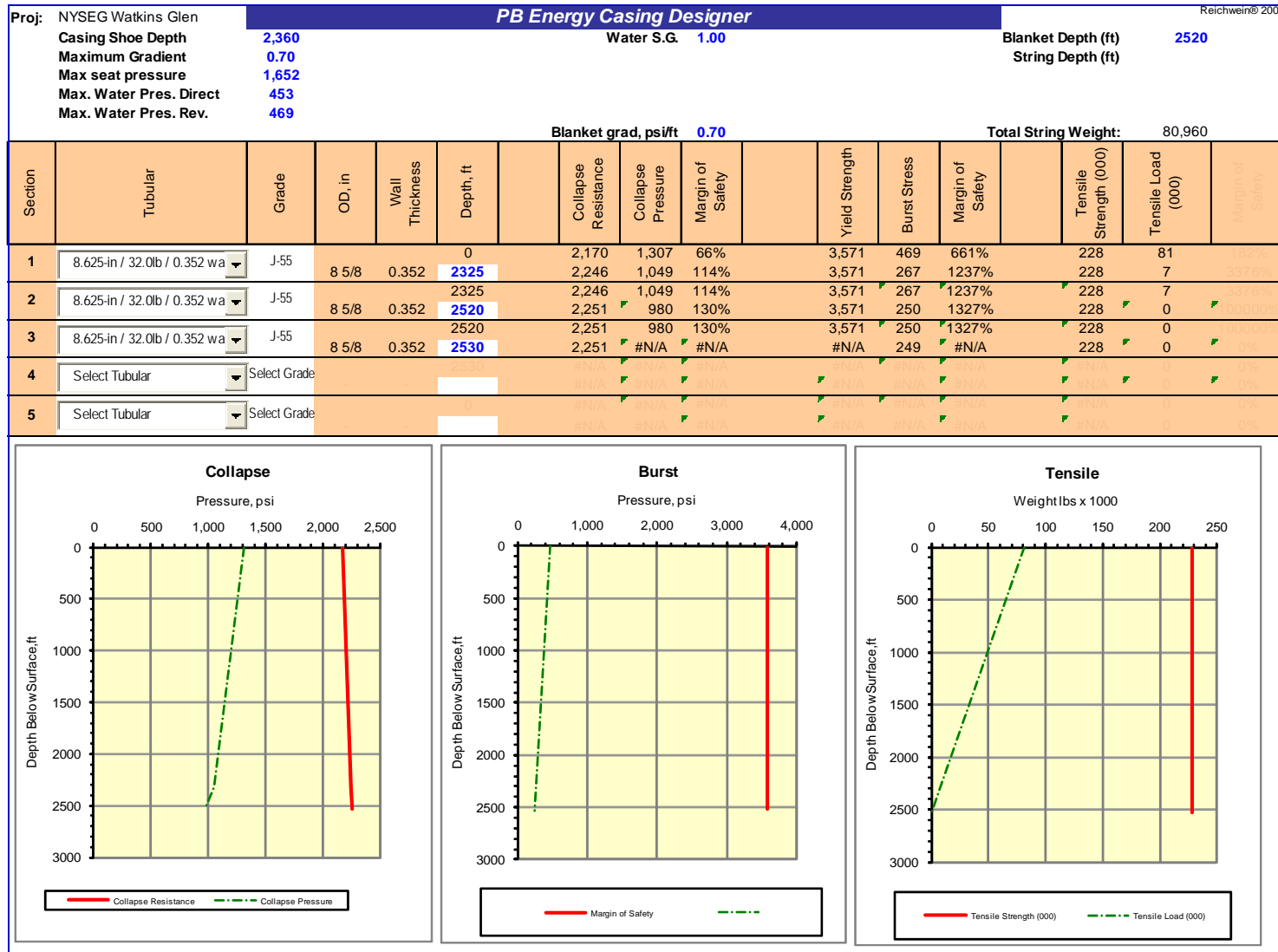


Figure 10 - Outer Leach String Calculations Cavern No. 1

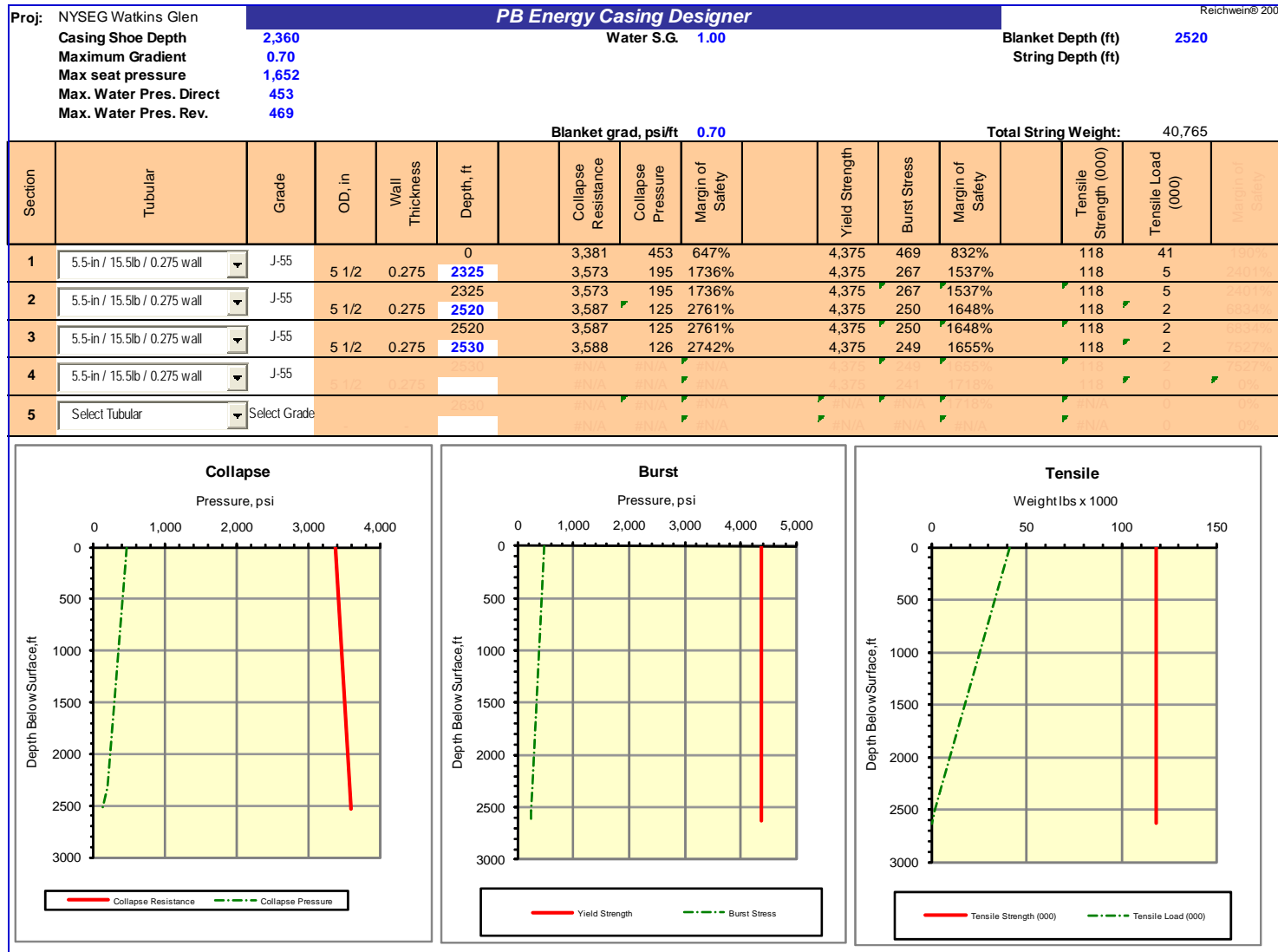


Figure 11 - Inner Leach String Calculations Cavern No. 1

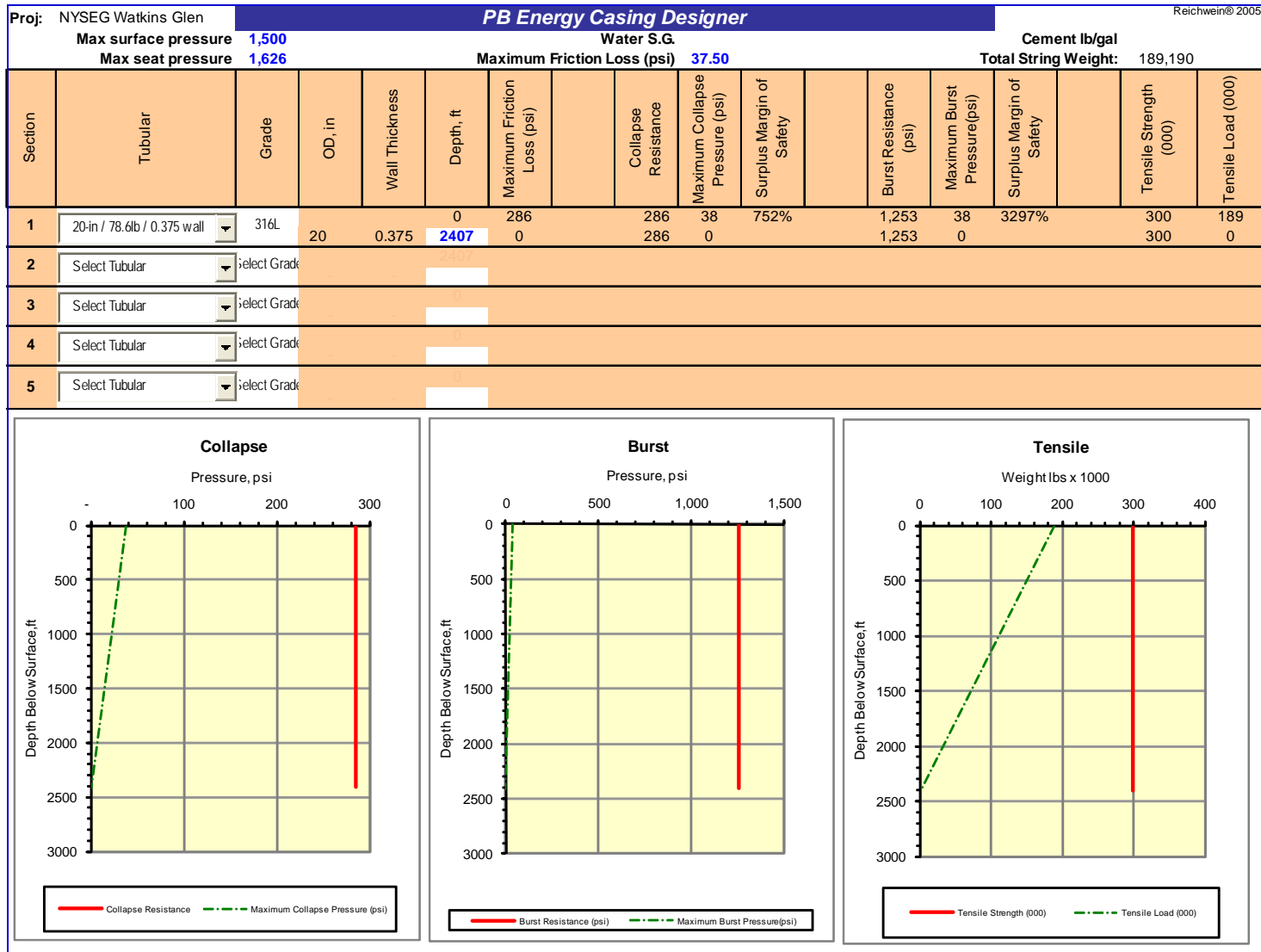


Figure 12 - Stainless Steel Production Liner Calculations Cavern No. 1

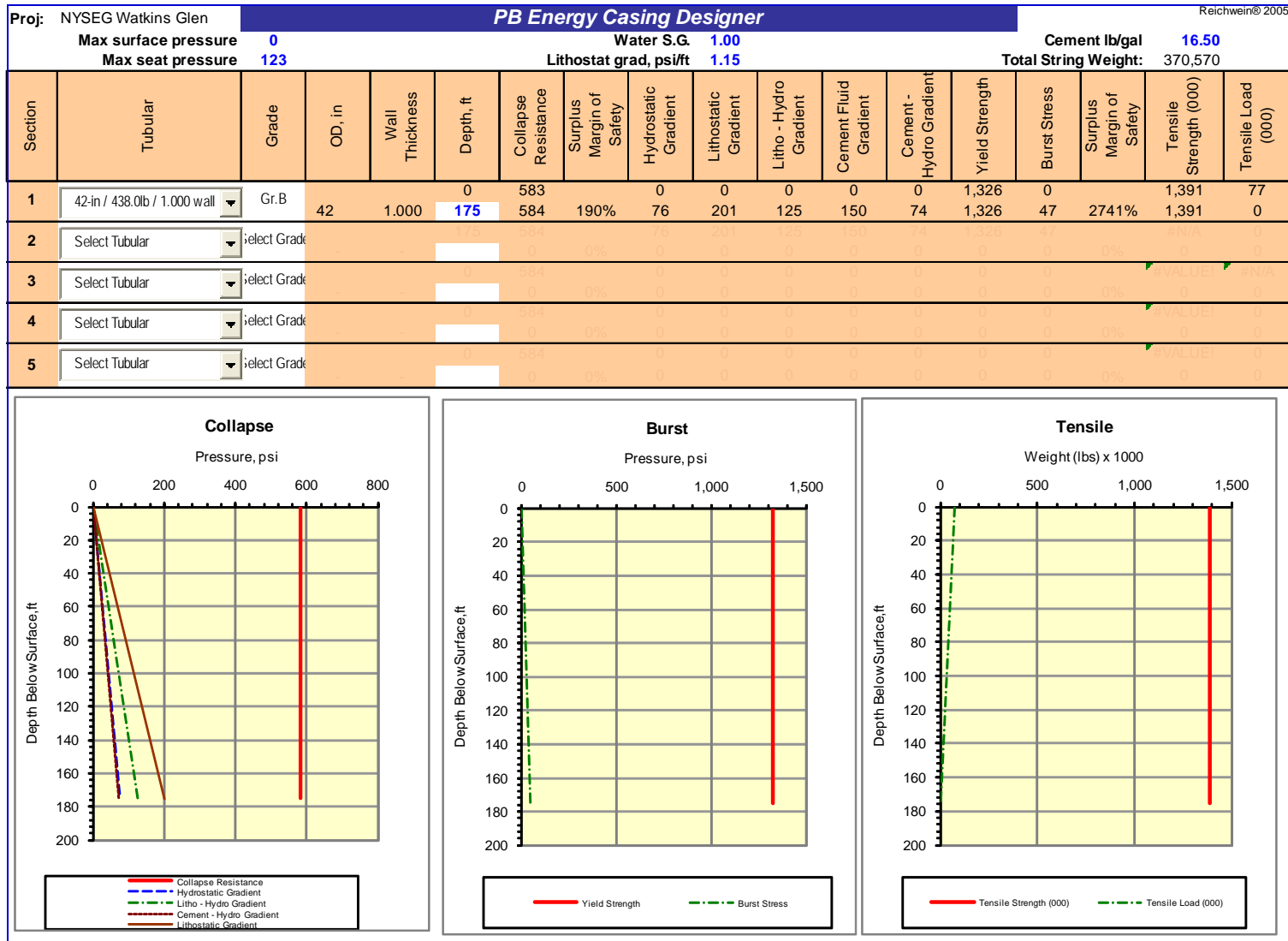


Figure 13 - Conductor Pipe Calculations Caverns No. 2 & 3

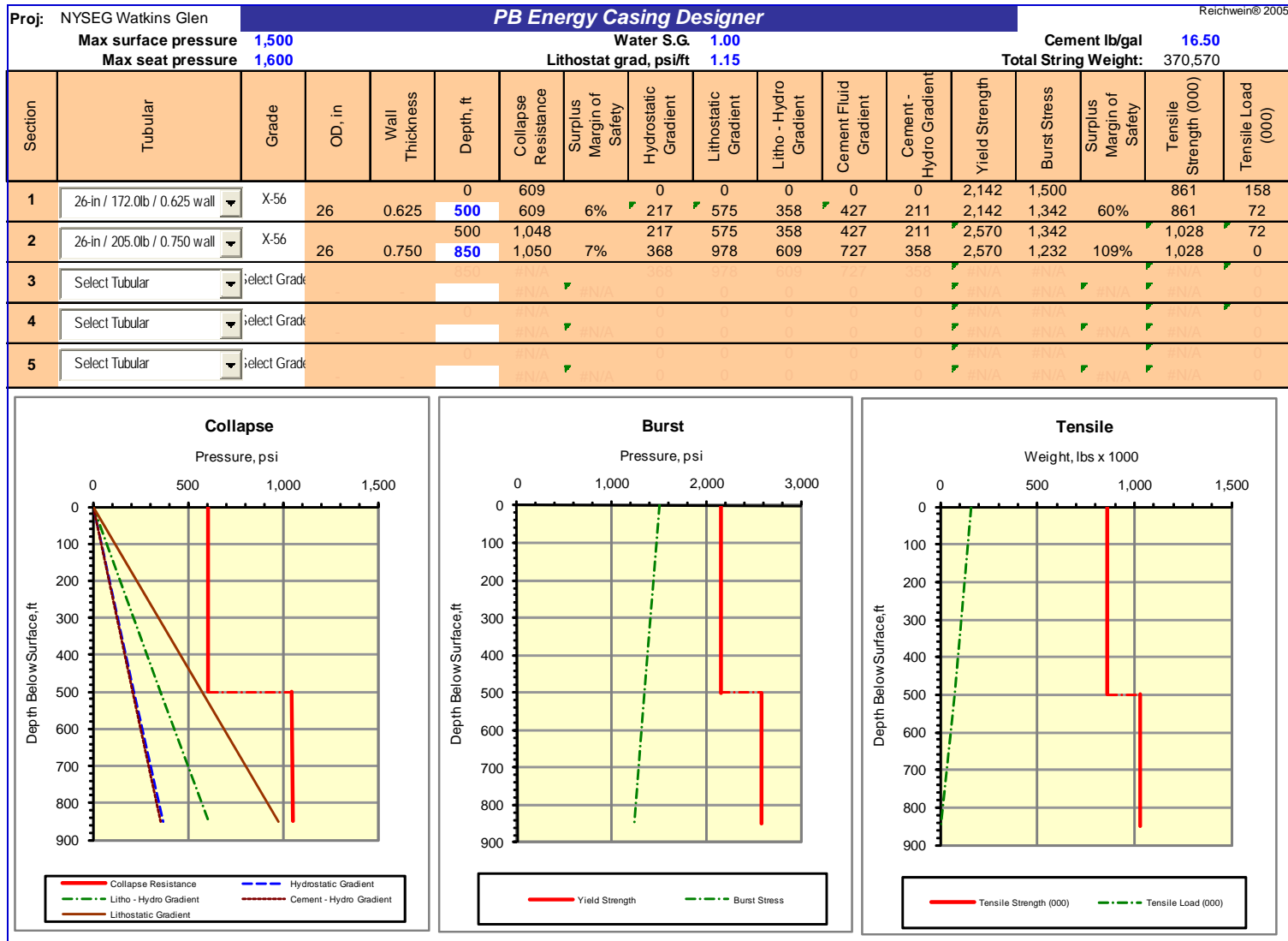


Figure 14 - Surface Casing Calculations Caverns No. 2 & 3

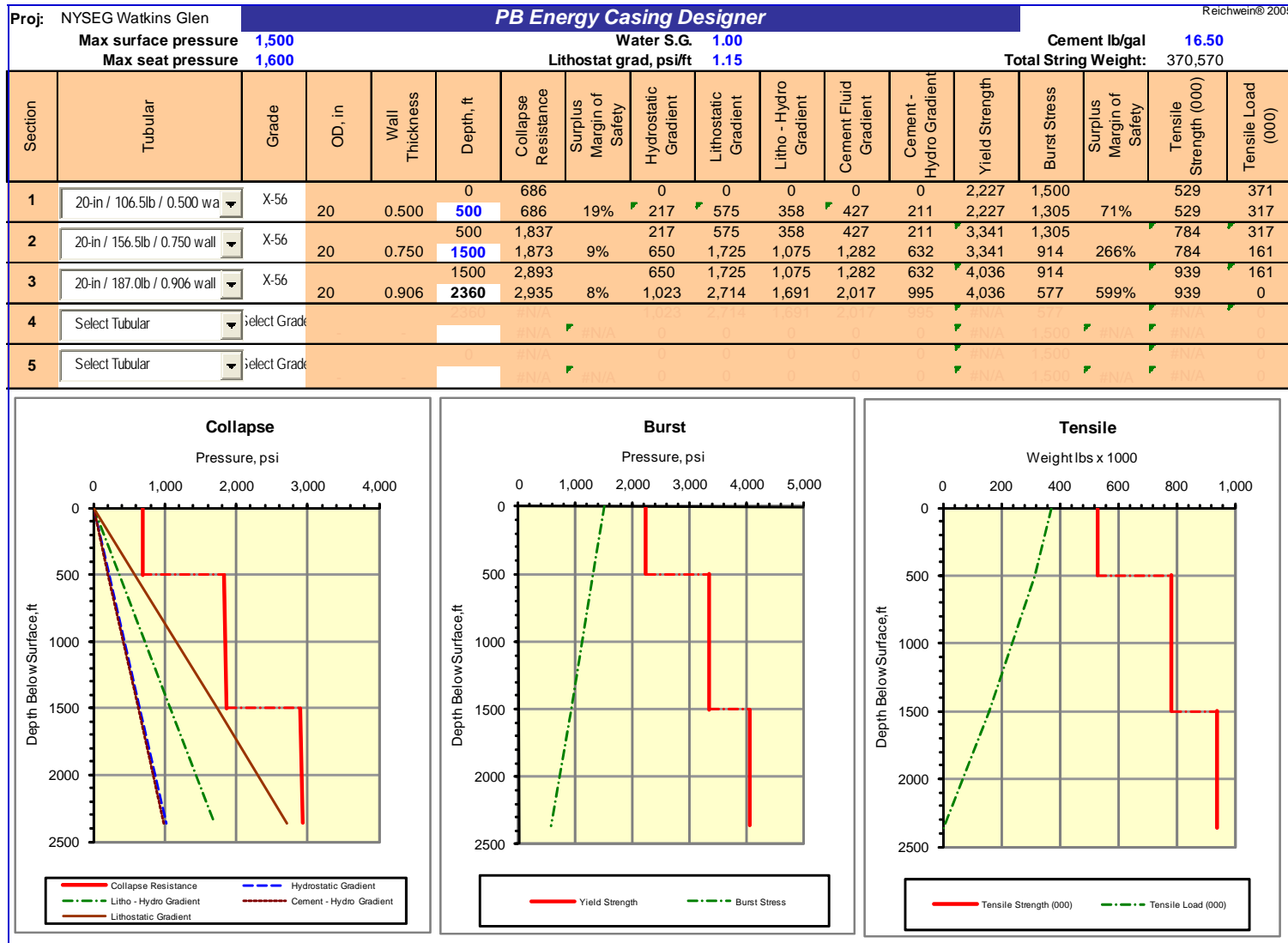


Figure 15 - Production Casing Calculations Caverns No. 2 & 3

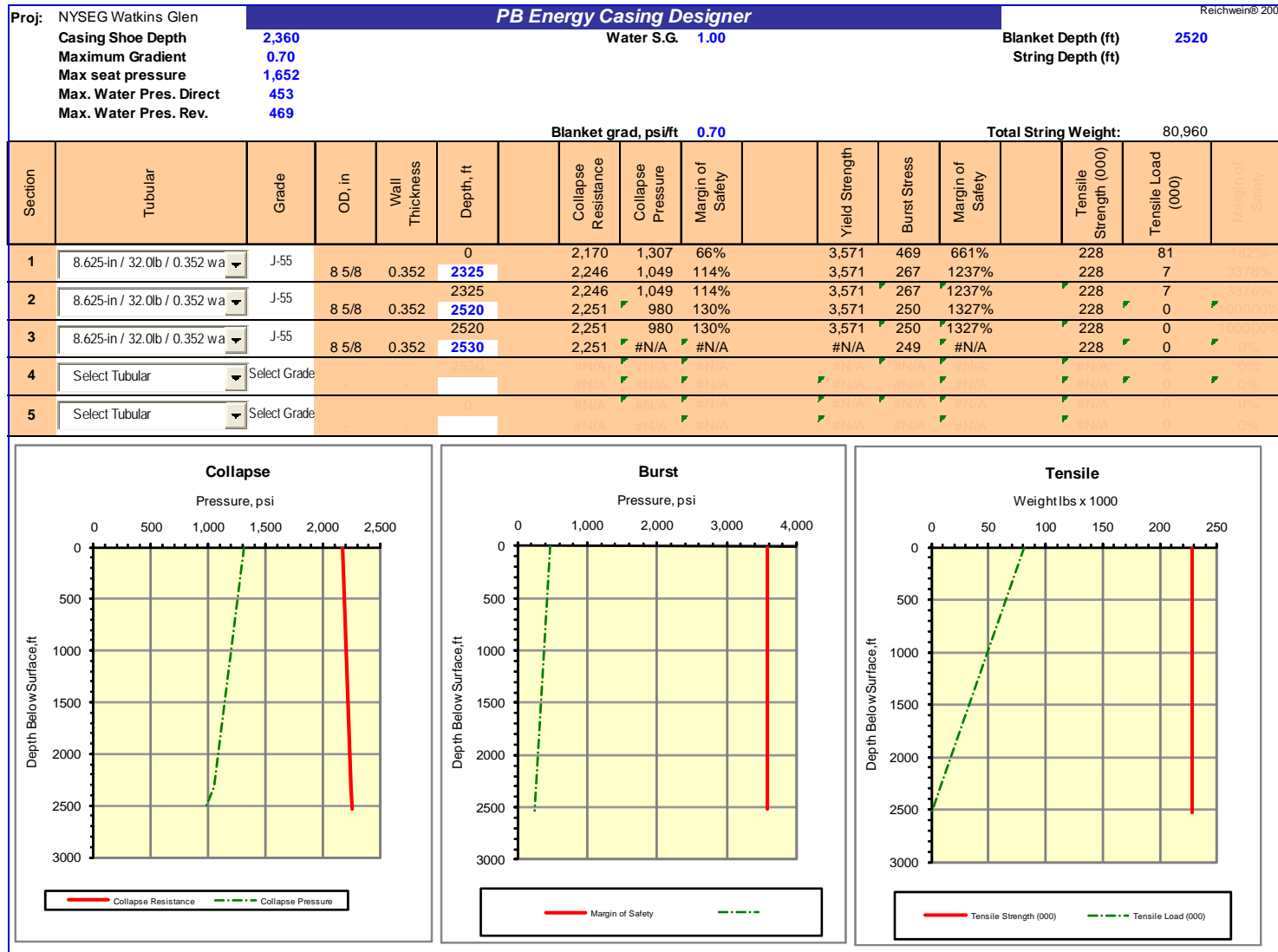


Figure 16 - Outer Leach String Calculations Caverns No. 2 & 3

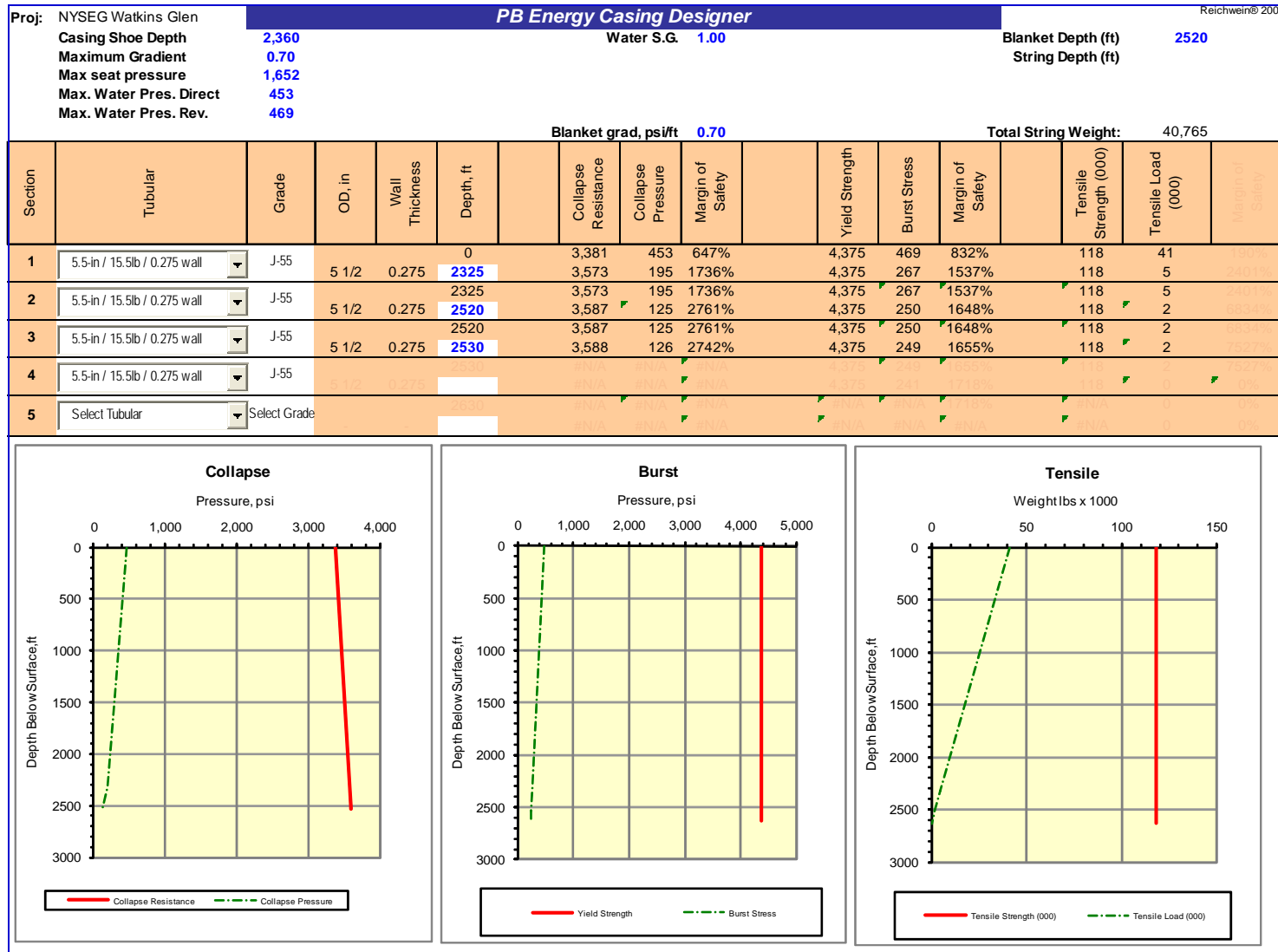


Figure 17 - Inner Leach String Calculations Caverns No. 2 & 3

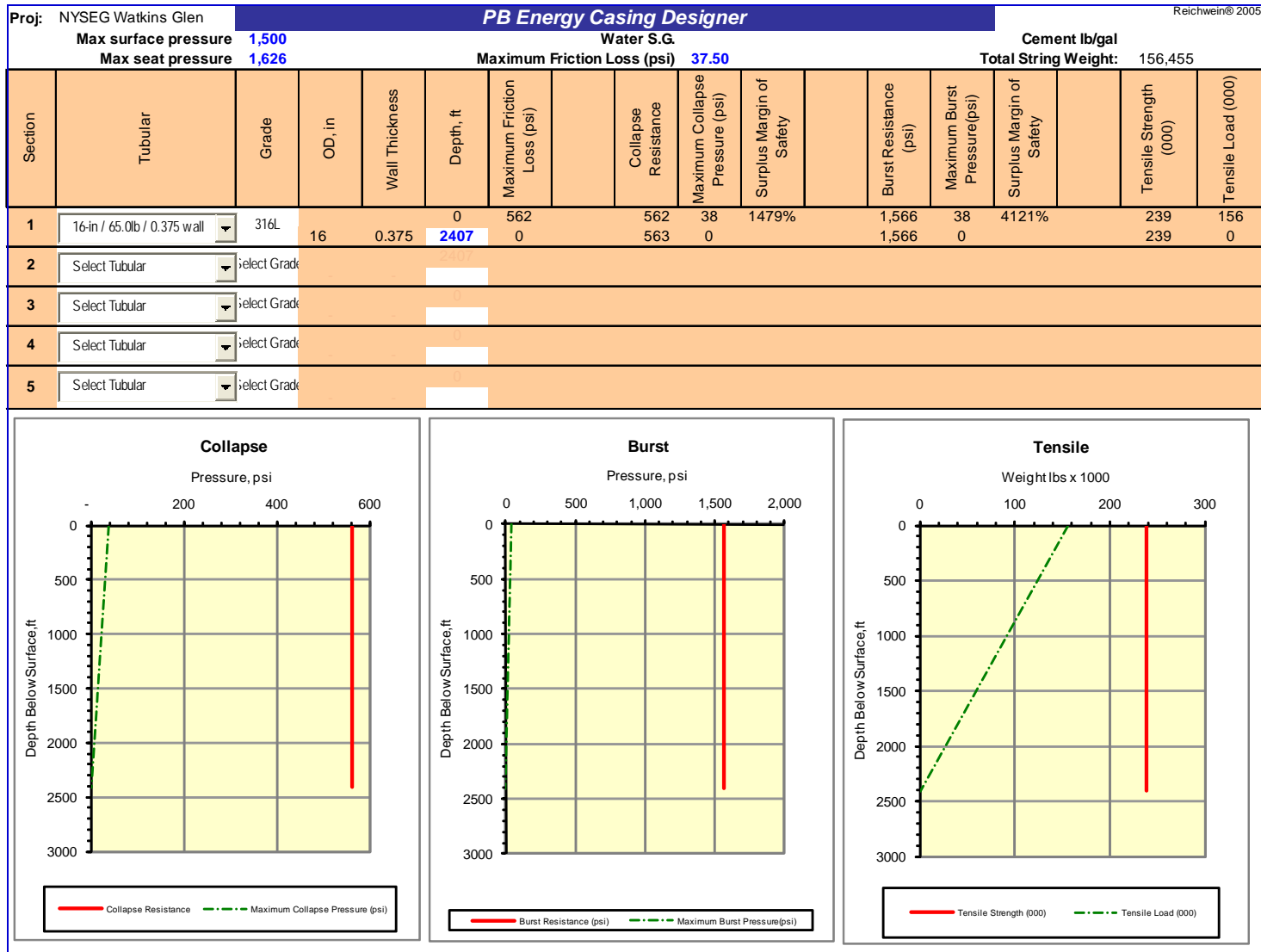


Figure 18 - Stainless Steel Production Liner Calculations Caverns No. 2 & 3

Table 3 - Slip Crushing Calculation Well No. 1

Outer Diameter (in)		20
String Length		2402
Inside Diameter (in)		19.25
Minimum Yield Strength (psi)		42000
Length of Slips (in)		16
Taper of Slips (degrees)		9.4625
Coefficient of Friction (slips to bowl)		0.08
API Tensile Design Factor		1.25
Cross Sectional Area (in ²)	23.12	
Tensile Capacity (lb)	776,837	
Tan ⁻¹ (m)	4.5739	
Transverse Load Factor	4.00	
Hoop Stress to Tensile Ratio	3.12	
Maximum Allowable Tensile Load	248,790	
String Weight	186,596	
Available For Dynamic Loading	<u>62,193</u>	

Table 4 - Slip Crushing Calculation Well Nos. 2 & 3

Outer Diameter (in)		16
String Length		2402
Inside Diameter (in)		15.25
Minimum Yield Strength (psi)		42000
Length of Slips (in)		16
Taper of Slips (degrees)		9.4625
Coefficient of Friction (slips to bowl)		0.08
API Tensile Design Factor		1.25
Cross Sectional Area (in ²)	18.41	
Tensile Capacity (lb)	618,501	
Tan ⁻¹ (m)	4.5739	
Transverse Load Factor	4.00	
Hoop Stress to Tensile Ratio	2.65	
Maximum Allowable Tensile Load	233,774	
String Weight	148,564	
Available For Dynamic Loading	<u>85,210</u>	